(4)

GL-TR-89-0198

Feasibility of Radio Blackout Mitigation in the Braking Phase of AOTV Operations

Didier Rault
Edward P. Szuszczewicz

Science Applications International Corp
P.O. Box 1303
1710 Goodridge Drive
McLean, VA 22102

October 1988

Scientific Report No. 17

GEOPHYSICS LABORATORY
AIR FORCE SYSTEMS COMMAND
UNITED STATES AIR FORCE
HANSCOM AIR FORCE BASE, MASSACHUSETTS 01731-5000

"This technical report has been reviewed and is approved for publication"

JOHN F. PAULSEN
Contract Manager

JOHN E. RASMUSSEN
Branch Chief

FOR THE COMMANDER

ROBERT A. SKRIVANEK
Division Director

This report has been reviewed by the ESD Public Affairs Office (PA) and is releasable to the National Technical Information Service (NTIS).

Qualified requestors may obtain additional copies from the Defense Technical Information Center. All others should apply to the National Technical Information Service.

If your address has changed, or if you wish to be removed from the mailing list, or if the addressee is no longer employed by our organization, please notify GL/DAA, Hanscom AFB, MA 01731. This will assist us in maintaining a current mailing list.

Do not return copies of this report unless contractual obligations or notices on a specific document requires that it be returned.

Unclassified

SECURITY CLASSIFICATION OF THIS PAGE

REPORT DOCUMENTATION PAGE

Form Approved OMB No. 0704-0188

1a REPORT SECURITY CLASSIFICATION Unclassified	1b. RESTRICTIVE MARKINGS
2a SECURITY CLASSIFICATION AUTHORITY	3. DISTRIBUTION/AVAILABILITY OF REPORT Approved for public release; Distribution unlimited.
2b DECLASSIFICATION/DOWNGRADING SCHEDULE	
4 PERFORMING ORGANIZATION REPORT NUMBER(S)	5 MONITORING ORGANIZATION REPORT NUMBER(S) GL-TR-89-0198
6a NAME OF PERFORMING ORGANIZATION Science Applications International Corp 6b OFFICE SYMBOL (If applicable)	7a. NAME OF MONITORING ORGANIZATION Northwest Research Associates
6c ADDRESS (City, State, and ZIP Code) P.O. Box 1303 1710 Goodridge Drive McLean, VA 22102	7b. ADDRESS (City, State, and ZIP Code) 300 120th Avenue, NE Bldg 7, Suite 220 Bellevue, WA 98005
8a NAME OF FUNDING/SPONSORING ORGANIZATION Geophysics Laboratory 8b OFFICE SYMBOL (If applicable) LID	9 PROCUREMENT INSTRUMENT IDENTIFICATION NUMBER F19628-87-C-0003
8c ADDRESS (City, State, and ZIP Code) Hanscom AFB Massachusetts 01731-5000	10 SOURCE OF FUNDING NUMBERS PROGRAM ELEMENT NO: 62101F; PROJECT NO: 4643; TASK NO: 10; WORK UNIT ACCESSION NO: AC
11. TITLE (Include Security Classification) **Feasibility of Radio Blackout Mitigation in the Braking Phase of AOTV Operations**	
12 PERSONAL AUTHOR(S) Didier Rault, Edward P. Szuszczewicz	
13a TYPE OF REPORT Scienticic #17	13b TIME COVERED FROM _____ TO _____
14. DATE OF REPORT (Year, Month, Day) 1988 October	15. PAGE COUNT 94
16 SUPPLEMENTARY NOTATION	

17. COSATI CODES			18. SUBJECT TERMS (Continue on reverse if necessary and identify by block number)
FIELD	GROUP	SUB-GROUP	Aerobraking Orbit Transfer Vehicle Hypersonic Reentry Vehicle Wake Transition Flow Direct Simulation Monte Carlo Method

19. ABSTRACT (Continue on reverse if necessary and identify by block number)

SEE REVERSE FOR ABSTRACT

20 DISTRIBUTION/AVAILABILITY OF ABSTRACT ☐ UNCLASSIFIED/UNLIMITED ☐ SAME AS RPT ☐ DTIC USERS	21. ABSTRACT SECURITY CLASSIFICATION Unclassified
22a NAME OF RESPONSIBLE INDIVIDUAL John Paulson	22b. TELEPHONE (Include Area Code) 22c. OFFICE SYMBOL GL/LID

DD Form 1473, JUN 86 *Previous editions are obsolete.*

SECURITY CLASSIFICATION OF THIS PAGE

Unclassified

An ability to simulate the flowfield produced in the wake of the Aerobraking Orbit Transfer Vehicle (AOTV) is needed to investigate mitigation of the expected ratio blackout by means of injecting SF_6 gas into the flow. This complex problem is characterized by a density in the wake that is well below ambient and very intense shock fronts in the ram flow. Consequently, the free molecular flow, transition flow, and continuum flow are simultaneous present in the AOTV problem. We show that Direct Simulation Monte Carlo (DMSC) code can be used to simulate the flowfield in an AOTV wake. The DMSC code produces reasonable results for air only flow, including many of the features known from investigations of continuum flow wakes. When SF_6 is added to the wake flow, the SF_6 is the dominant species controlling the flow near the vehicle, is well mixed with the ambient gas, and is largely confined to the wake. While our results demonstrate the utility of the DMSC code for the blackout problem, we recommend additional effort to perform simulations in a 3-D axisymetric geometry and to anchor our input data to ram flow calculations by NASA-Langley.

CONTENTS

LIST OF FIGURES

1. Introduction

Communications with a space vehicle reentering into the Earth's atmosphere are severely disturbed by the dense electron population surrounding the vehicle. These high electron densities occur through ionization of the ambient air which is elevated to very high temperature by a very strong bow shock. Signal loss, or blackout, occurs when the electron density in the shock layer reaches the critical values for the selected signal frequencies. For frequencies of 0.28 GHz, 2.8 GHz and 28 GHz, the critical electron densities are respectively 10^9, 10^{11}, and 10^{13} electron/cm^3. The blackout problem can be mitigated by injection of an electrophile gas which, in effect, converts the highly mobile electrons into massive negative ions. At the high radio frequencies, electromagnetic waves are practically unaffected by these massive ions. One such electrophile gas is sulfur hexaflouride (SF_6) which has been used in numerous programs, both experimentally and theoretically.

This report describes work done by SAIC to evaluate the feasibility of injecting SF_6 gas into the wake of an Aerobraking Orbital Transfer Vehicle (AOTV) for the purpose of alleviating blackout during the brief reentry of the vehicle into the atmosphere. The AOTV, or its scaled down precursor experimental vehicle called Aerobraking Flight Experiment (AFE), relies on aerodynamic forces to dissipate orbit energy in order to transition into a lower orbit.

The problem will first be stated and our approach will be described in the following section. It will be shown that, in the present work, no attempt is made to solve for the whole flow field over the vehicle due to the inherent complexities of such a simulation. Rather, we focus our attention on the wake flow field which we analyze using a transition flow model, namely the Direct Simulation Monte Carlo model (devised by Bird), since the flow in the near wake always remains either in the transition or free molecule regime throughout the aerobraking maneuver. Results obtained for the ram flow field by NASA-Langley are used as input boundary conditions in our simulation. In the third section, the basic structure of the flow field in the wake of supersonic blunt bodies will be described. It will be shown that the supersonic wake is very rich in features: expansion fan, recompression shocks, free shear layer, boundary layer and viscous effects. Additional rarefaction effects in the wake of aerobraking vehicle further complicate the flow structure. Section 4 summarizes the main results obtained during the prior year. In that effort, we tried to gain basic insights into the problem and derive first order estimates of the air and SF_6 flow field characteristics.

Section 5 describes the present simulation method. The main features of the Direct Simulation Monte Carlo code are explained and the diagnostic tools which we constructed to monitor the progress of the code are described. In Section 6 we present

results obtained with this code for three problems. The fundamental problem of the presence or absence of vortices in the wake of supersonic blunt bodies is analyzed in the first problem. The expansion of SF_6 into the AOTV wake is analyzed in the second and third problems. The results presented here are preliminary, however, and further work should be done in several areas (see Section 7), such as 3- dimensional geometry, the effect of computational grid structure on flow field, and the effect of actual ram conditions.

2. Problem Statement and Methodology for Solution

The ultimate objective of the present task is to assess the potential of SF_6 injected into the wake of a reentering AOTV/AFE vehicle in an effort to decrease the electron density below critical values along some path through which radio communication can travel. To evaluate the merit of such an experiment, one has to answer the following question:

(a) Where are the large electron populations located around the reentering vehicle and what is the magnitude of these electron densities?

(b) Where does the SF_6 go once injected into the vehicle wake? Can SF_6 counterflow against the air, or is it swept along by the high velocity air flow? Does SF_6 penetrate and destroy the "recirculation vortices" which are formed at the bases of blunt supersonic vehicles, or is SF_6 contained in the "recirculation zone" and later entrained through the "neck" of the wake shear layer? (See below for explanation of the terms within quotation marks.)

(c) How much SF_6 has to be injected into the wake to lower the electron density to values less than the critical densities for the working frequencies?

The answer to the first question would come from the study of the air flow field around the AOTV/AFE vehicle. This air flow field is inherently very complex and extremely difficult to simulate with any accuracy, due to the high enthalpy of the gas with respect to the spacecraft and the relatively high altitude, and therefore low ambient density, at which the AOTV/AFE vehicle reenters the atmosphere. As shown in Fig. 1, the flight domain of these aerobraking vehicles is very different from the ones contemplated for the Apollo program or the RAM program, and no experimental data is available. The answer to question (a) would therefore have to come from a full 3-D simulation of the air flow field around the vehicle taking into account the chemistry (dissociation, recombination, ionization), internal energy exchange (translational, rotational, vibrational, electronic), nonequilibrium (in all internal energy modes and also in translational modes), gas-surface interaction (catalysis, outgassing, reflection accommodation coefficients), radiation energy exchange (in nonequilibrium), plasma effects (induced electric field, Earth's magnetic field, spacecraft charging), rarefaction effects (breakdown of pressure tensor isotropy, breakdown of Chapman-Enskoy relations for transport properties, discontinuities at boundary surfaces such as velocity slip and temperature jump). To understand the basic features of the flow field, however, reference should be made to Fig. 2. The flow around the reentering space vehicle is characterized by a wide, very strong bow shock which envelopes the whole forebody. Near the stagnation point, the shock is a strong compression wave with a downstream

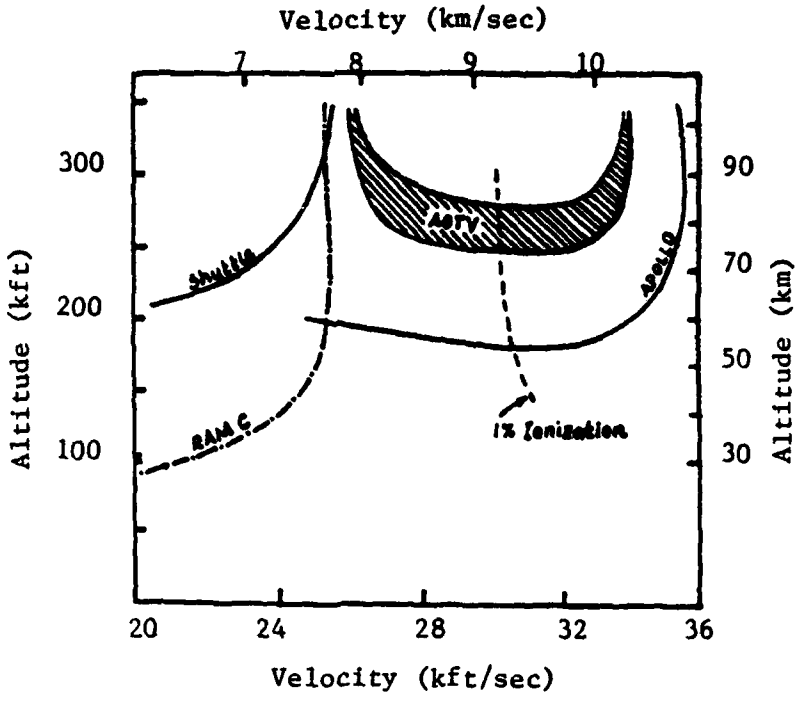

Fig. 1 Flight domain of AOTV/AFE vehicles. Comparison with Apollo and RAM experiment (Ref. 1).

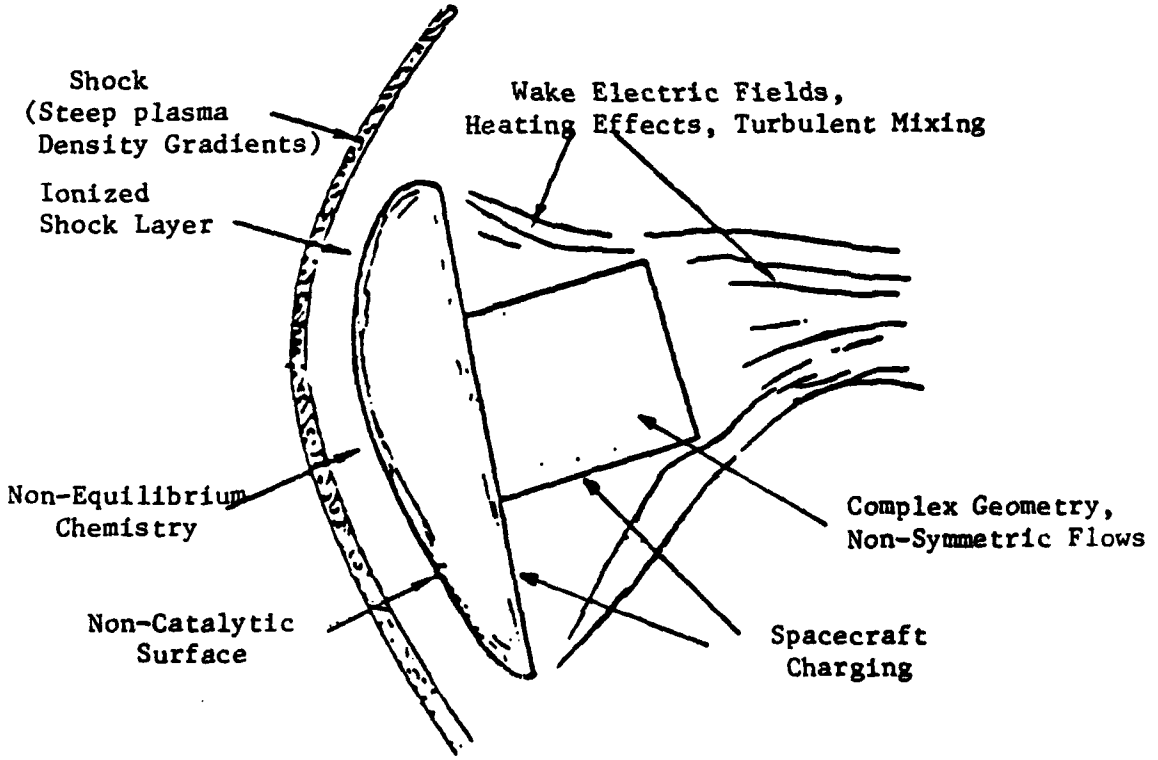

Fig. 2 Basic features of flow field around a reentering aerobraking vehicle (Ref. 1).

temperature of several eV. Intense dissociation and some ionization would then occur within the shock as shown in Fig. 3. Partial recombination and neutralization will then occur as the air flow passes around the vehicle. The presence of streaming charged particles elevates the spacecraft potential and induces electric fields, which in turn affect the distribution and density of charged particles around the spacecraft.

No attempts have been made in the present work to simulate the flow field in the ram region of the vehicle. Rather, we are relying on the results of 2-D and 3-D simulations which have been performed at NASA-Langley by Gnoffo, Moss and Celenligil. Gnoffo's results are applicable in the lower altitude region near the perigee of the AOTV/AFE vehicle, where the flow in the ram is in the continuum regime (low Knudsen numbers). The results obtained by Moss and Celenligil are applicable at higher altitudes (90-130 km) where the flow over the whole vehicle is either in the transition regime or the free molecular regime (medium and high Knudsen numbers). NASA's results are expressed in the form of neutral and charged particle densities over the whole vehicle, together with temperature (translational and internal), and flow speed (magnitude and direction). Since the main goal of NASA's simulations is the evaluation of the aerodynamic forces and moments, and the heat transfer to the vehicle, little emphasis is put on the wake region which contributes little to those parameters. Rarefaction effects in the wake are ignored in Gnoffo's simulation, whereas quasi vacuum conditions are deemed sufficient in Moss's simulation.

Our approach to answering questions (b) and (c) is to concentrate on first trying to solve for the air flow field structure and properties in the wake as accurately as possible, utilizing Gnoffo's (in continuum regime) and Moss's (in transition regime) results as boundary input conditions. Wake flows are usually very complex due primarily to the fact that their structural characteristics depend heavily on the upstream flow field. Furthermore, as shown in Section 3, the flow field structure in the wake of supersonic blunt bodies is complex due to the presence of

- numerous expansion and compression waves (shocks),
- a recirculation region (vortex),
- rarefaction effects (due to low densities),
- a shear layer (which is intrinsically unstable), and
- viscous effects (which distort the wave pattern, generate additional compression waves, thicken the shear layer and alter the flow separation process).

Hypersonic flows cannot "turn sharp angles." Hence, the gas density in the wake is expected to be one or more order of magnitude lower than the ambient density. Therefore, even at the lowest altitudes, where the flow in the ram could be well represented

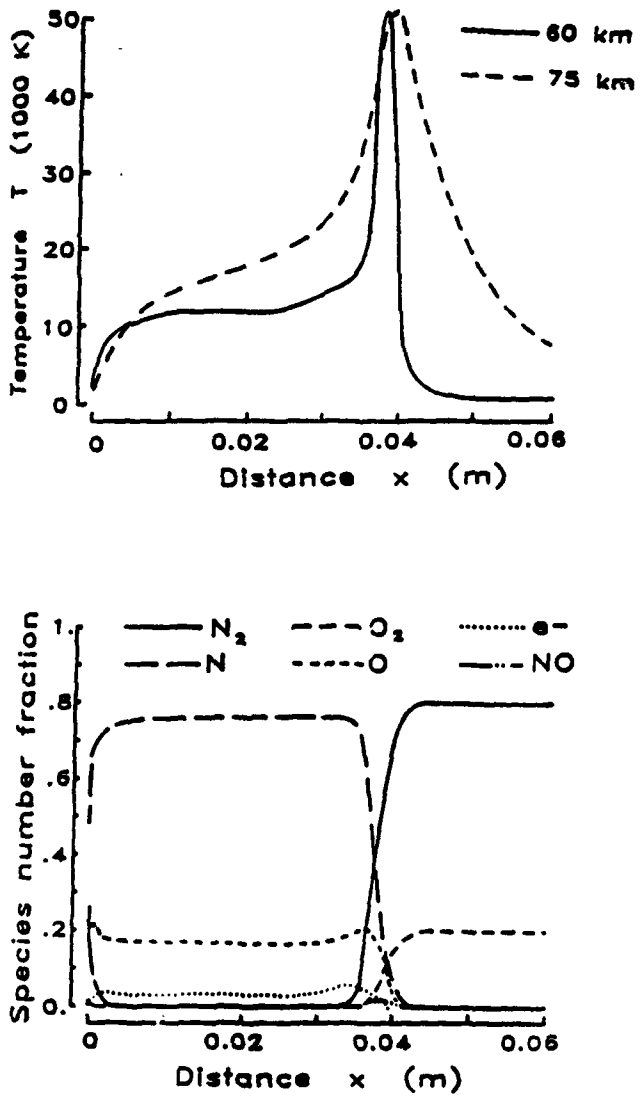

Fig. 3 Ionization along stagnation streamline of a reentering AOTV (Ref. 1).

under the continuum assumption, the near wake would remain in either transition or free molecule regime throughout the pass of the AOTV/AFE vehicle. Consequently, it was decided to select a transition flow model to simulate the air flow field in the wake of all cases. We have selected the method devised and developed by Bird (Direct Simulation Monte Carlo, or DSMC) due to its wide acceptance in the engineering community, its numerous critical reviews in literature and its relative simplicity of use. The SF_6 flow field in the wake is then studied by adding a source of SF_6 gas in the computer model.

3. General Features of Flow Fields in the Wake of Supersonic Blunt Bodies

Flow fields in the wake of supersonic blunt bodies are very complex and have not been well characterized. Little experimental data is available and only incomplete analysis have been made about them, as is shown in the book by S. Berger, entitled "Laminar Wakes" (Ref. 2). Additional uncertainties with regard to aerobraking vehicle wakes are due to the very low densities expected behind the vehicle which will induce important rarefaction effects. This section first reviews what is currently known about supersonic wakes in the continuum regime, i.e., in the absence of rarefaction effect. The last part highlights the main rarefaction effects expected in an AOTV wake.

3.1 Continuum Regime

The fundamental structure of a supersonic wake flow can best be understood by first considering the inviscid problem, i.e., neglecting the gas viscosity. As shown in Fig. 4, the supersonic flow turns at the sharp shoulder or corner through the Prandtl-Meyer expansion fan. Hypersonic flows, however, are unable to "turn sharply" around corners, and can be deflected only up to a maximum angle. Table I lists the values of the maximum deflection angles for several gases. As shown in Fig. 4, flow arriving at the vehicle shoulder would separate, thus creating a free shear layer which divides the bulk flow from a dead air zone.

Table I

SUPERSONIC DEFLECTION LIMIT IN DEGREES

GAS	γ	FLOW MACH NO.			
		1	2	4	10
Ar, He	1.67	90	68	40	17
O_2, H_2	1.41	128	102	62	27
H_2O	1.33	149	121	77	34

The incoming air streamlines first pass through the expansion fan and turn parallel to the free shear layer surface. The wake shock then bends the streamlines to turn the flow parallel to the initial direction. The intersection of the free shear layer with the axis of symmetry is called the rear stagnation point. Within the dead air zone, a recirculation vortex establishes itself. This vortex is stable due to the presence of the wake compression shock, i.e. the vortex is not shed away as in the case of subsonic flow.

The introduction of viscous effects somewhat changes this basic flow pattern, as shown in Figs. 5 and 6. Fig. 6 is a Schlieren photograph (i.e., it highlights density

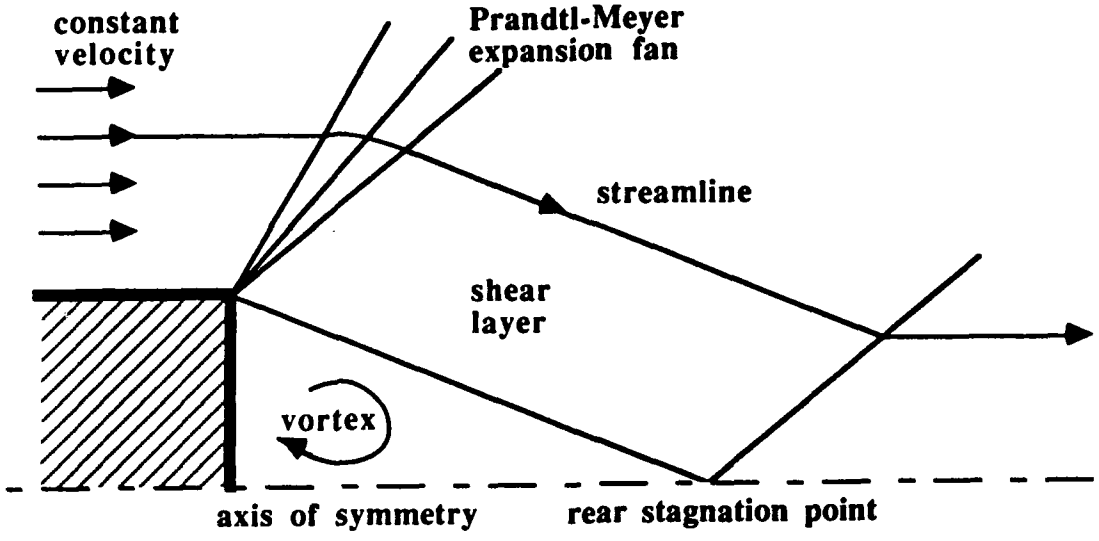

Fig. 4 Supersonic flow field structure in the wake of blunt bodies in the absence of viscous forces.

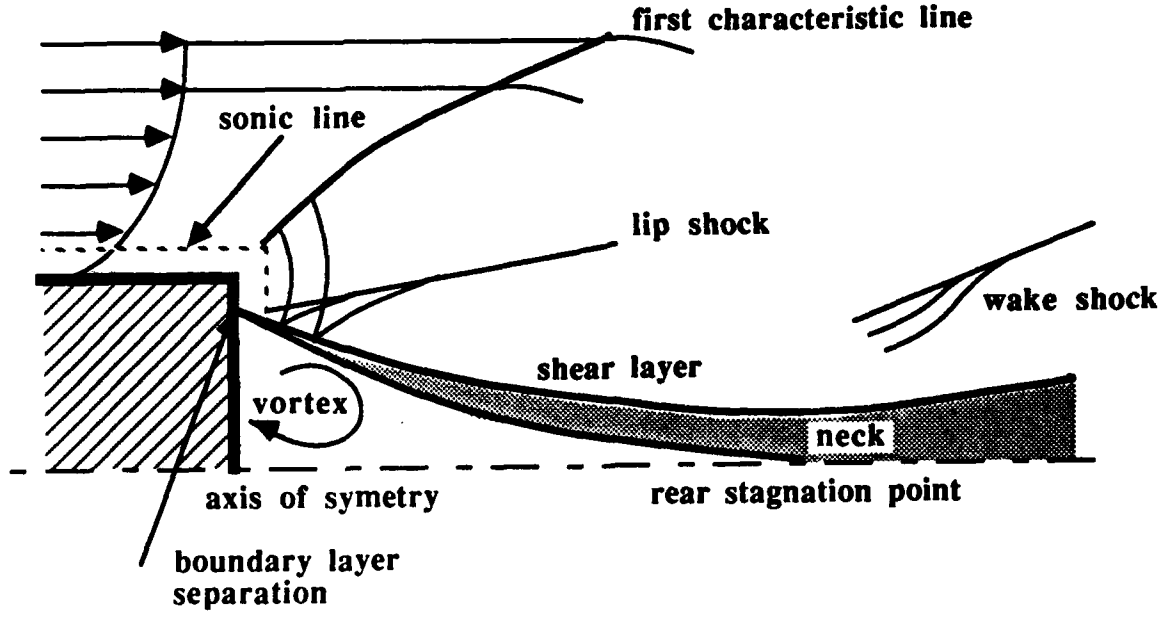

Fig. 5 Supersonic flow field structure in the wake of blunt bodies. Effect of viscous forces.

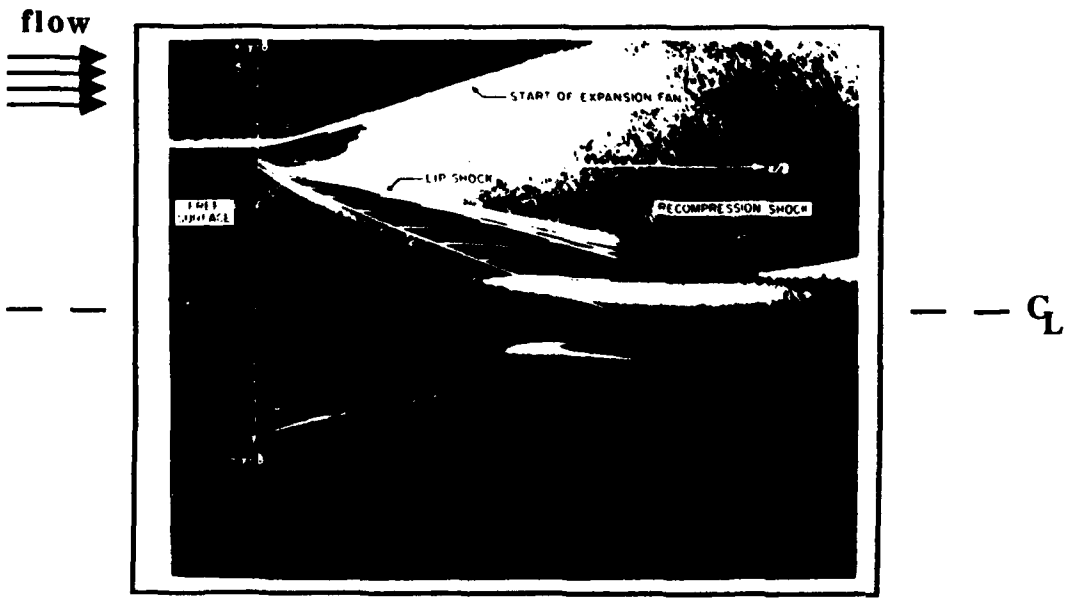

Fig. 6 Schlieren photograph of supersonic flow in the wake of a tangent ogive (Ref. 2).

gradients) of a flow over a tangent ogive. When the viscous boundary layer reaches the shoulder, part of it is subsonic and part of it is supersonic. The subsonic region is not constrained by the Prandlt-Meyer limitation and subsonic streamlines can turn sharply over the corner. The supersonic streamlines can only slightly bend across the expansion wave fan. Since the supersonic velocity profile is not uniform, the expansion waves are no longer straight lines, which give rise to cross waves (see Fig. 5). After turning around the sharp corner, the subsonic boundary layer separates from the wall (due to unsurmountable adverse pressure gradients) and forms a free shear layer. The boundary layer separation induces a separation lip shock. The lip shock extends into the freestream and is reinforced by the reflection of the cross waves on the sonic line (Fig. 5). Due to viscous transport across the shear surface, the shear layer grows as gases from the recirculation zone and the bulk flow mix together. A "neck" is formed near the rear stagnation point, i.e., the wake shock is no longer attached. Through the neck, subsonic gases are allowed to "leak" from the recirculation zone.

3.2 Transition and Free Molecular Flow

At the extreme limit of collisionless or free molecular flow, no compression waves or vortices can materialize in the wake of the body. The wake is "filled" according to the transverse thermal velocity distribution of the molecules and the flow field appears to uniformly turn around the corner. No studies, either experimental or theoretical, have yet been done to determine the Knudsen number at which bulk recirculation starts occurring in the wake. Therefore, it is difficult to predict the flow field structures in the transition regime and to validate wake simulation codes in rarefied gas conditions. If the simulation code fails to generate a vortex, the reason could be either physical (too low a density) or numerical (insufficient spatial resolution, or two few collisions between molecules). Further discussions on this point can be found in Section 6.

4. Review of Prior Year Method and Results

In the first phase of our work, we attempted to obtain basic information on the overall problem by evaluating first order estimates of the air flow field and SF_6 expansion. Our prime objective was to determine a first order estimate of the required flux of injected SF_6 to "neutralize" electrons in a 1% ionized wake. The "neutralization" process would proceed according to

$$SF_6 + \ electron \ \longrightarrow SF_6^- .$$

To do this, we represented the AOTV as a disk, 27 m in diameter and 10 m in length (see Fig. 7). We used an Euler equation solver, i.e., a continuum fluid code which neglects molecular transport (viscosity, thermal transfer, diffusion), nonequilibrium effects, and assumes a perfect gas (no dissociation, ionization, chemical reaction). The Euler equation solver we selected was based on the Godunov method which accurately simulates flows with strong shock discontinuities. The geometry was assumed to be axisymmetric. The numerical method is described in subsection 4.4.

In the first part of this section, we review the air flow field around the simulated AOTV and discuss the results. In the second part, we describe the method we have devised to characterize the flow field of SF_6 as it expands from feed nozzles into the wake region. In the third part, we present our results and show that, in order to achieve a 1% SF_6/air ratio in the wake region, the SF_6 input flux must be on the order of 200g/sec.

4.1 Air Flow field

Figs. 8a and b show the air density and flow field around the simulated AOTV for the following nominal conditions:

AOTV velocity = 9000 m/sec

Ambient pressure = 6.5 mTorr, and

Ambient density = 3.3 10^{14} cm^{-3}.

The ambient pressure and density correspond to a nominal altitude of 80 km where the ram flow can be considered to be in the continuum flow regime. The flow field is characterized by a strong bow shock with a pressure jump on the order of 500:1 at a standoff distance of about 7 m from the AOTV front surface. Gas temperatures in front of the AOTV are on the order of 30,000 K, which is a "frozen condition" temperature since the code does not allow for dissociation, ionization or chemical reactions.

The flow field in the wake is characterized by a toroidal vortex and fairly low

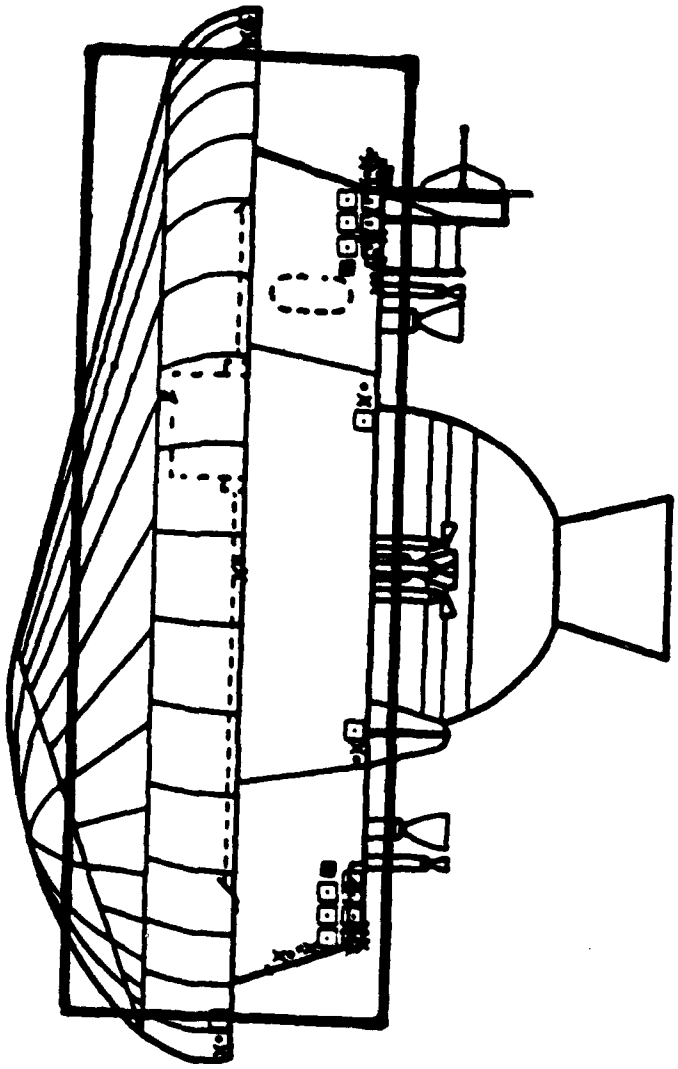

Fig. 7 Simple geometry representation of AOTV used for first phase computation.

density. The low air densities near the edge of the disk are due to the inability of a supersonic flow to turn around sharp corners (Prandtl-Meyer expansion). The densities shown is Fig. 8, however, are lower limits on the actual densities. Viscous effects would tend to increase the density in the wake region through several mechanisms:

- Low velocity gases in the boundary layer along the side walls would not be constrained by the Prandtl-Meyer limitation and could sharply turn into the wake region.
- Strong shear stresses are present in the vortex region. These stresses would become unstable and create large scale turbulence in the wake. The large scale turbulence could dramatically alter the flow field in the wake.

4.2 SF_6 Flow Configuration and Computation Method

Review and analysis of the flow field results in Fig. 8 suggest that the optimum locations for SF_6 injectors in the wake correspond to the velocity shear intercept with the aft body. These locations should provide efficient mixing of the injected SF_6 with the ambient neutral and plasma distributions in the wake. To accurately track the SF_6 expansion from the supply nozzle into the surrounding ambient air, it is necessary to solve the complete set of Navier-Stokes equations for a two-species gas in 3 dimensions, taking into account the exchange of mass, momentum and energy between air and SF_6. A simpler approach is adopted here to obtain a first order estimate of the SF_6 density field and, therefore, the magnitude of the SF_6 flux required to achieve sufficient SF_6/air ratio in the wake region. The method is as follows:

(a) We require that the mean SF_6 concentration be fairly small compared to air concentration (i.e., only 1 - 2%). We can, therefore, assume that the injection of SF_6 does not alter the flow field configuration of air. This assumption is rigorously valid in most of the wake region, but breaks down in the close vicinity of the SF_6 supply nozzle where air density is very low and SF_6 density is high.

(b) Due to its low concentration with respect to air, SF_6 is assumed to instantaneously take the temperature of surrounding air.

(c) SF_6 exchanges momentum with the surrounding air at a rate

$$\rho_{SF_6} \frac{\nu}{n} (u_{air} - u_{SF_6})$$

where u_{air} and u_{SF_6} are the local stream velocities of air and SF_6, respectively, ρ_{SF_6} is the local SF_6 density, ν is the mean collision frequency between a molecule of SF_6 and surrounding air molecules, n is the transfer efficiency coefficient which stipulates that n collisions are necessary to "equilibrate" the air and SF_6 velocities.

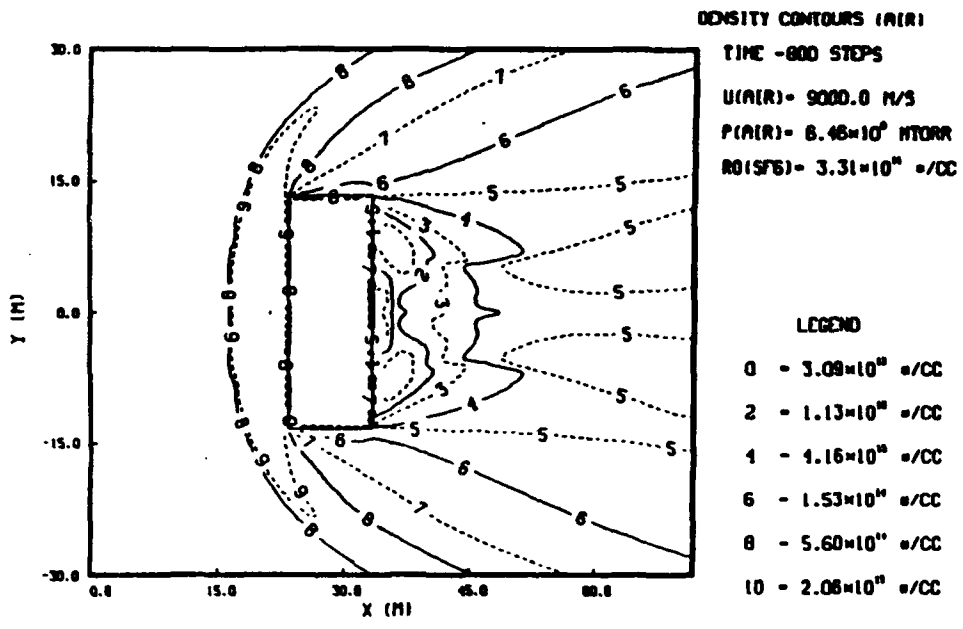

Fig. 8a Air density distribution around a simplified geometry AOTV.

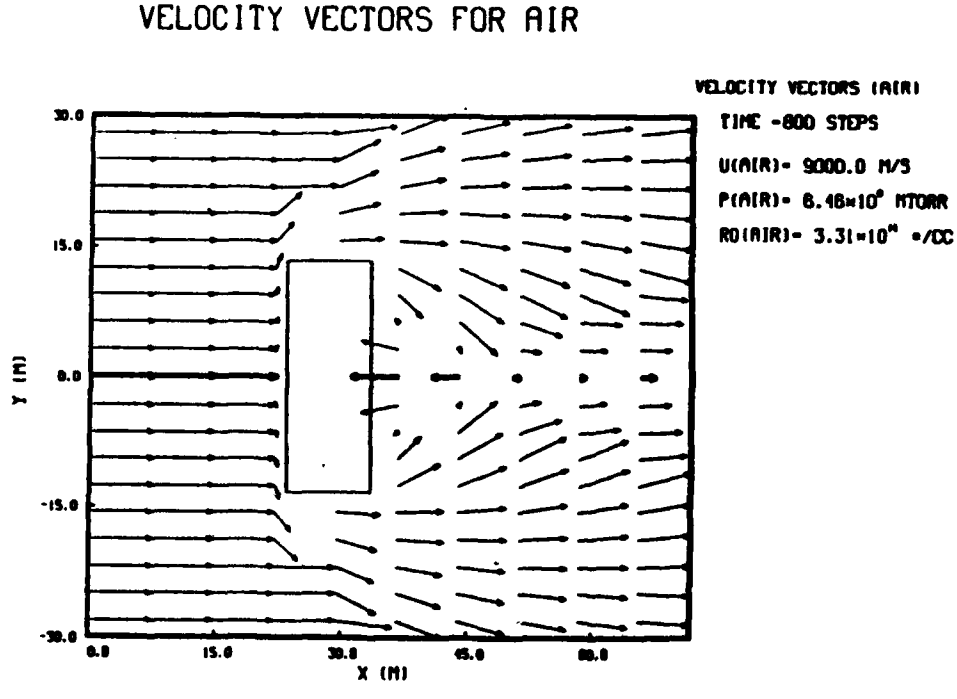

Fig. 8b Flow field around a simplified geometry AOTV.

The conservation equations for SF_6 can therefore be written as

$$\frac{\partial U}{\partial t} + \frac{\partial F}{\partial z} + \frac{\partial G}{\partial r} = S_1 + S_2,$$

where

$$U = \begin{vmatrix} \rho \\ \rho u \\ \rho v \end{vmatrix},$$

$$F = \begin{vmatrix} \rho u \\ P + \rho u^2 \\ \rho u v \end{vmatrix},$$

$$G = \begin{vmatrix} \rho v \\ \rho u v \\ P + \rho v^2 \end{vmatrix},$$

$$S_1 = \begin{vmatrix} -\rho v / r \\ -\rho u v / r \\ -\rho v^2 / r \end{vmatrix}, \text{and}$$

$$S_2 = \begin{vmatrix} 0 \\ F_z \\ F_r \end{vmatrix},$$

with

$$F_z = \rho_{SF_6} \frac{\nu}{n}(u_{air} - u_{SF_6}), \text{and}$$

$$F_r = \rho_{SF_6} \frac{\nu}{n}(v_{air} - v_{SF_6}).$$

This set of equations is similar to the ones solved for air (see Section 4.4) with two exceptions: the additional term S_2 which represents the momentum transfer from air to SF_6, and the energy equation, which is not solved for SF_6 since it is assumed that air and SF_6 are at the same temperature at all times. Hence, the partial pressure of SF_6 is

$$P = \frac{\rho_{SF_6} M_{air}}{\rho_{air} M_{SF_6}},$$

where M_{air} and M_{SF_6} are the molecular weight of air and SF_6, respectively.

It is understood that the assumptions described above might not be rigorously correct. The results obtained should be regarded as a limiting case.

4.3 Results and Discussion

Figs. 9a and b show the real time evolution of the SF_6 gas expansion from an annular shaped supply nozzle under the following conditions:

Transfer efficiency n = 50,

Total SF_6 flux = 193 g/sec,

Inlet pressure = 12.9 mTorr,

Inlet velocity = 1000 m/sec,

Inlet nozzle inner annulus radius = 6.4 cm, and width = 0.33 cm.

The following observations can be made:

- Within 10 msec, steady state is closely achieved within the "window" shown on the figure.
- The sideways expansion of the SF_6 cloud is limited by the high velocity air.
- At steady state, the SF_6/air ratio in the bulk of the wake region is in the range 0.5% to 1.5% with a higher concentration near the nozzle exit.

4.4 Numerical Code

The Euler equation solver we selected is based on the Godunov approach. In this section, the approach is outlined. Further description of the code can be found in last year's report (Ref. 1).

The unsteady 2-D axisymmetric Euler equations describing the air flow field can be written as

$$\frac{\partial U}{\partial t} + \frac{\partial F}{\partial z} + \frac{\partial G}{\partial r} = S,$$

where

$$U = \begin{vmatrix} \rho \\ \rho u \\ \rho v \\ e \end{vmatrix},$$

$$F = \begin{vmatrix} \rho u \\ P + \rho u^2 \\ \rho u v \\ (e+P)u \end{vmatrix},$$

$$G = \begin{vmatrix} \rho v \\ \rho u v \\ P + \rho v^2 \\ (e+P)v \end{vmatrix}, \text{and}$$

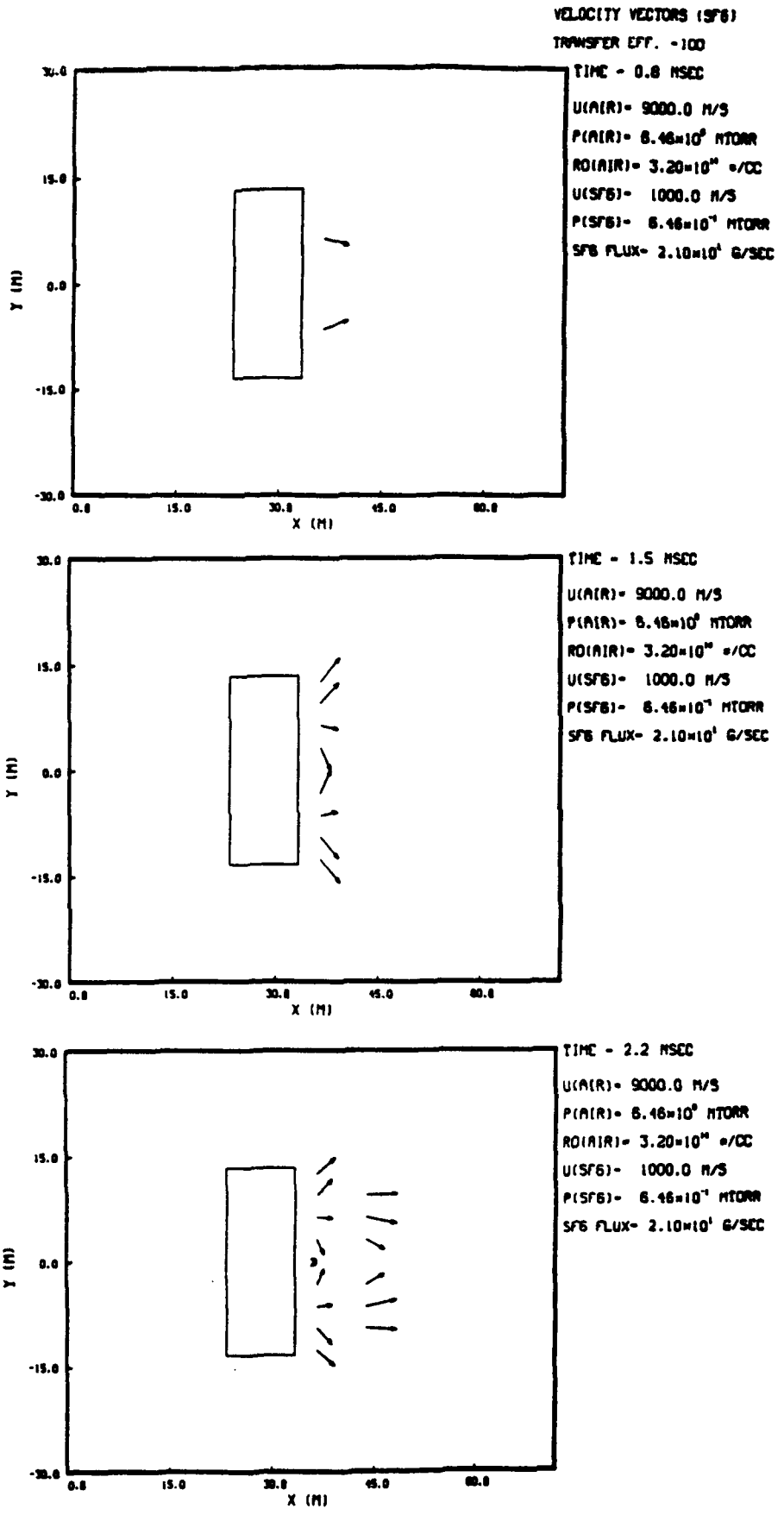

Fig. 9a SF_6 flow expansion. Density distribution.

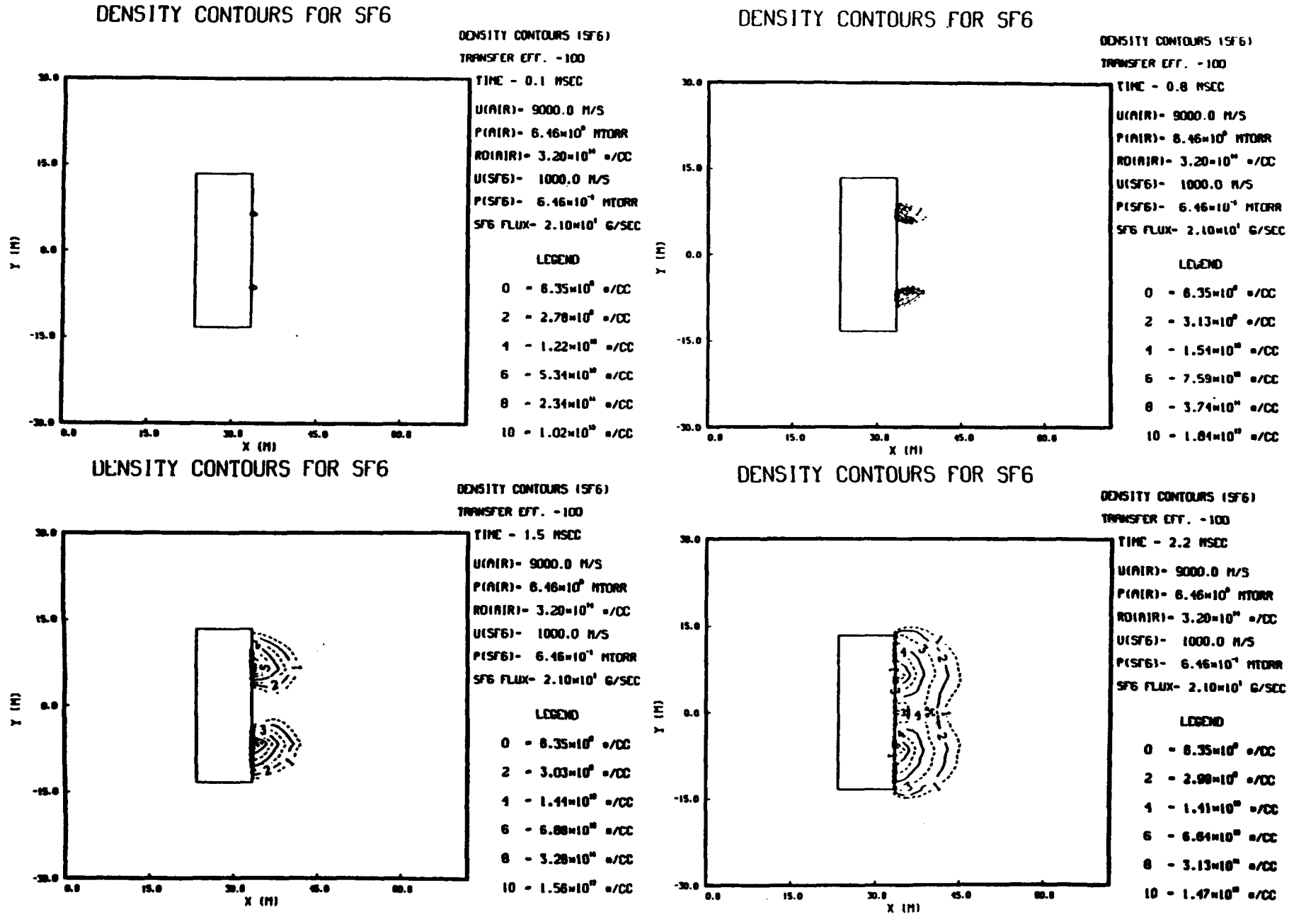

Fig. 9b SF_6 flow expansion. Flow field.

$$S = \begin{vmatrix} -\rho v/r \\ -\rho uv/r \\ -\rho v^2/r \\ -(e+P)v/r \end{vmatrix}.$$

Here ρ is the density, u and v are the velocity components in the axial and radial coordinate directions, P is the pressure and γ is the ratio of specific heats. The energy per unit of volume, e, is defined by

$$e = \rho(\epsilon + \frac{u^2 + v^2}{2}),$$

where $\epsilon = \frac{P}{(\gamma-1)\rho}$ is the internal energy.

5. Present Simulation Method

As explained above, the simulation of the flow in the wake of an AOTV/AFE vehicle requires the use of a code which is explicitly designed to model flows in a non-continuum region. In this flow regime, the Euler and Navier-Stokes equations are not applicable. The gas cannot be considered as a fluid and must be treated as an ensemble of molecules. In principle, the governing equation in this flow regime is the Boltzmann equation. For the AOTV problem, the Boltzmann equation should be solved in 3-D over a complex geometry. The solution to the Boltzmann equation would be the molecular velocity distribution functions over the whole computation domain, and the macroscopic flow properties would be computed as the moments of the distribution functions. This approach, however, is impossible, except for a very simple flow geometry in 1-D. An alternative method is to simulate the gas as a large ensemble of gas particles, and track each molecule as it collides with other molecules and bounces on the surface boundaries. Bird (Refs. 8 and 9) has constructed such a code, and over the years, has perfected it into a tool which is now widely used in the engineering community. We have supplemented this Direct Simulation Monte Carlo (DSMC) code with a set of diagnostic tools to monitor the time evaluation and the initial setup of the code.

5.1 DSMC Code Summary Description

Bird's code tracks only a relatively small number of molecules. In a real gas, even at low density, molecular number densities are on the order of 10^{19} per cubic meter. Therefore, it is impossible to follow each molecule. However, it can be shown that the statistics of the flow are well represented when only a few thousand "simulated molecules" are considered in the flow field (Ref. 9). In the code, the position and velocity vectors of the simulated molecules are stored in the computer and are periodically reevaluated as molecules intercollide and interact with the computational domain boundaries. The computation marches in time with the help of a clock. At each clock tick, the position and velocity of each simulated molecule in the computational domain are advanced, and subsequently some molecules are allowed to collide with their nearest neighbors. Molecular motion and collisions are thus decoupled. It has been demonstrated that as long as the clock time increment is small with respect to the mean collision time, this decoupling has no secondary effect on the flow properties (Ref. 9). To define the nearest neighbor collision dynamics and evaluate the spatial distribution of the macroscopic thermodynamics and flow properties, the computation domain has to be divided into a network of cells, the size of which has to be less than the local mean free path. Subcells, i.e., "cells within cells," have recently been added to the simulation model to allow better control over the code. Subcells allow the decoupling

of requirements for (1) a small spatial region to evaluate the closest neighbor collision, and (2) a sufficiently large number of simulated molecules to evaluate macroscopic thermodynamic properties. Subcells are especially useful in regions where high vorticity is expected. In the computation of wake flow, for example, special care must be given to conserving rotational motion if emphasis is put on reproducing the structure of the recirculation zone.

The cells in the computational domain are arranged in a series of "regions," each of which has its own clock (with a given time increment) and its own ratio (FNUM) of real molecules to simulated molecules. Proper use of these regions can help tune the code so that the simulation requirements can be met without unduly penalizing the overall computer time and memory. The number of allowed collisions between simulated molecules in a given cell per clock tick is determined so as to make the simulation computer time proportional to the number of simulated molecules. (Note that in other rarefied flow simulation codes, the computer time is proportional to the square of the number of simulated molecules.) The choice of the collision parameters, together with the selection of the scattering parameters, is made on a probabilistic manner, using random number generators (see Appendix A).

Collisions are computed with the VHS model, a tool which has been extensively used and proved adequate in numerous engineering problems. In this model, molecules are assumed to be spherical, i.e. isotropic scatterers, with a variable diameter which depends on the relative velocity between the colliding partners.

A DSMC calculation is always unsteady and non-interactive. A converged flow solution is obtained as the simulation is allowed to evolve over a long time from a known steady state, such as either a vacuum or uniform flow. The simulation has been shown to have no numerical instabilities. It is also thought to be ergodic, i.e., similar results can be expected with either a small number of simulated molecules and long run time or a large number of simulated molecules and a short run time.

5.2 Diagnostic Tools

We have developed a set of graphic diagnostics to assist in the implementation of Bird's code. These tools, described in Appendix B, allows us to check the initial setup of the code, monitor the time evolution of the code and optimize the run conditions. With these tools, we can verify that the following conditions are met during a run:

- Cell size is 1/3 of the local mean free path, or less.
- During a clock tick, the molecule travels no more than 1/3 to 1/2 of a cell length.
- The number of molecules per cell is about 10.

6. Problem Setup and Main Results

The complexity of the hypersonic rarefied gas wake flow problem dictates a step by step approach to the present problem. Fundamental issues have to be dealt with such as:

- Are vortices present in the wake of hypersonic blunt bodies in rarefied conditions?
- Can Bird's code reproduce such vortices?
- If no vortices materialize in Bird's code, should we conclude that, physically, there cannot be vortices in rarefied wakes, or that the lack of vortices in the solution shows the failure of Bird's code to conserve flow rotationality?

The first problem we study with Bird's code is aimed at trying to answer these questions. The second and third test runs are directed towards the problem of SF_6 injection into the vehicle wake.

6.1 First Computational Case

The first problem we solve with Bird's code has a fairly simple geometry, as shown in Fig. 10. We consider the flow of an initially uniform velocity stream past a rectangular slab of 1 m height. The gas is assumed to be monatomic (Argon) and the reference frame is 2-D Cartesian. The gas density corresponds to air density at 100 km altitude and the gas temperature is initially set at 300 K. The initial condition around the slab is a vacuum. Three runs are made under these conditions with initial free stream gas velocities of 500 m/sec (Mach 1.5), 1300 m/sec (Mach 4), and 8000 m/sec (orbital velocity).

The computational domain is divided into four regions (Fig. 11). The first region is setup to deal with the inlet stream. The second region, which in effect is the source of the gases flowing into the wake, is divided into a fine grid of small cells, each subdivided into four subcells, in order to try to "capture" the initial flow rotationality and ensure a good transfer of the flow vorticity into the lower region. The ratio of the number of real molecules to simulated molecules (FNUM) is selected so that each cell contains about 10 simulated molecules. The third region encompasses the near wake. Gas densities are lower in this region, but cell size is kept to a very small fraction of the local mean free path. Cells are subdivided into 16 subcells to try to conserve and properly transfer vorticity. The ratio of real molecules to simulated molecules is selected so that the low density cells near the base face contain about 10 simulated molecules. The fourth region is the "post-wake" and constraints on the cell size and ratio FNUM are slightly relaxed. Further information on the input data can be found in Appendix C.

Figs. 12 through 15 show the results of the simulation in the case where the uniform

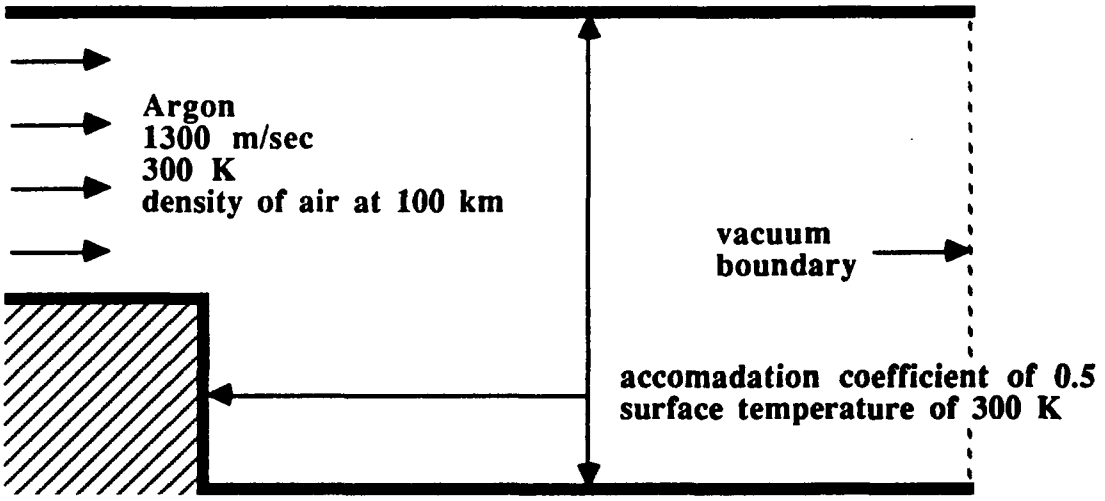

Fig. 10 Flow geometry for Computational Case # 1.

velocity is 1300 m/sec (Mach 4). At 500 m/sec, no recirculation zone was observed as the flow turned sharply over the corner. At 8000 m/sec, the code was difficult to tune up, owing to the large density drop in the wake, and it was not possible to reach steady state within the computer time allocated for this program.

Fig. 12 shows the direction of the velocity vectors in the wake, from which we can visualize the flow steamlines. A thin recirculation zone near the body base plate is clearly visible, with fluid counterflowing upwards near the surface. The solid inclined line represents the Prandtl-Meyer limit which indicates the maximum deflection of the flow if it were in the continuum regime.

Fig. 13 shows the number density contours. The expansion fan centered at the body shoulder is clearly visible. The high density contours near the top wall are due to the build up of a viscous boundary layer. (The top wall is assumed to have a momentum accommodation coefficient of 0.5.) The density in the near wake is less than 5% of the ambient density.

Fig. 14 shows the magnitude of the flow speed vectors. The flow speed in the near wake is very small, less than 7% of the original flow speed. The presence of a growing boundary layer near the top wall is clearly visible. Fig. 15 shows the number density gradient in the horizontal direction within the wake. This figure is similar to a Schlieren photograph with a slit axis parallel to the body base plate, and can be used to visualize pressure waves. (More information is provided in this figure, however, through the sign of the gradient.) A recompression region can be observed just downstream of the body shoulder. This recompression could be the lip shock. Moreover, a fairly steep recompression zone can also be observed downstream of the wake. This region could be the foot of the wake shock.

6.2 Second and Third Computational Cases

The second and third computational cases constitute an attempt to run the code under conditions close to the ones encountered in the flight of an AOTV/AFE vehicle during reentry into the atmosphere. As shown in Fig. 16, inlet flux in these cases is non-uniform, with gas velocities ranging from 500 m/sec on the body skirt surface to 3000 m/sec on the outer edge. This profile is a coarse approximation of the velocity distribution computed by Gnoffo. Approximately at the center of the base face, we allow SF_6 to be injected into the wake at a velocity of 300 m/sec (about Mach 1) and a temperature of 300 K. The mass flux of SF_6 was varied by changing the feed pressure (or number density). Computational Case #2 corresponds to a relatively low feed pressure. Computational Case #3 corresponds to a higher feed pressure.

The flow geometry is identical to that used for Computational Case #1. Addi-

PR- 76 NPRNT- 12 (IFX- 0 IOS- 0 INS- 0 RWF- 0.00 NIS- 10 NSP- 10 NPS- 11)
(NSS- 1 NSSR- 0 IRA- 0 MNVT- 0 MAXRE- 0 FND- 1.00×10^{19} FMTP- 0.0
FNUM()- 16.0/ 15.3/ 14.9/ 15.8/ 15.3/
DTM()- -4.0/-4.3/-4.0/-4.0/-4.0/
TIME()- 0.0/-0.4/ 0.0/ 0.0/ 0.0/
DUPLIC(W.R.T. REG. 2)- -0.4/ 0.0/ 0.7/-0.2/ 0.3/

REG 1 SIDES: 5/3/5/7/
SUBCELLS: 1/10/ 1/ 1/
REG 2 SIDES: 7/7/5/7/
SUBCELLS: 40/12/ 2/ 2/
REG 3 SIDES: 2/5/7/7/
SUBCELLS: 40/40/ 4/ 4/
REG 4 SIDES: 7/7/5/8/
SUBCELLS: 10/ 3/ 1/ 1/
REG 5 SIDES: 2/7/7/8/
SUBCELLS: 40/40/ 4/ 4/

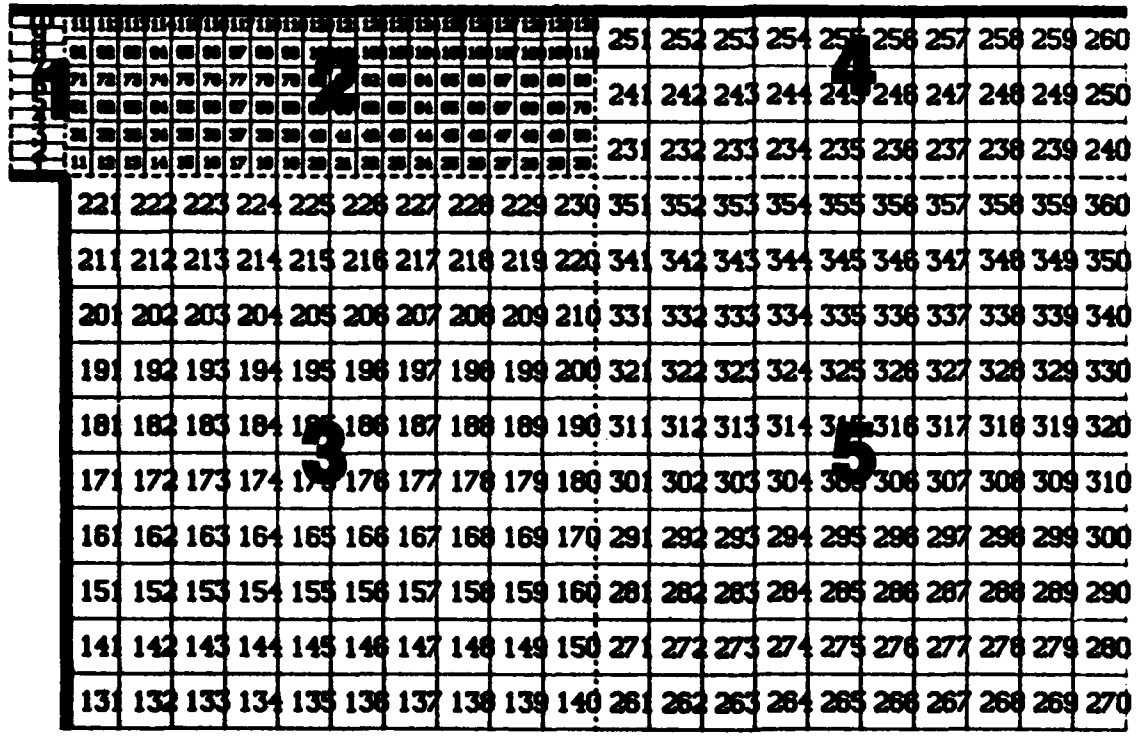

GRID AND BOUNDARY CONDITIONS CHECKUP DATE-22-Sep-88
TIME- 16:53:17 RUN * A1300

Fig. 11 Code setup for Computational Case # 1.

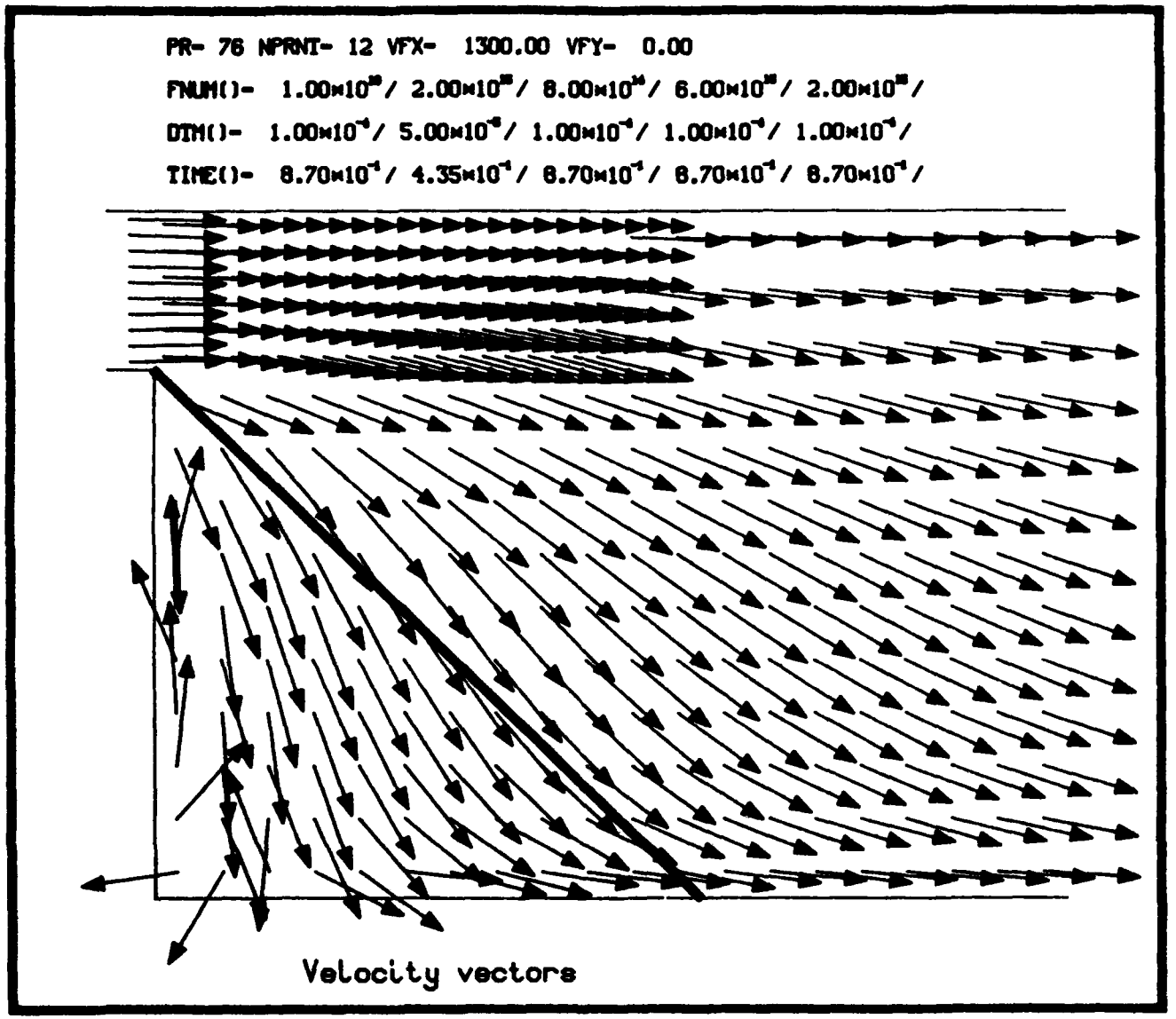

Fig. 12 Flow field for Computational Case # 1.

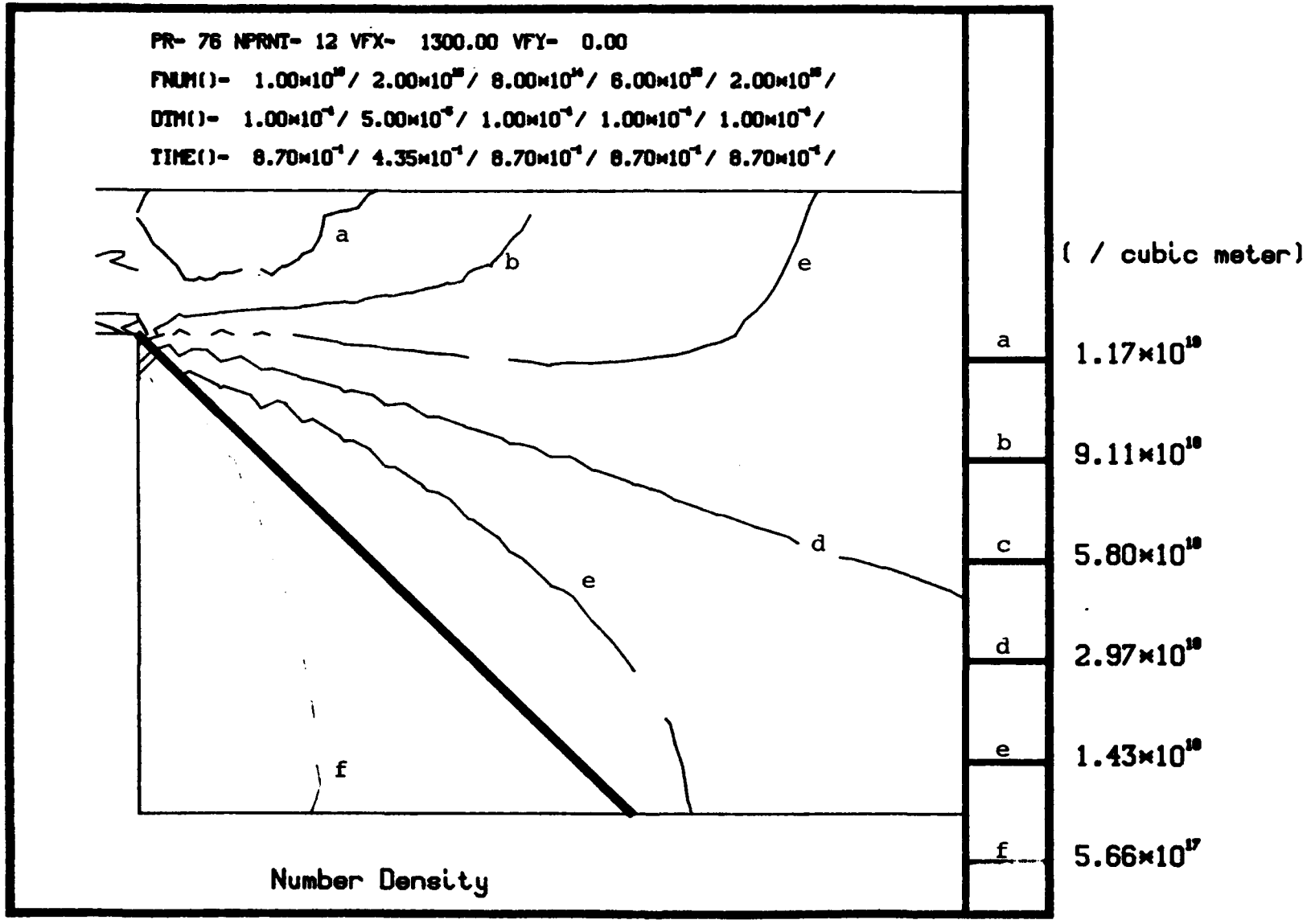

Fig. 13 Number density contours for Computational Case # 1.

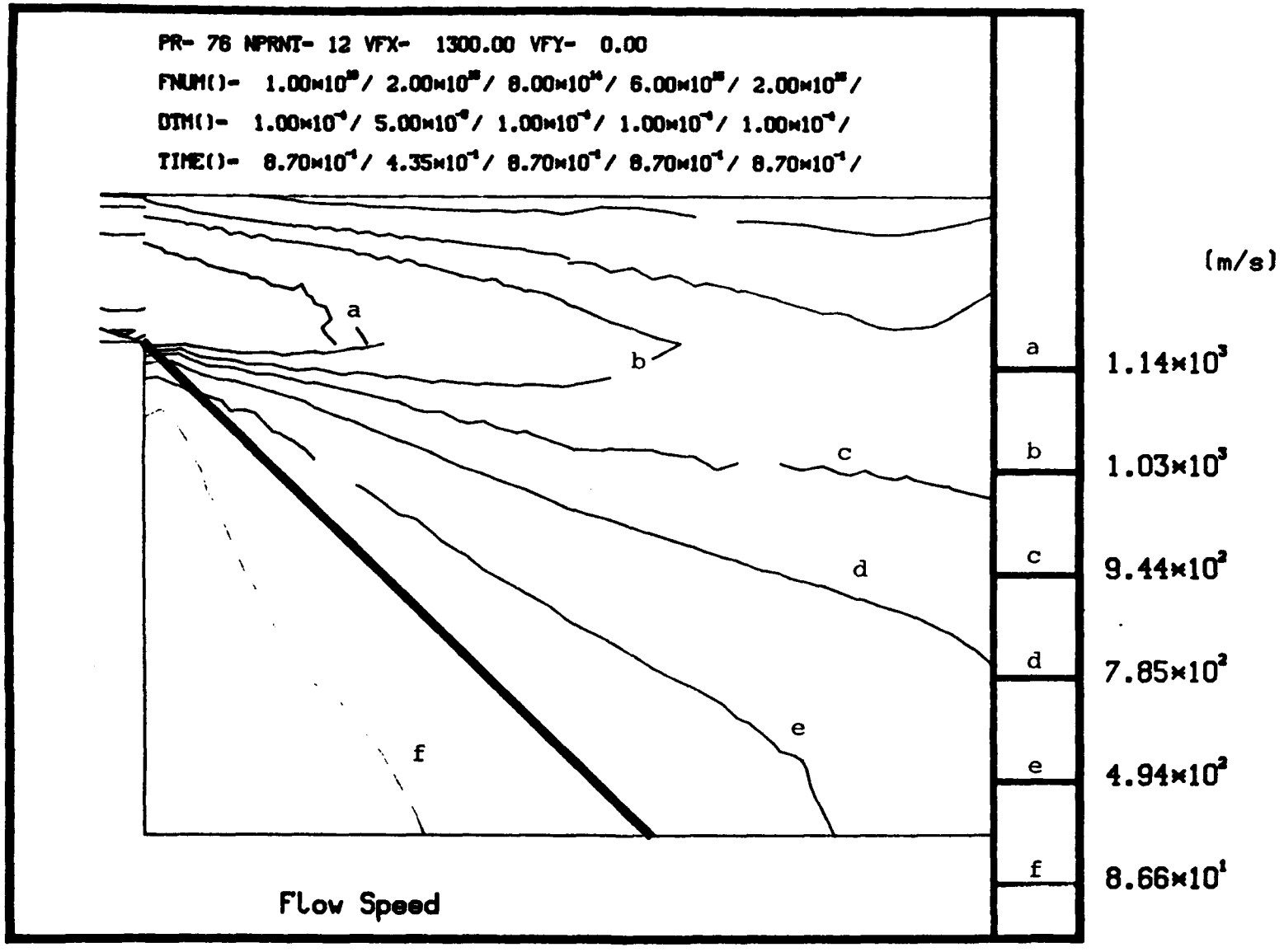

Fig. 14 Magnitude of flow velocity vectors for Computational Case # 1.

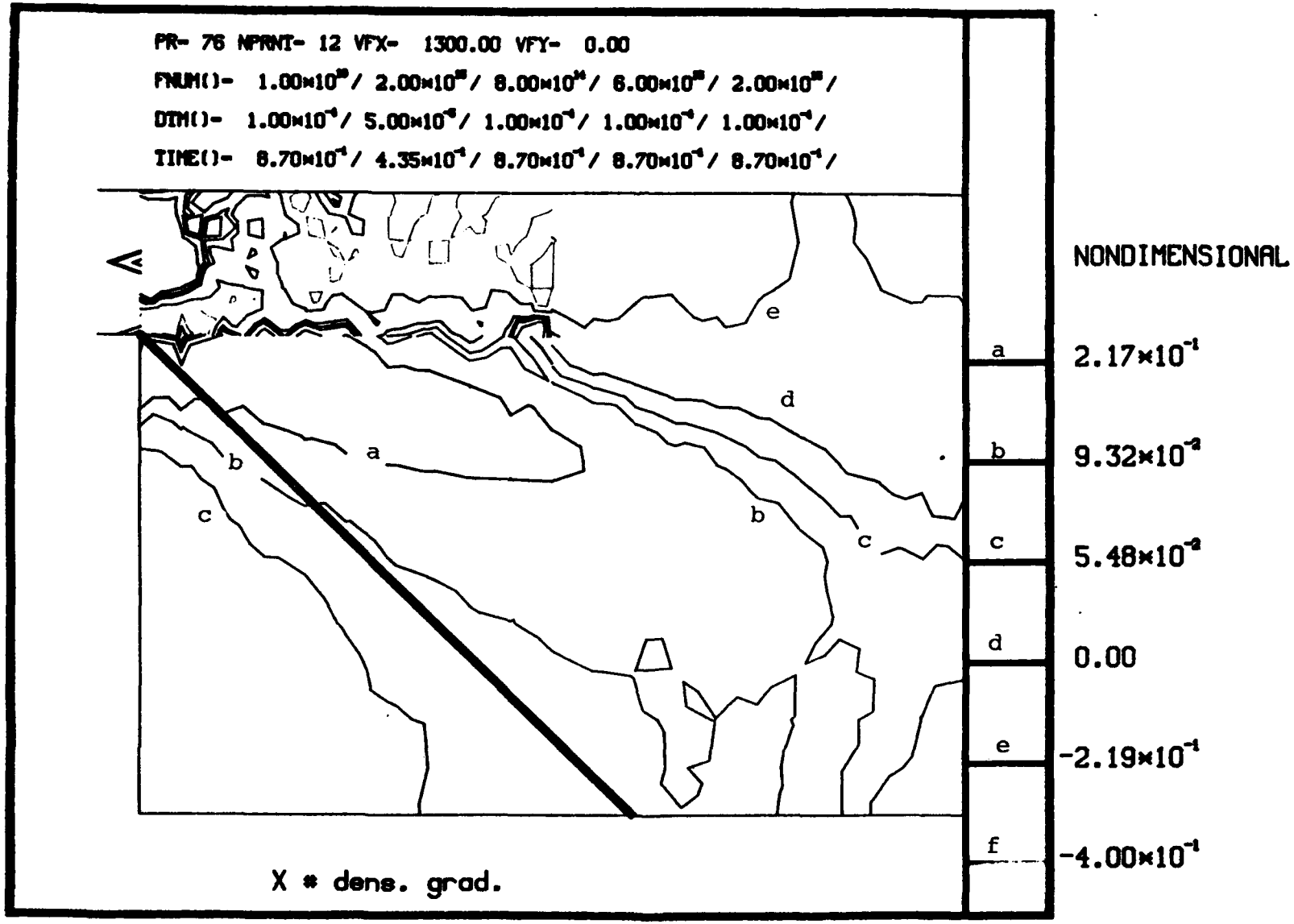

Fig. 15 Density gradient for Computational Case # 1.

tional regions are, however, introduced in order to either smooth the transition between the primary regions described above, better tune the code, or allow for SF_6 injection (see Fig. 10). The top wall in this case is assumed to be specularly reflective (accommodation coefficient of 1). Air is represented by diatomic nitrogen and is assumed to be initially at 300 K.

Figs. 17 through 34 shows the results obtained for a SF_6 feel density of 10^{17}/cc (Computational Case #2) and 10^{18}/cc (Computational Case #3). In these figures, the velocity vector direction, and the density are shown over the whole domain for the mean composition, and also for both species (air and SF_6). The flow velocity magnitude is given for the mean composition, and the density fraction is given for both species. As can be seen from the velocity vector plots, the structure of the flow field in the wake is dramatically altered by the SF_6 injection. The total momentum (density $\times$ velocity) of the SF_6 gas dominates the air momentum in the near wake. Any vortex structure that might have existed in the air flow prior to the SF_6 injection would therefore be swept away under these conditions.

At the lower feed density, it can be seen that SF_6 barely penetrates into the "free stream," i.e., barely leaves the wake area. Even at the higher feed density, the 1% SF_6 fraction contour remains practically aligned with the spacecraft skirt.

PR- 31 NPRNT- 12 (IFX- 0 IOS- 0 INS- 0 RWF- 0.00 NIS- 10 NSP- 10 NPS- 11)
(NSS- 2 NSSR- 0 IRA- 0 MNVT- 0 MAXRE- 0 FND- 1.00×10^{10} FMTP- 0.0
FNUM()- 15.3/ 15.3/ 13.3/ 15.8/ 14.8/ 14.7/ 15.0/ 13.3/ 13.7/
DTM()- -5.0/-5.3/-4.2/-4.7/-4.0/-4.7/-4.7/-3.9/-3.9/
TIME()- -1.4/-1.7/-0.6/-1.1/-0.4/-1.1/-1.1/-0.3/-0.3/
DUPLIC(W.R.T. REG. 2)- 0.3/ 0.0/ 3.0/ 0.1/ 1.8/ 1.2/ 0.9/ 3.4/ 3.0/

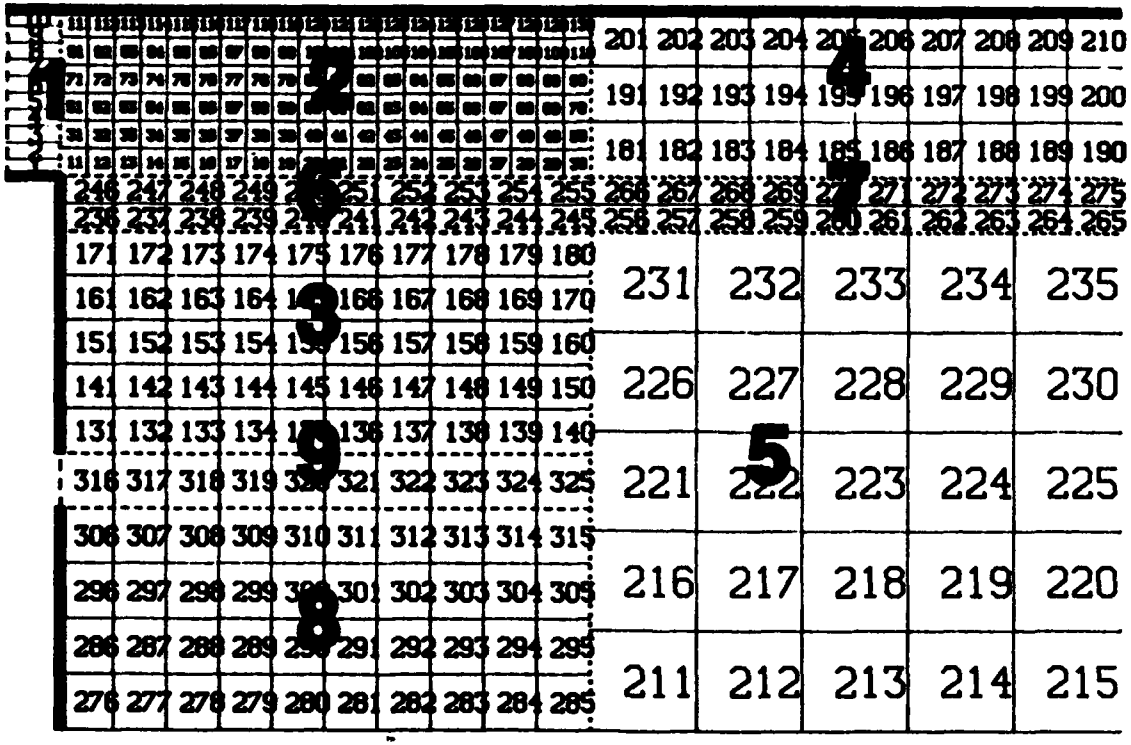

REG 1 SIDES: 5/4/5/7/
SUBCELLS: 1/10/ 1/ 1/
REG 2 SIDES: 7/7/5/7/
SUBCELLS: 40/12/ 2/ 2/
REG 3 SIDES: 7/5/7/7/
SUBCELLS: 40/20/ 4/ 4/
REG 4 SIDES: 7/7/5/8/
SUBCELLS: 10/ 3/ 1/ 1/
REG 5 SIDES: 2/7/7/8/
SUBCELLS: 10/10/ 2/ 2/
REG 6 SIDES: 7/5/7/7/
SUBCELLS: 40/ 4/ 4/ 2/
REG 7 SIDES: 7/7/7/8/
SUBCELLS: 20/ 4/ 2/ 2/
REG 8 SIDES: 2/5/7/7/
SUBCELLS: 40/16/ 4/ 4/
REG 9 SIDES: 7/4/7/7/
SUBCELLS: 40/ 4/ 4/ 4/

GRID AND BOUNDARY CONDITIONS CHECKUP DATE-22-Sep-88
SPECIES * MEAN TIME- 09:59:14 RUN * PROF7

Fig. 16 Code setup for Computational Case # 2.

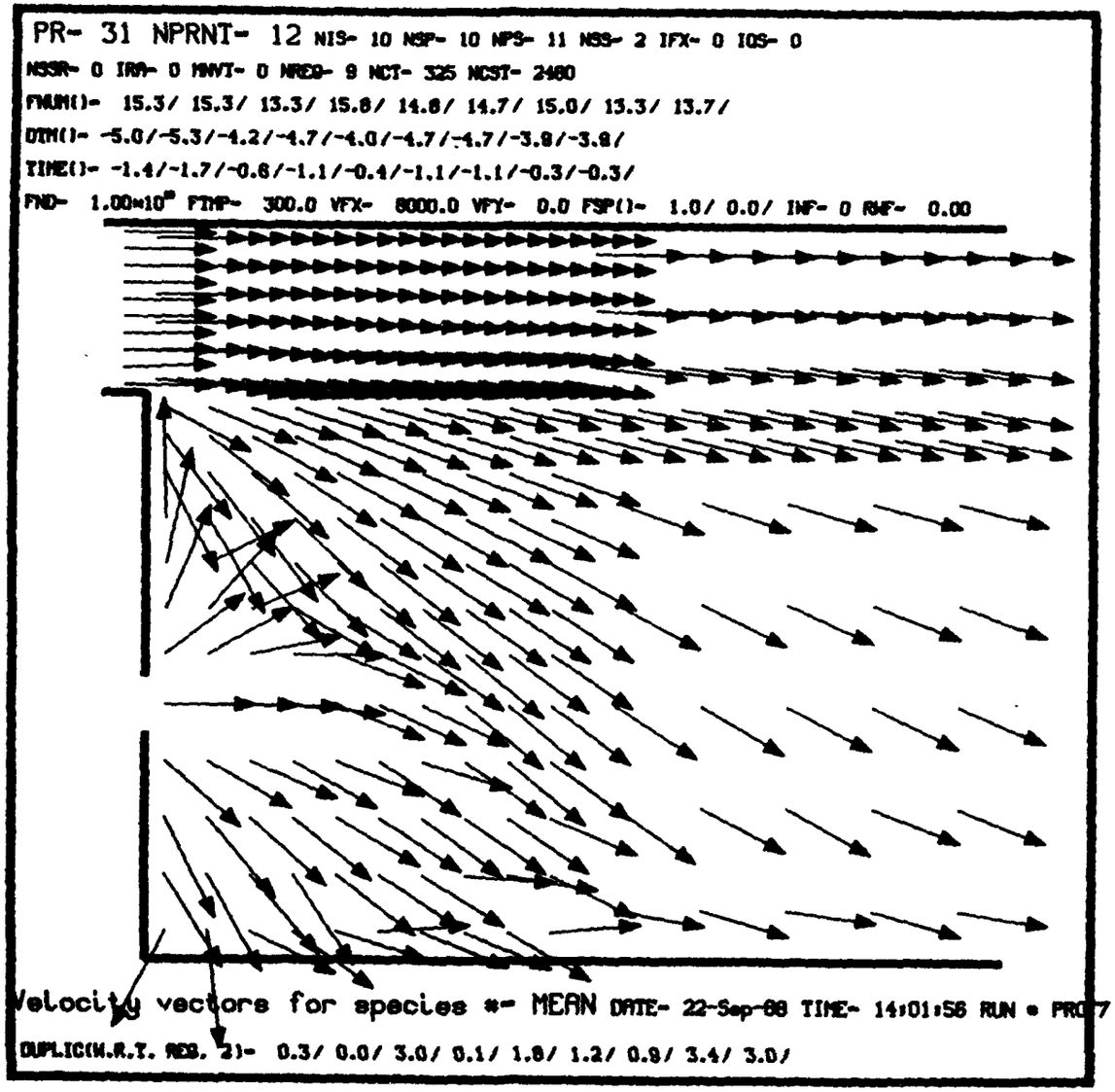

Fig. 17 Flow field for Computational Case # 2 (mean).

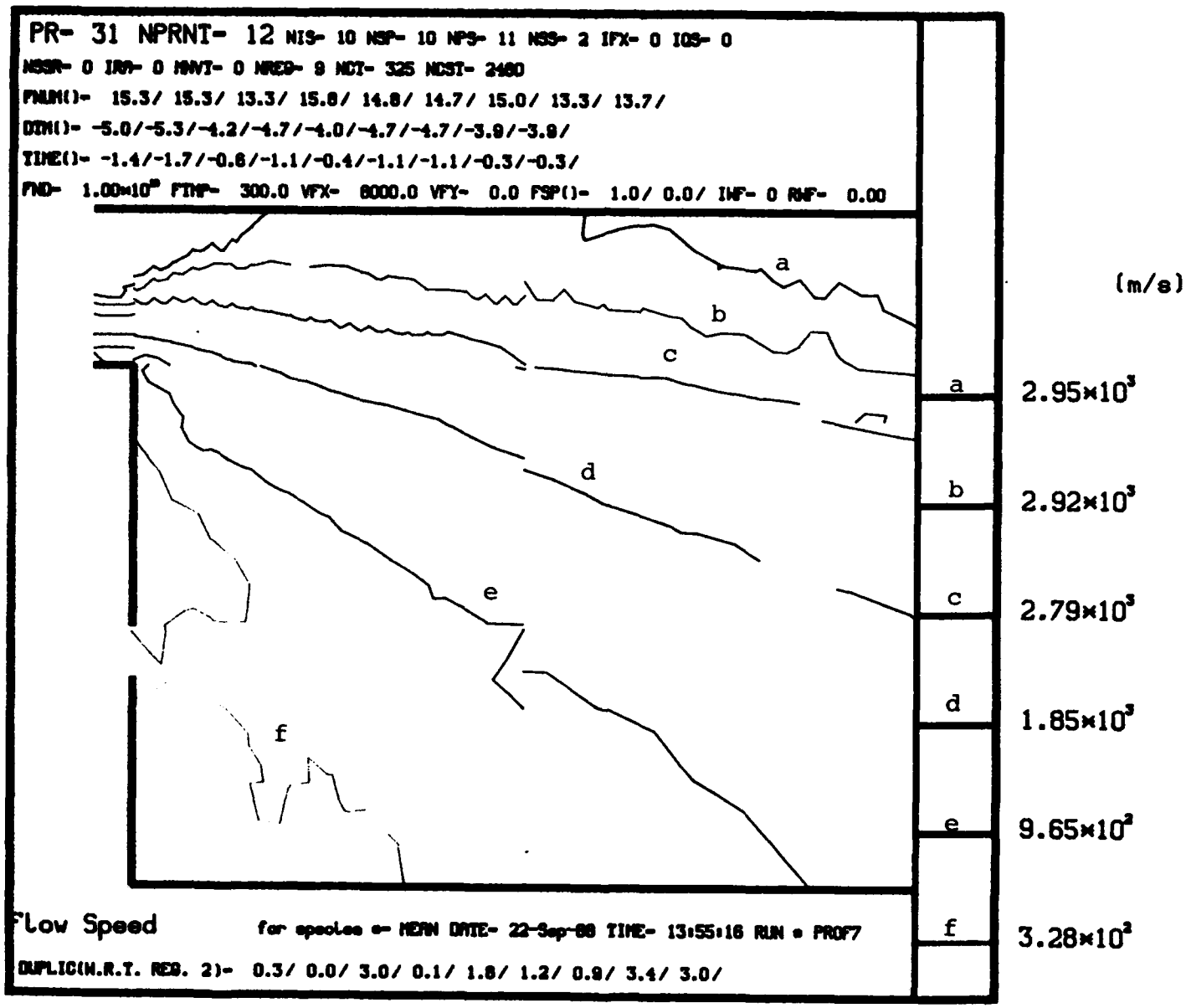

Fig. 18 Magnitude of flow velocity vectors for Computational Case # 2 (mean).

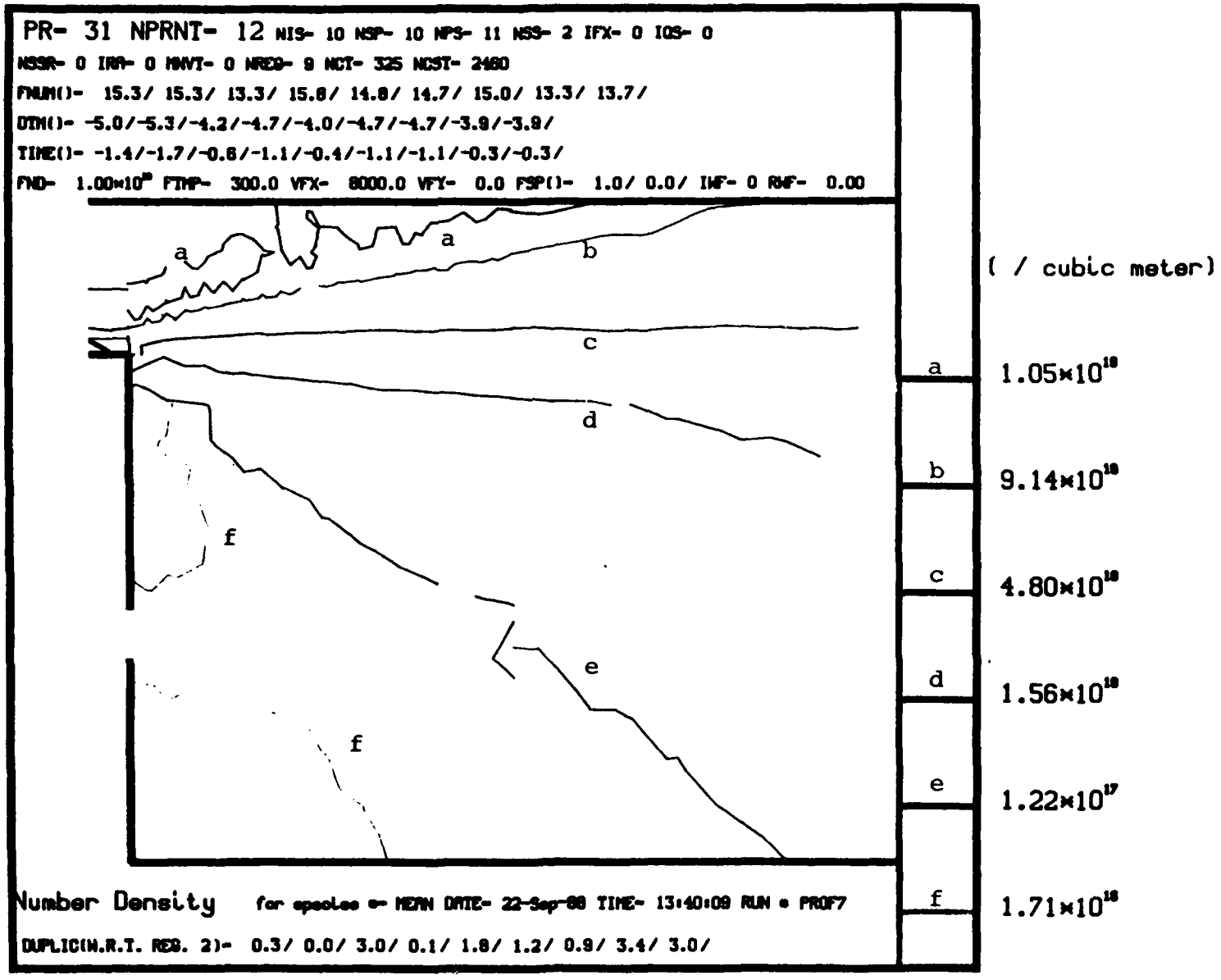

Fig. 19 Number density contours for Computational Case # 2 (mean).

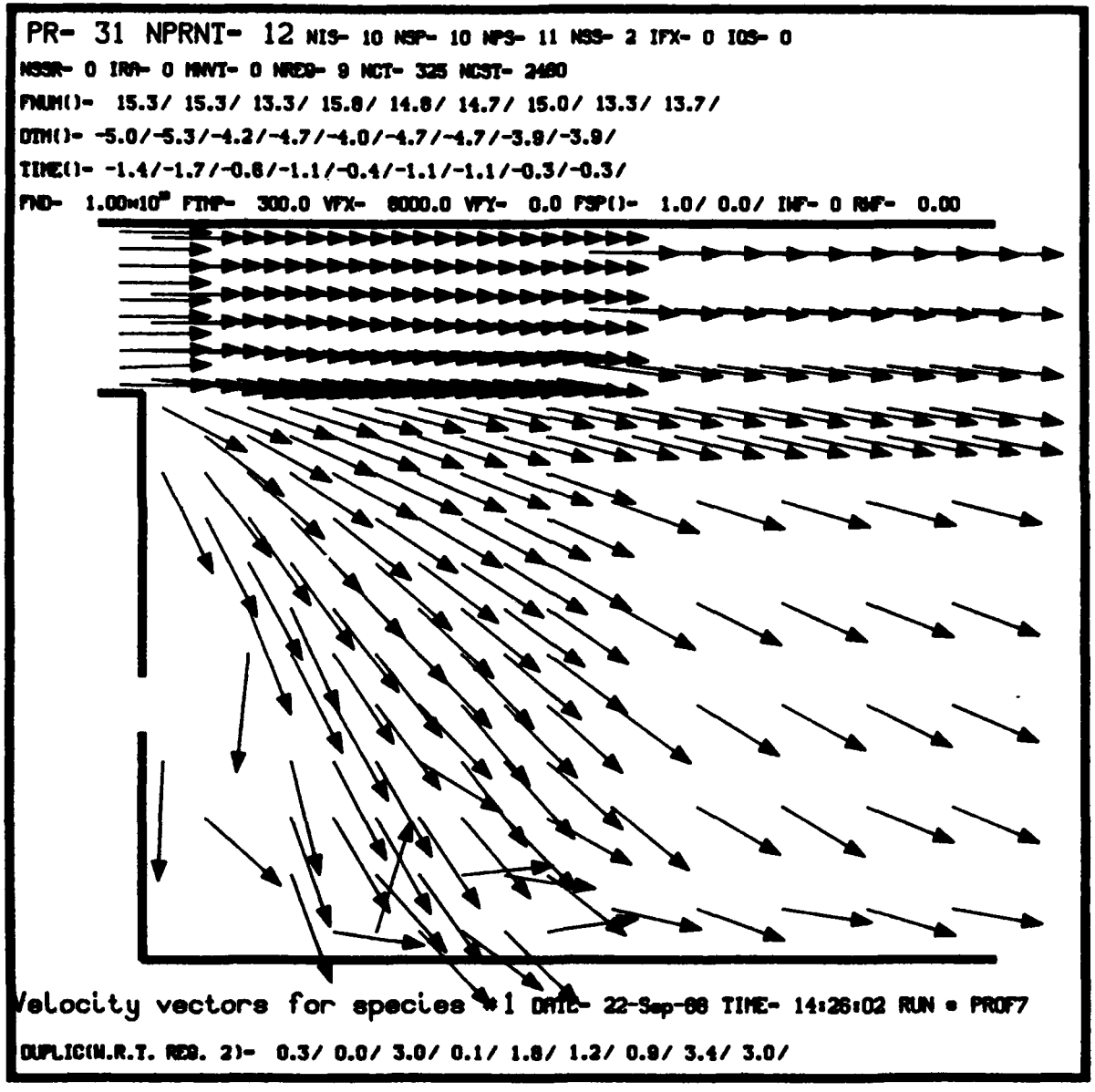

Fig. 20 Flow field for Computational Case # 2 (air).

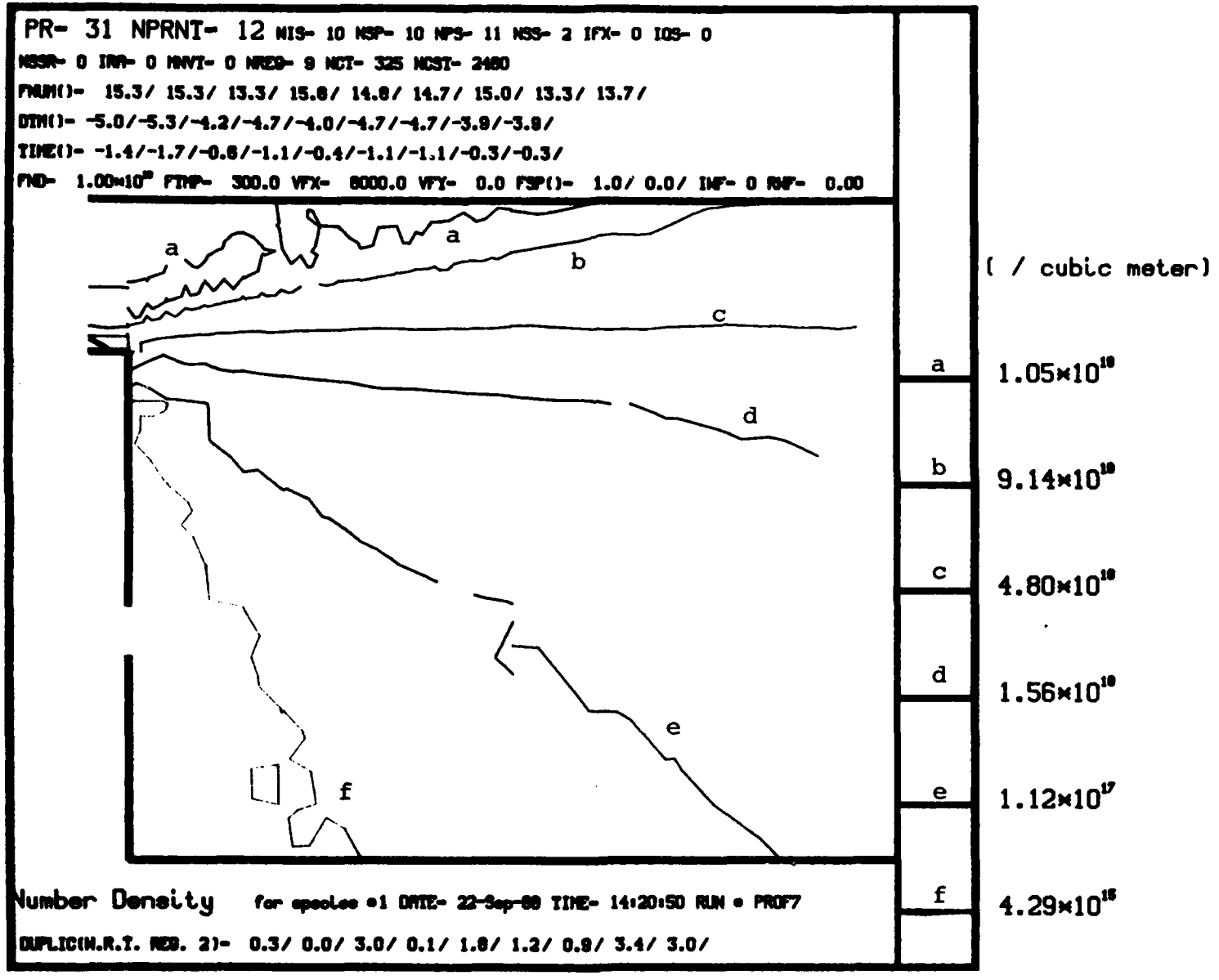

Fig. 21 Number density contours for Computational Case # 2 (air).

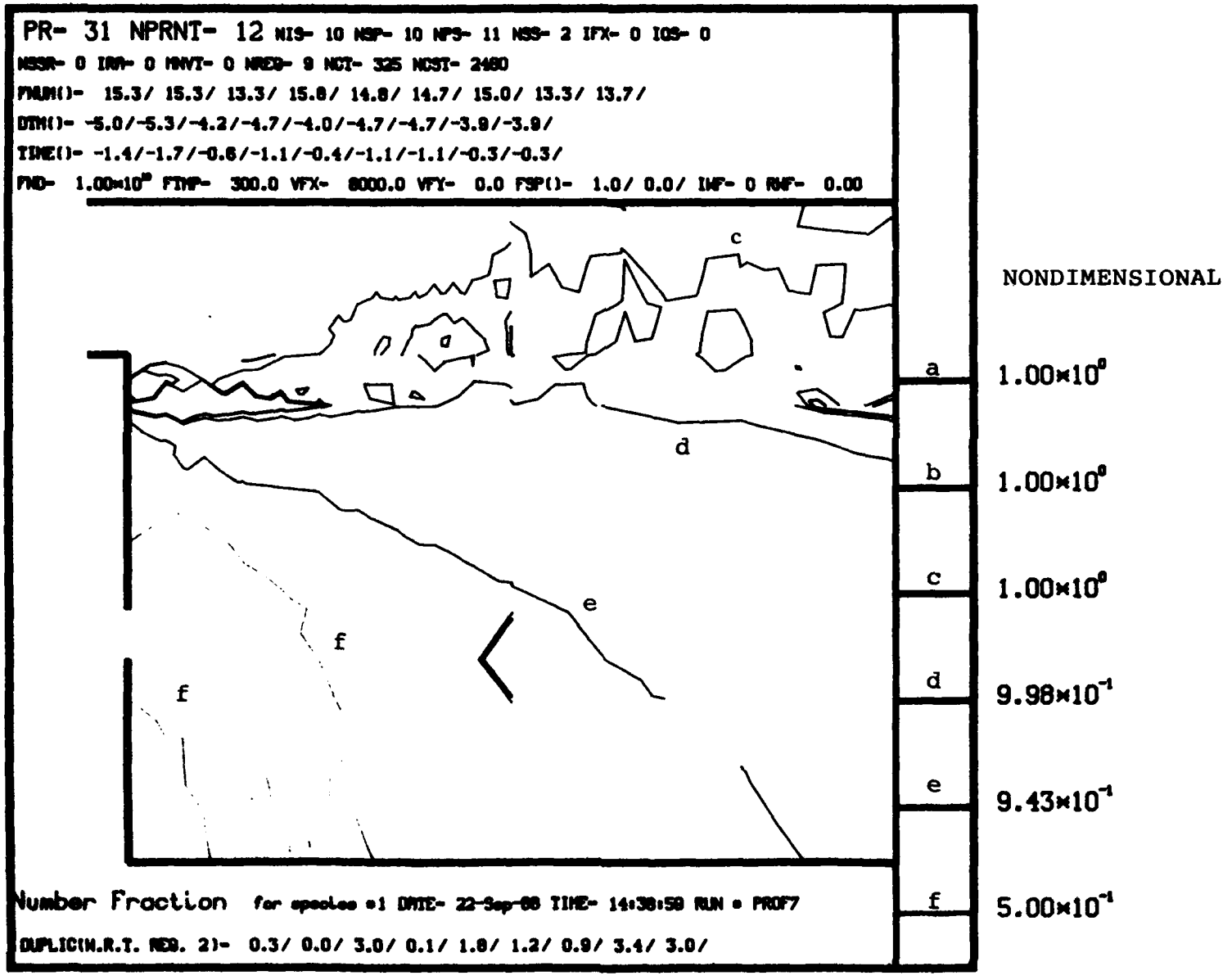

Fig. 22 Number density fraction for Computational Case # 2 (air).

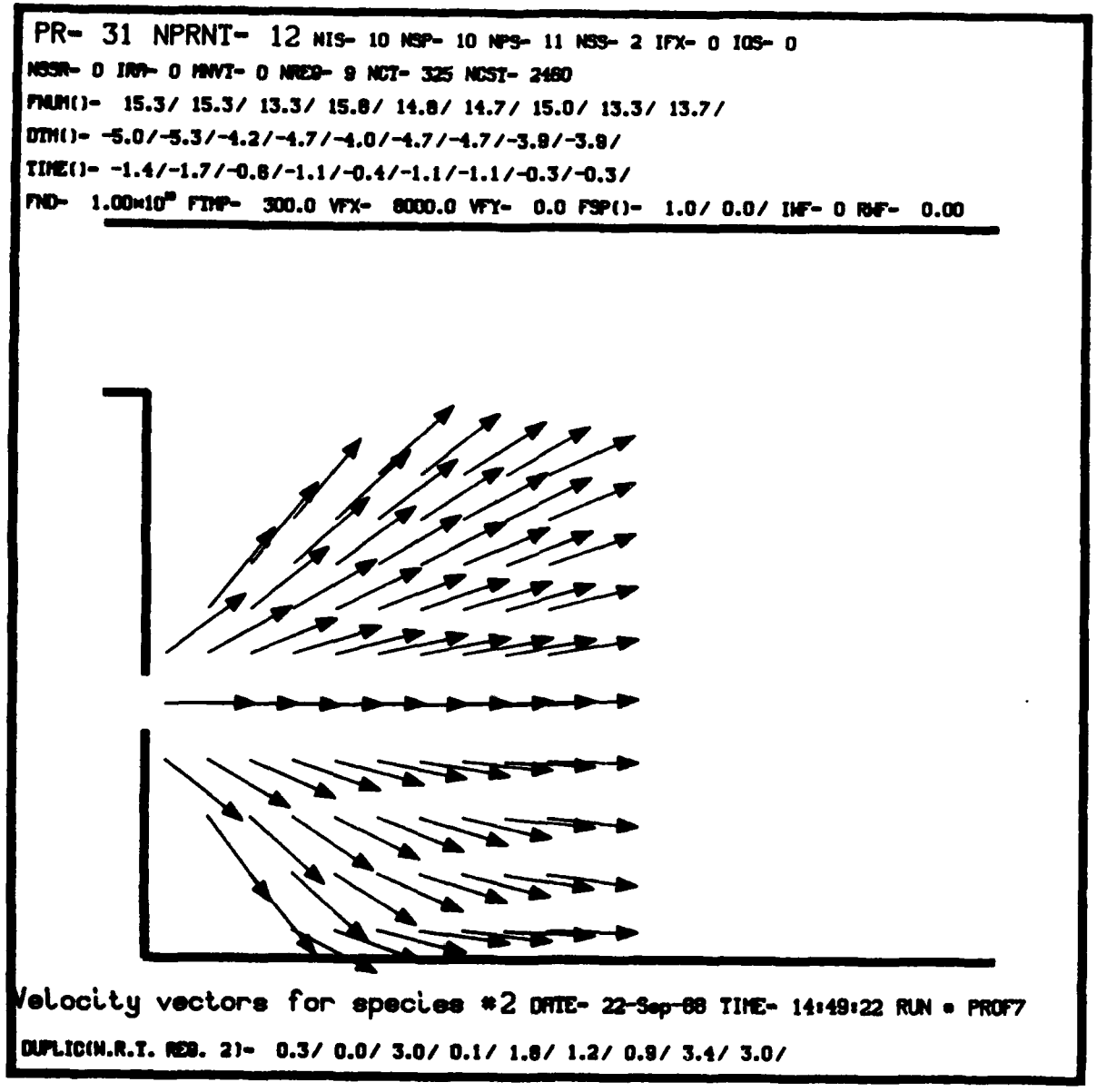

Fig. 23 Flow field for Computational Case # 2 (SF_6).

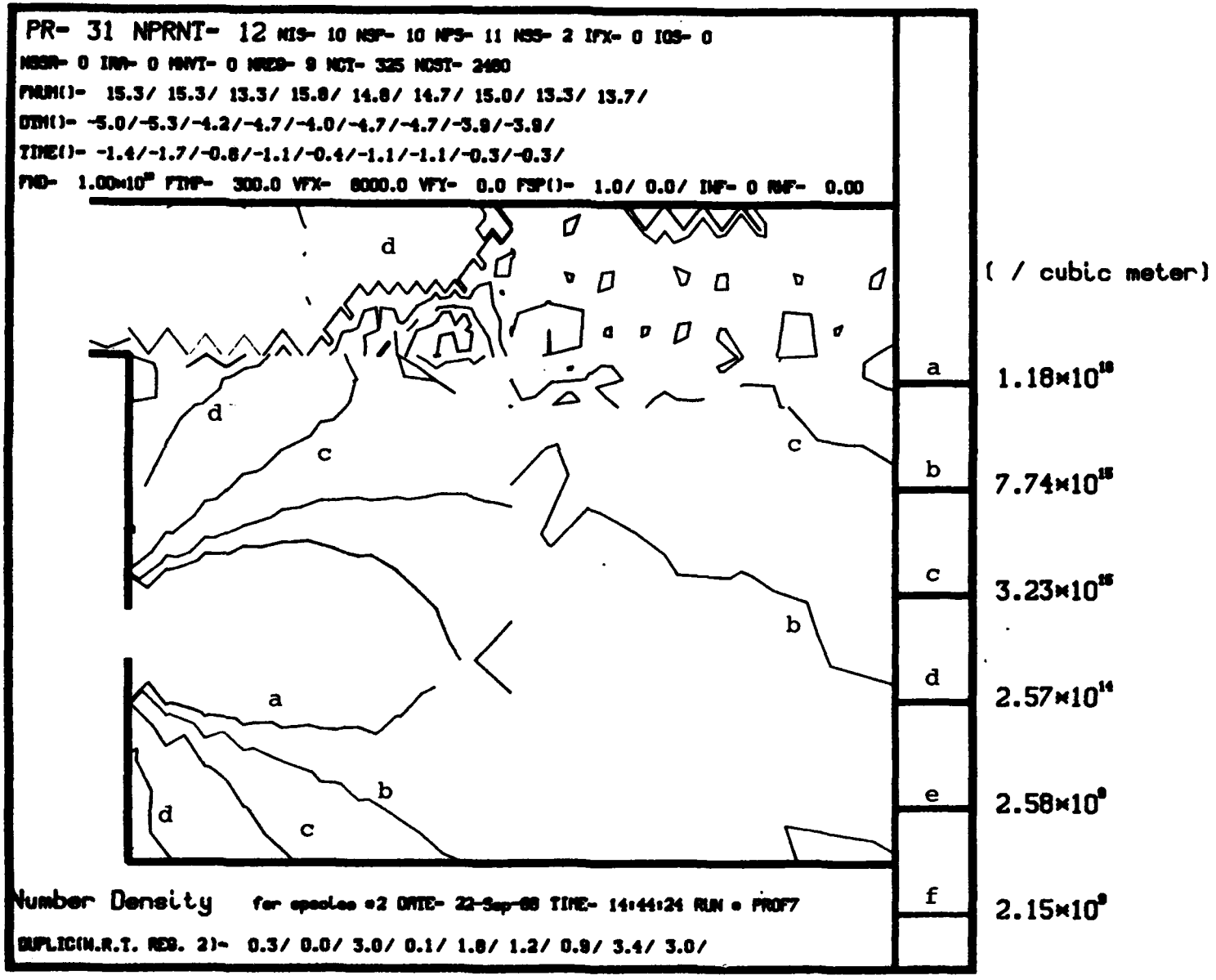

Fig. 24 Number density contours for Computational Case # 2 (SF_6).

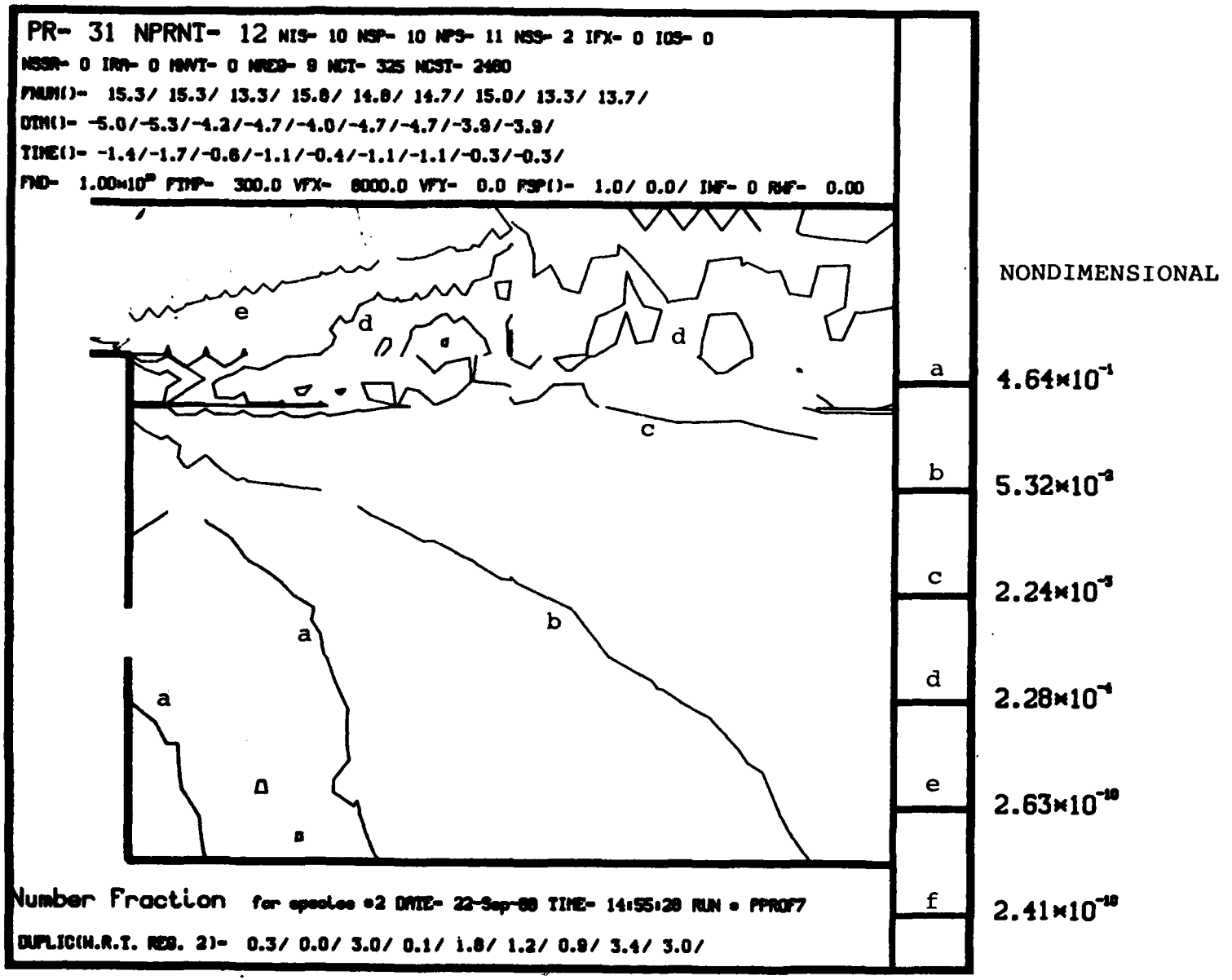

Fig. 25 Number density fraction for Computational Case # 2 (SF_6).

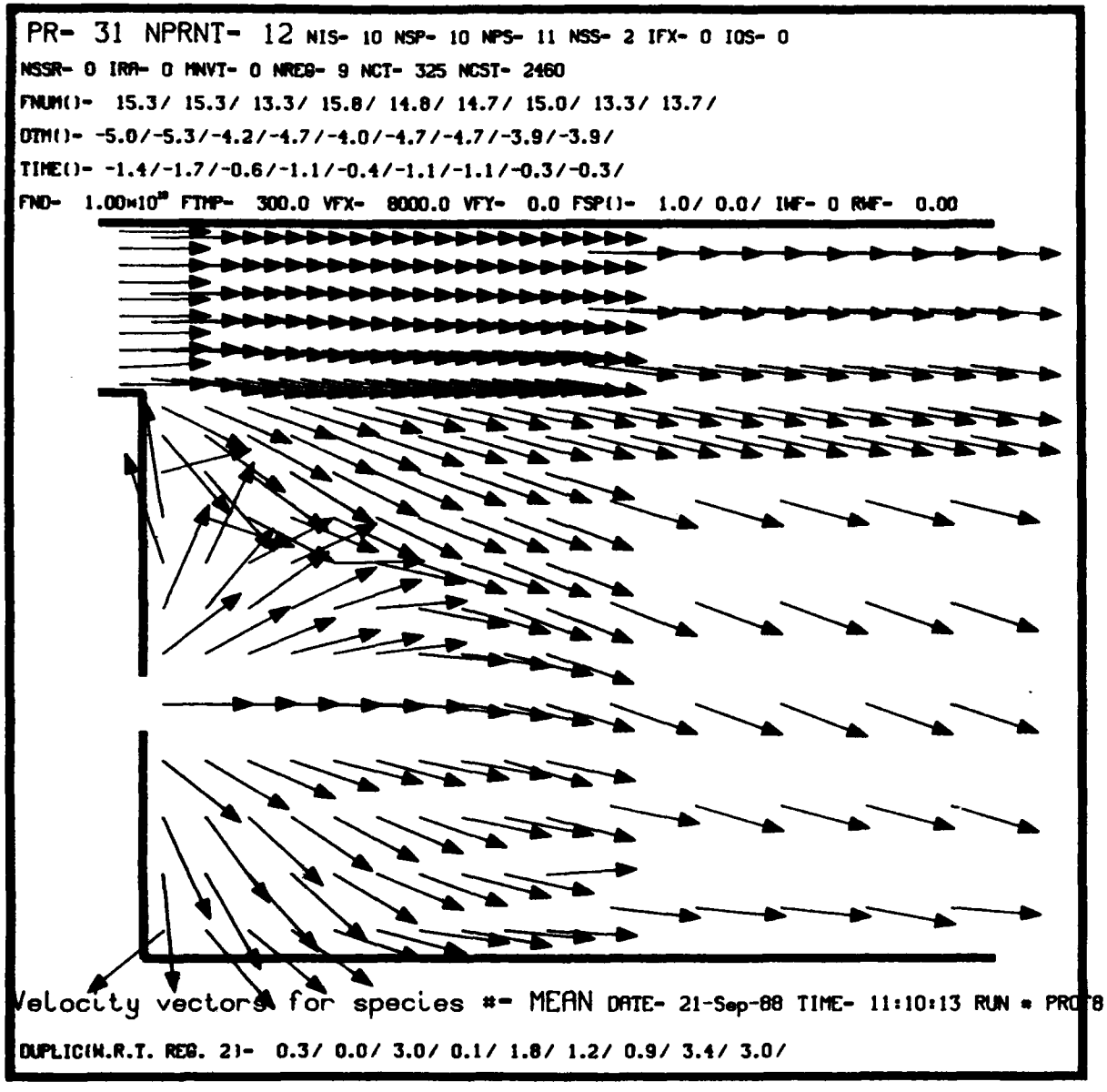

Fig. 26 Flow field for Computational Case # 3 (mean).

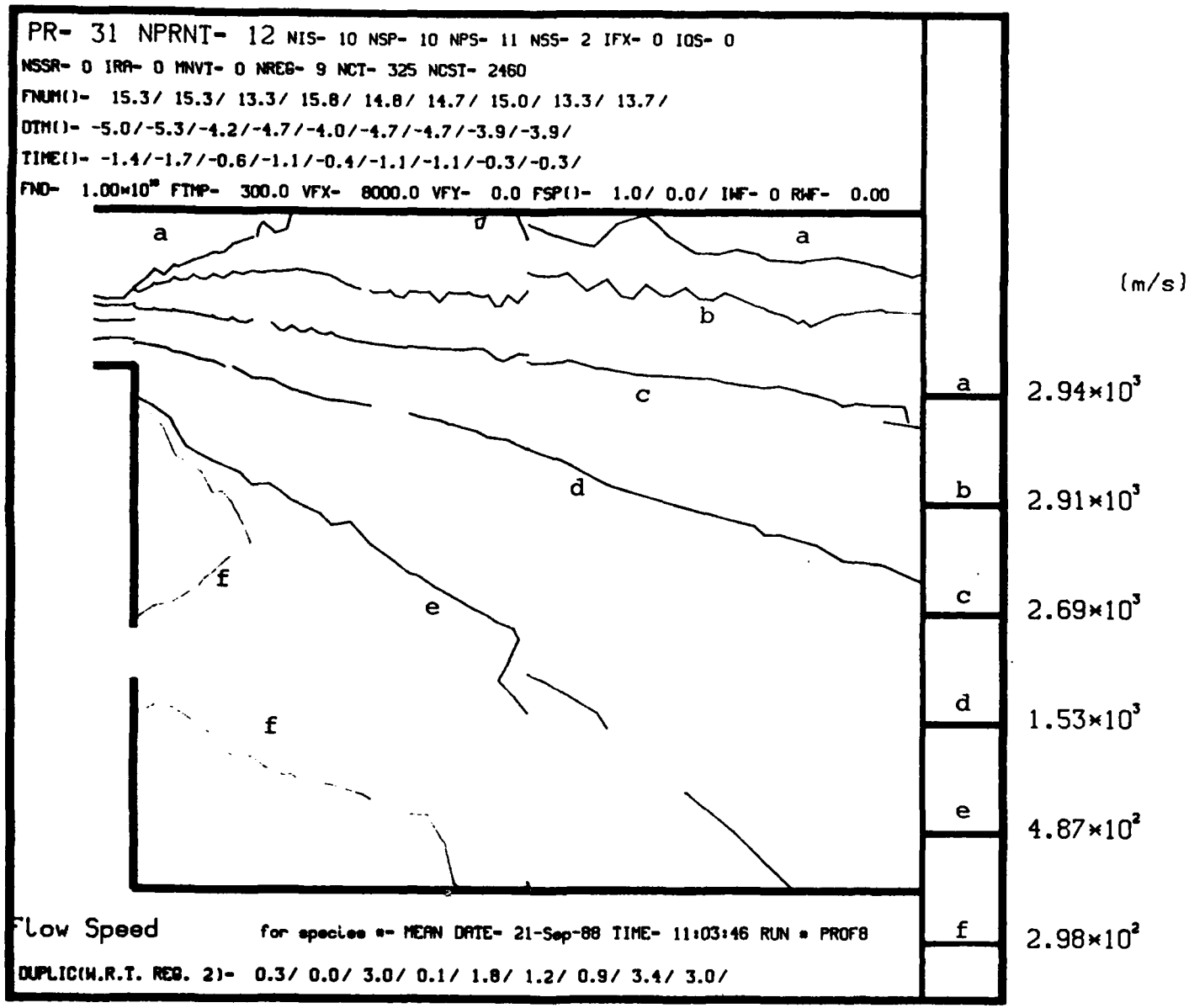

Fig. 27 Magnitude of flow velocity vectors for Computational Case # 3 (mean).

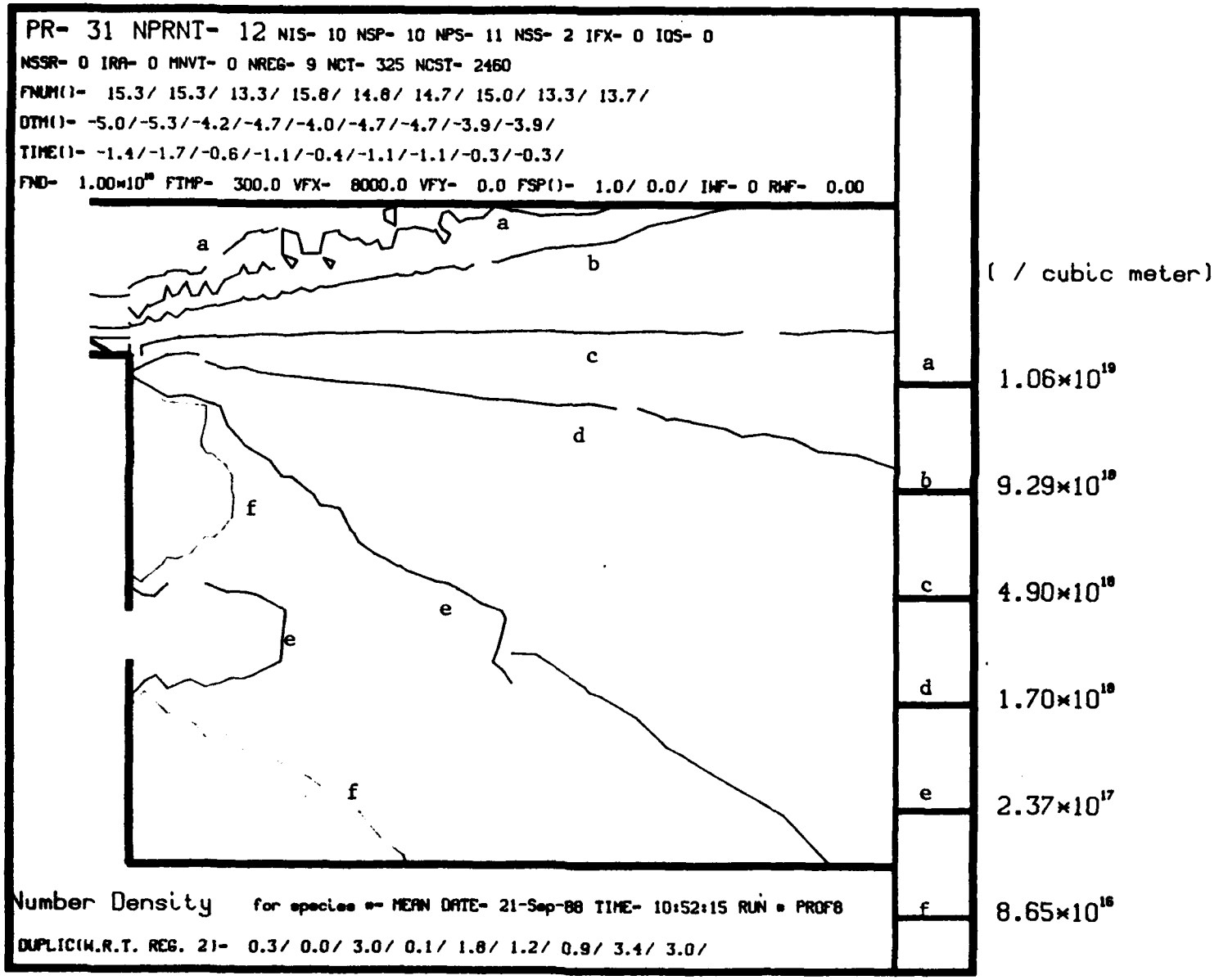

Fig. 28 Number density contours for Computational Case # 3 (mean).

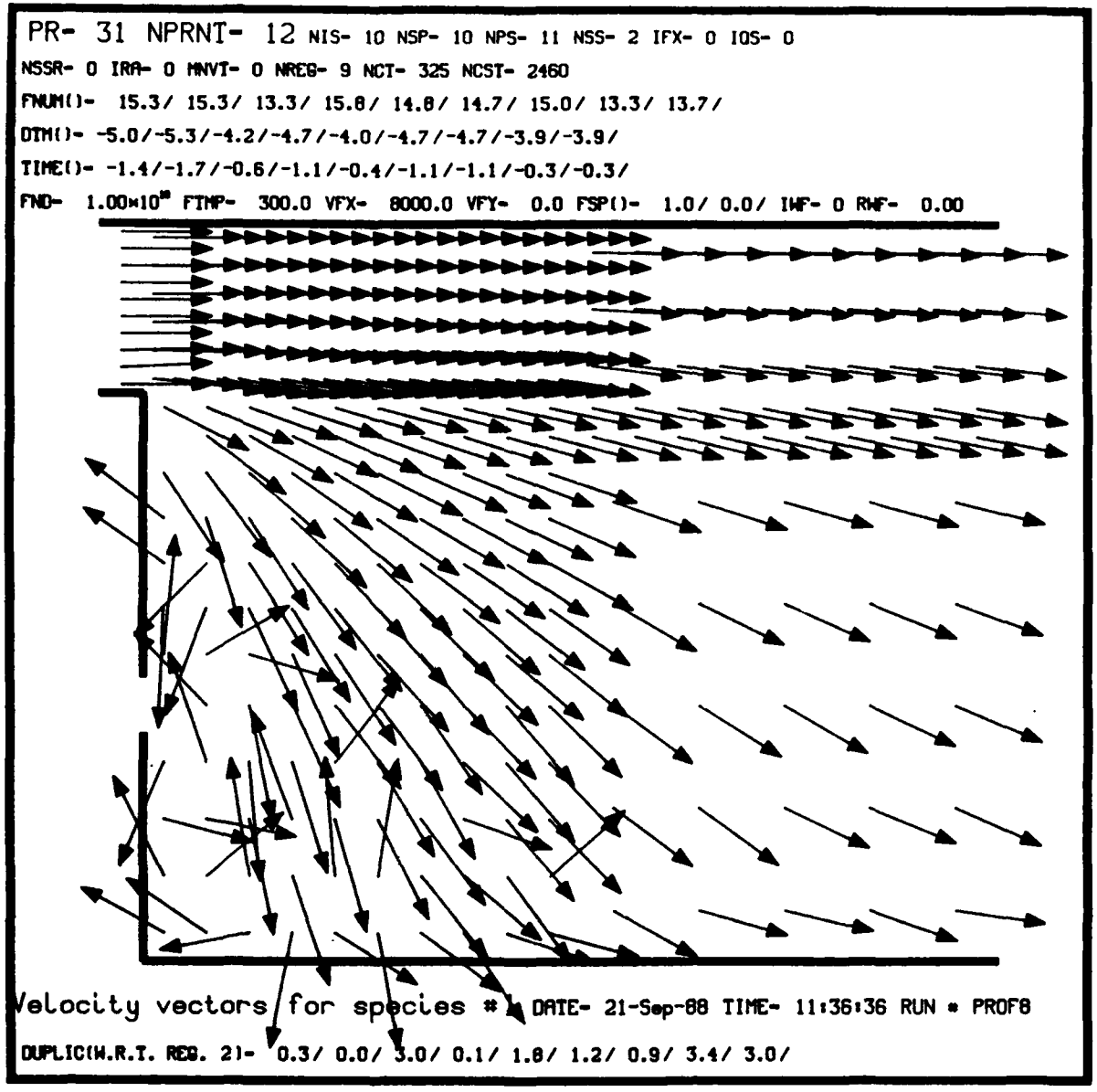

Fig. 29 Flow field for Computational Case # 3 (air).

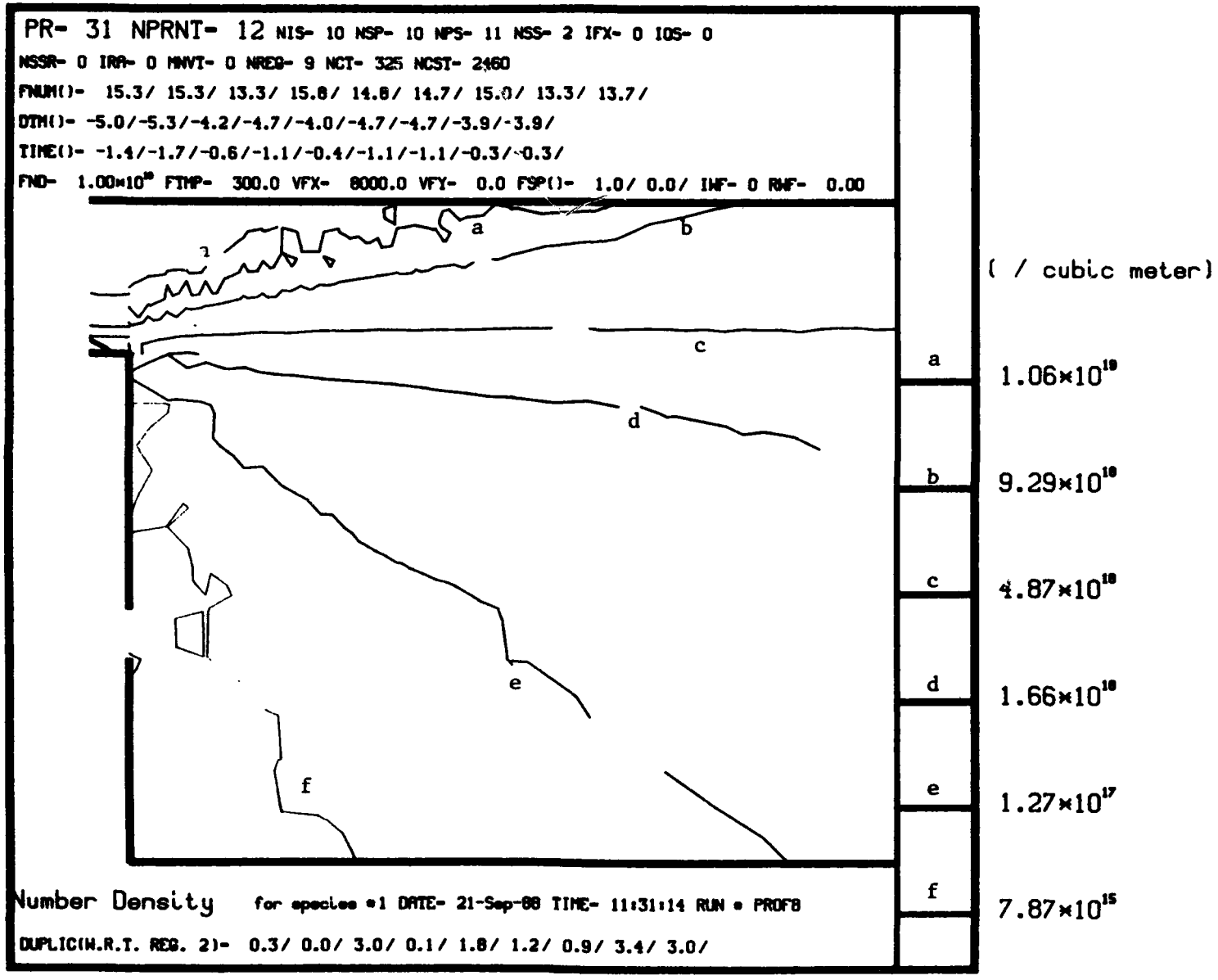

Fig. 30 Number density contours for Computational Case # 3 (air).

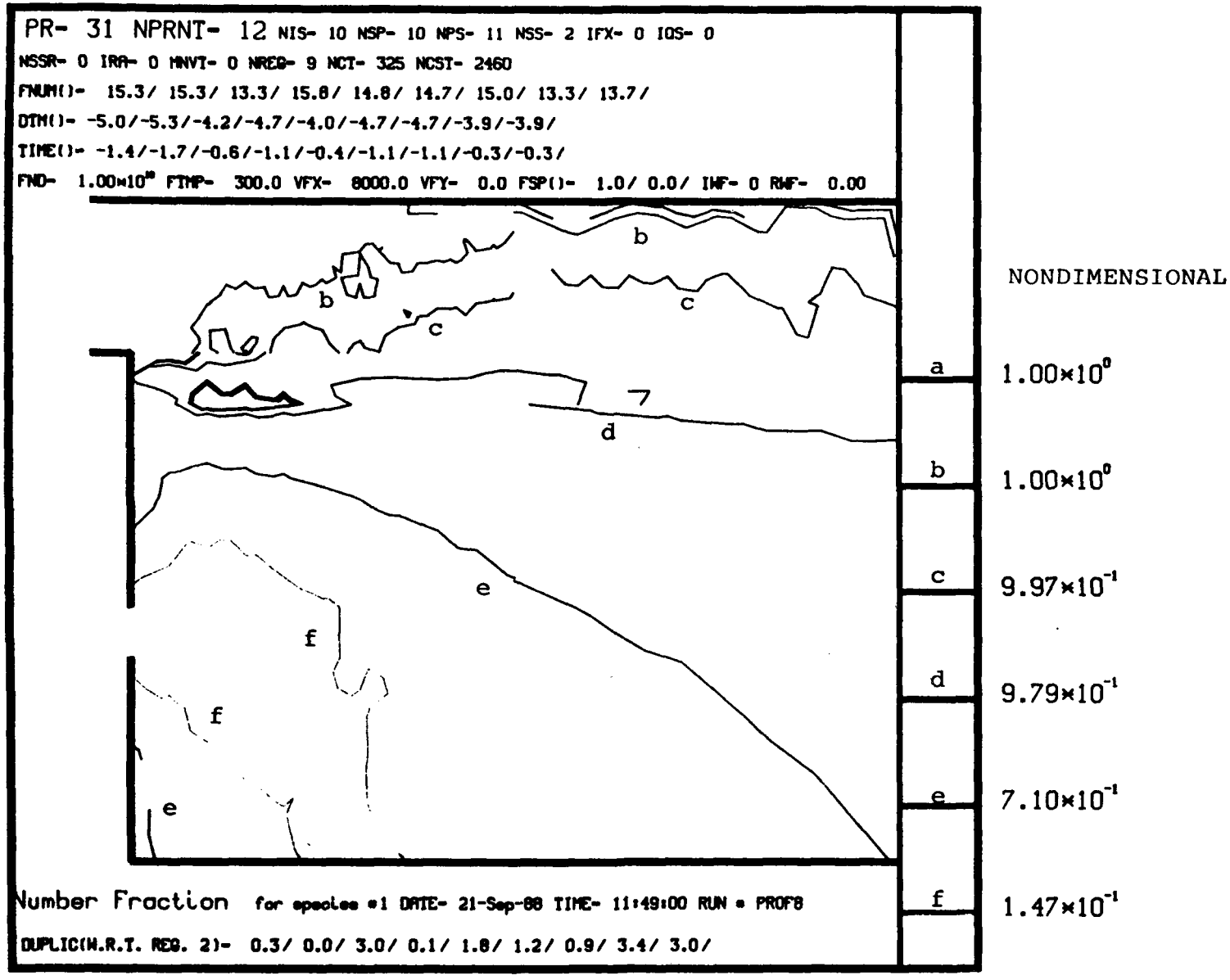

Fig. 31 Number density fraction for Computational Case # 3 (air).

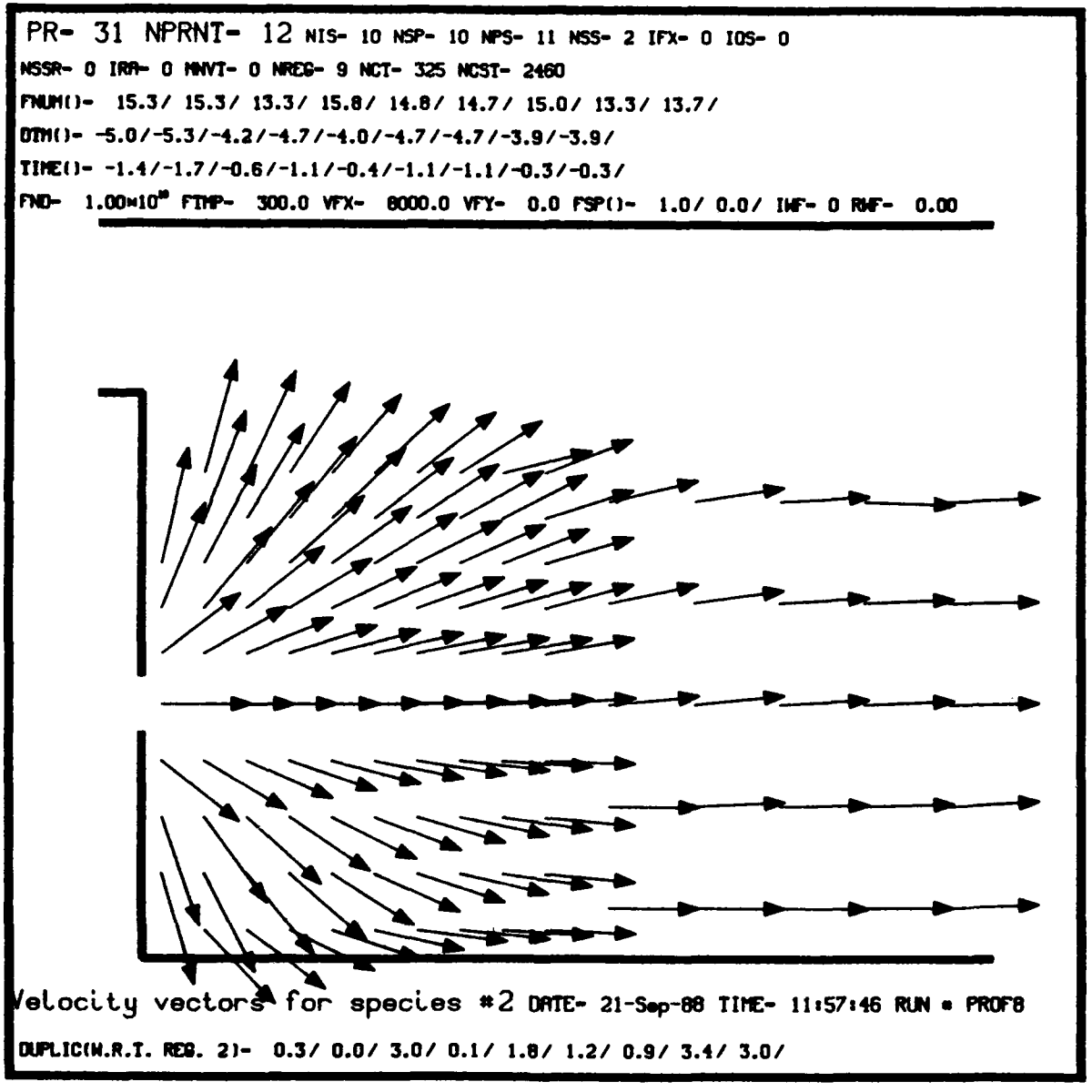

Fig. 32 Flow field for Computational Case # 3 (SF_6).

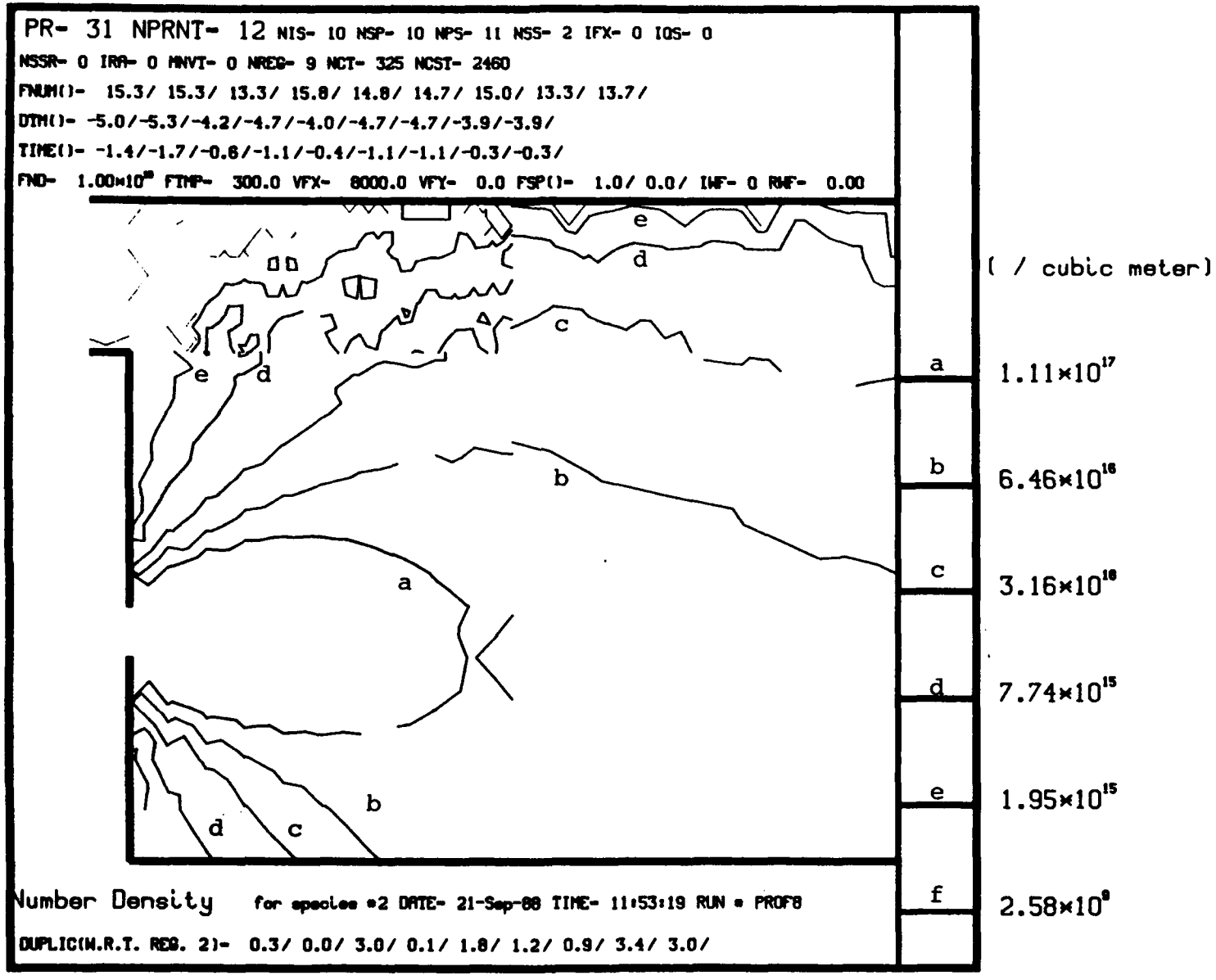

Fig. 33 Number density contours for Computational Case # 3 (SF_6).

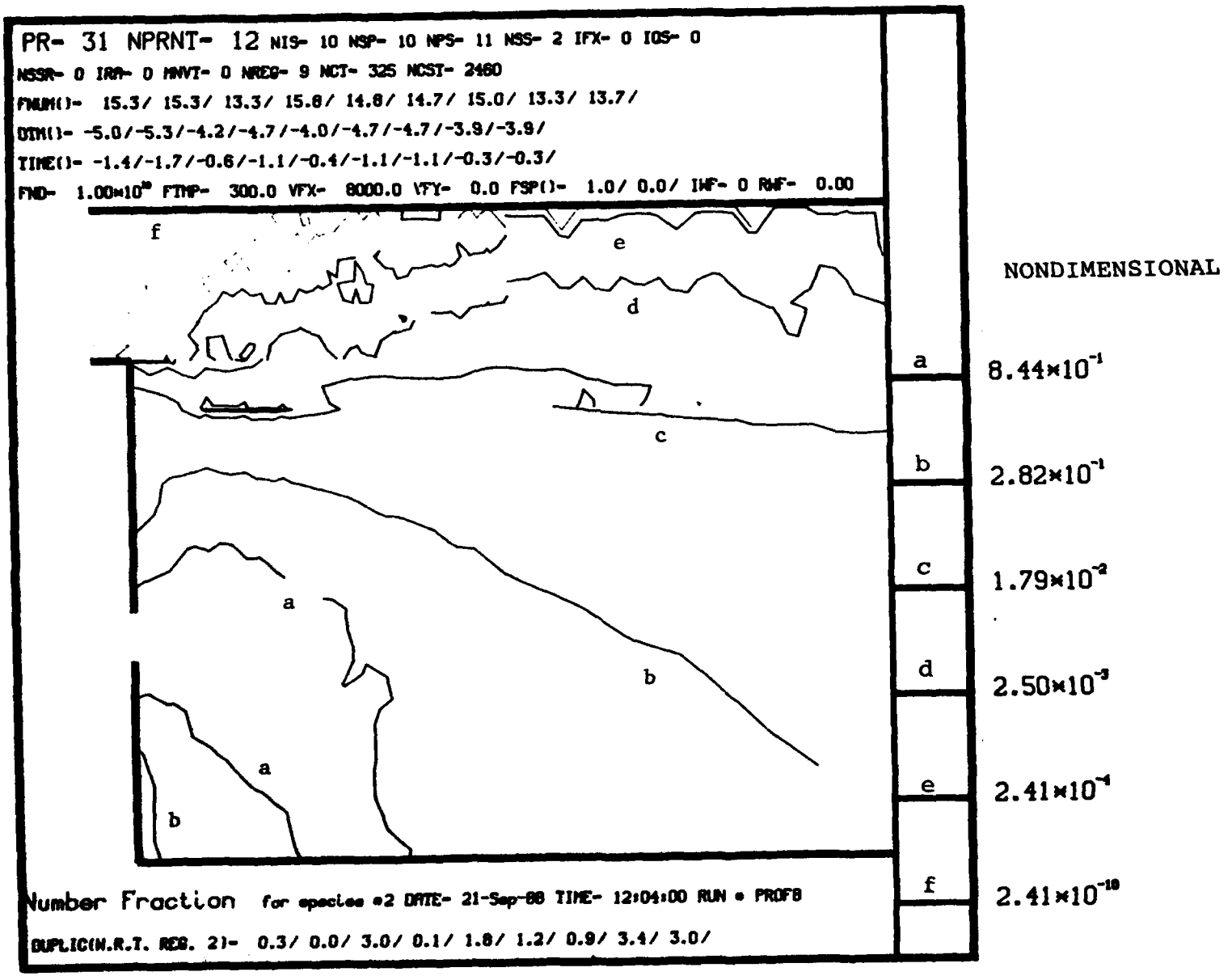

Fig. 34 Number density fraction for Computational Case # 3 (SF_6).

7. Future Plans

The results presented herein are preliminary. This initial effort affords a first look at Bird's code as a tool to study gas injection into the wake of reentering AOTV/AFE vehicles. Results are very promising and the method appears to give the expected results, including the characteristic features of wake flow seen in past studies in the continuum regime. However, work in several areas should be pursued:

- The dependence of the computation grid structure on the flow pattern has to be analyzed. The vortex seen on the body base at Mach 4 is very thin, and we must determine whether this result is due to cell/subcell sizes that are too large.
- To account for 3-D effects, the computation should be carried out in a 2-D axisymmetric frame of reference. Such computation will allow us to determine the flux of SF_6 needed to achieve a given threshold of SF_6/air mass fraction.
- The results obtained by Gnoffo (at low altitudes) and Moss and Celenligil (at higher altitudes) should be used as boundary conditions to the present simulation. The use of these numerical results to anchor the present code should yield fairly reliable estimates of the SF_6 flow field in the wake region of the AOTV.
- Conditions for which rarefaction effects are so important that the Navier-Stokes equatins are no longer valid, i.e., the "breakdown" surface, should be identified from Gnoffo's results at lower altitudes, when the ram is in the continuum flow regime. The breakdown surface, shown on Fig. 35, is characterized as the locii of the points for which the parameter

$$P = 1.5\sqrt{\pi}\ \ s\lambda\ \frac{d}{dx}\ell n\rho = 0.05,$$

  where s is the ratio of the flow velocity to the most probable molecular velocity, λ is the near free path, and ρ is the gas density (Ref. 13). The flow field and thermodynamic properties on this surface can be used as input boundary conditions to our wake flow model. Preliminary investigation of Gnoffo's data have been made in the vicinity of the spacecraft. Results are reproduced in Fig. 36. The computer programs developed to obtain these results can be used to determine the location of the whole breakdown surface over the AOTV wake region, and specify the density and flow speed of the air flow at the breakdown surface.
- The chemistry between SF_6 and electrons should be inserted into the code.
- More diagnostics should be developed to monitor the progress of the code. Such diagnostics would include a check for steady state attainment, check for global mass, momentum, energy conservation, monitor the molecular collision process,

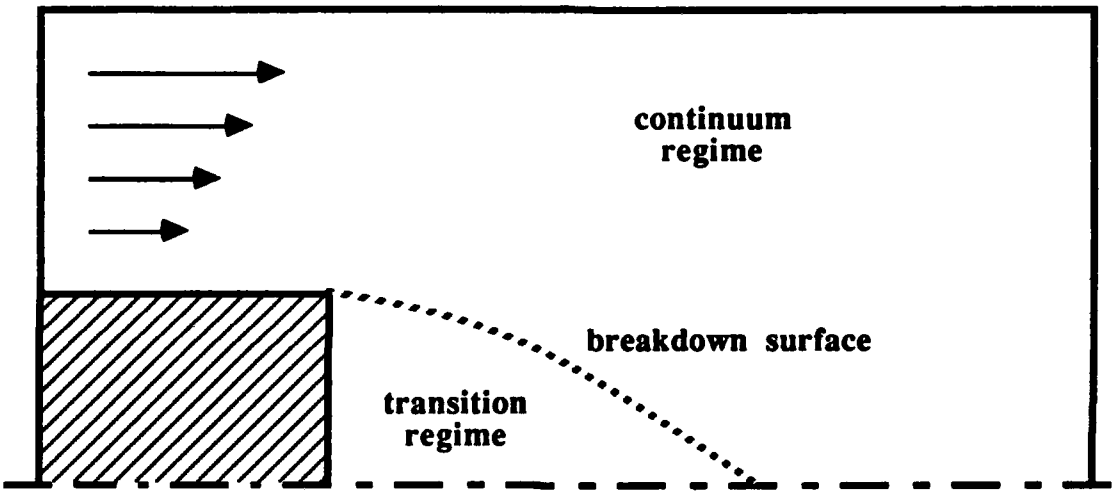

Fig. 35 Breakdown surface for an AOTV near perigee.

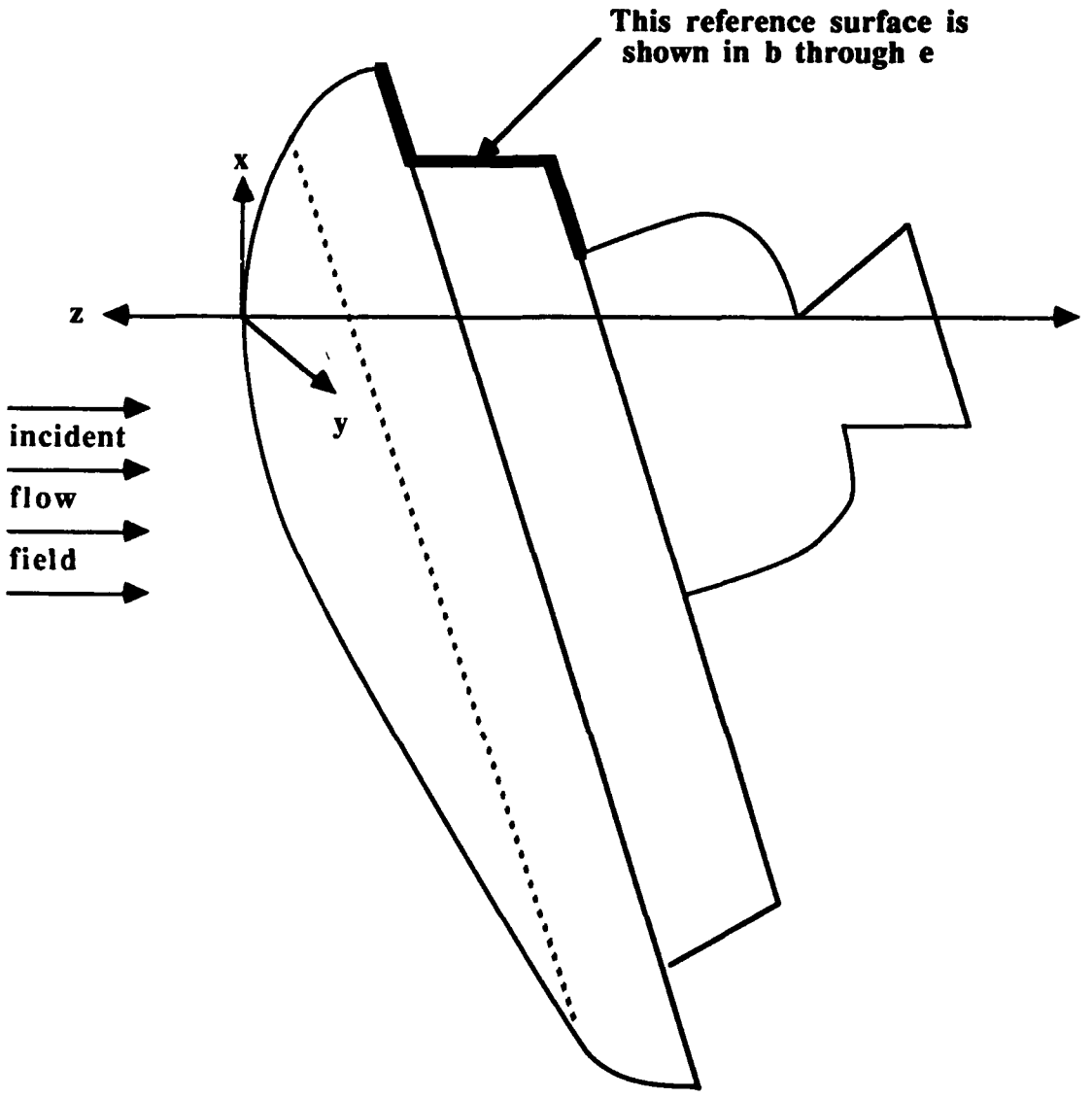

Fig. 36a. Vehicle Configuration

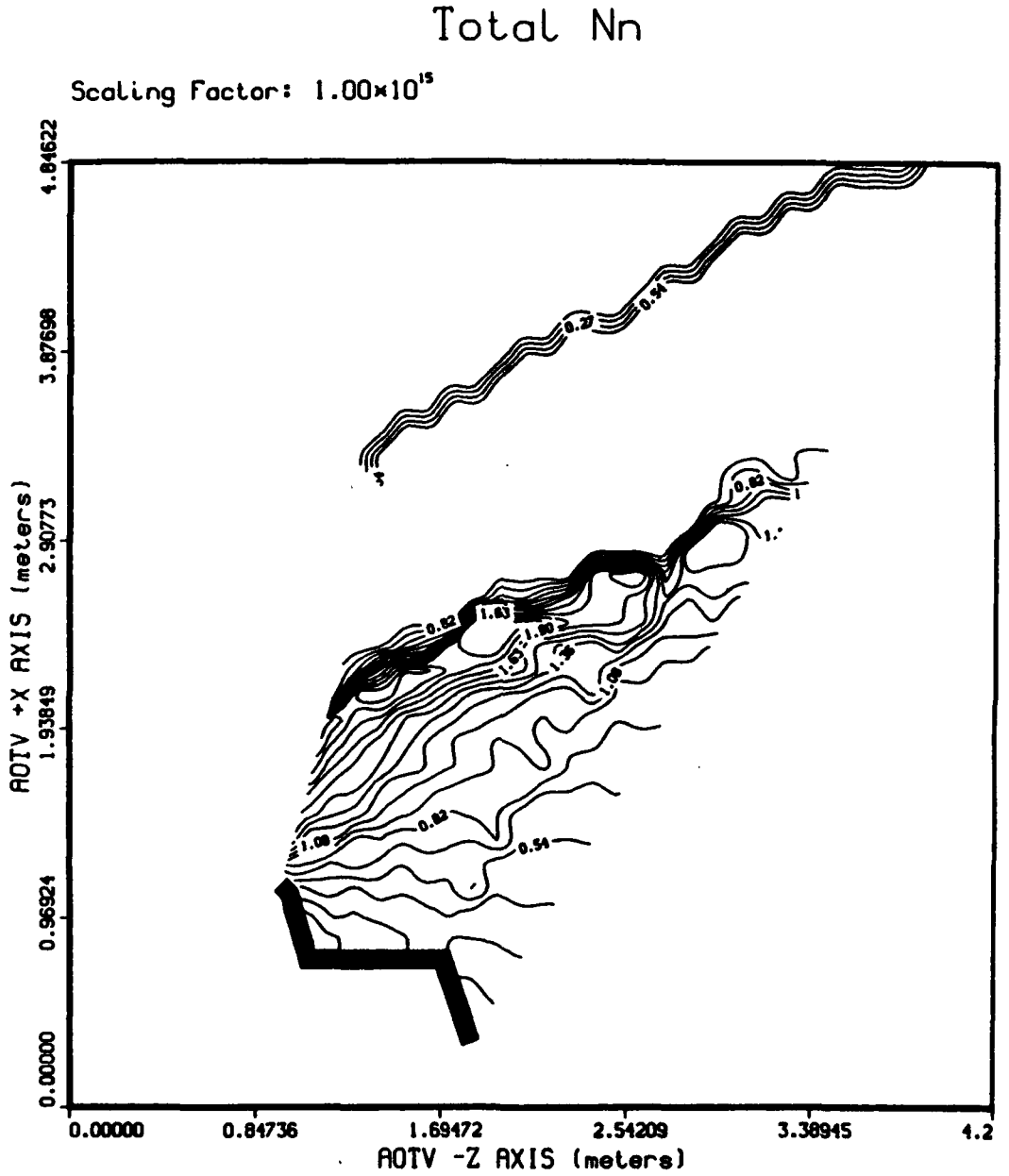

Fig. 36b. Results obtained by Gnoffo

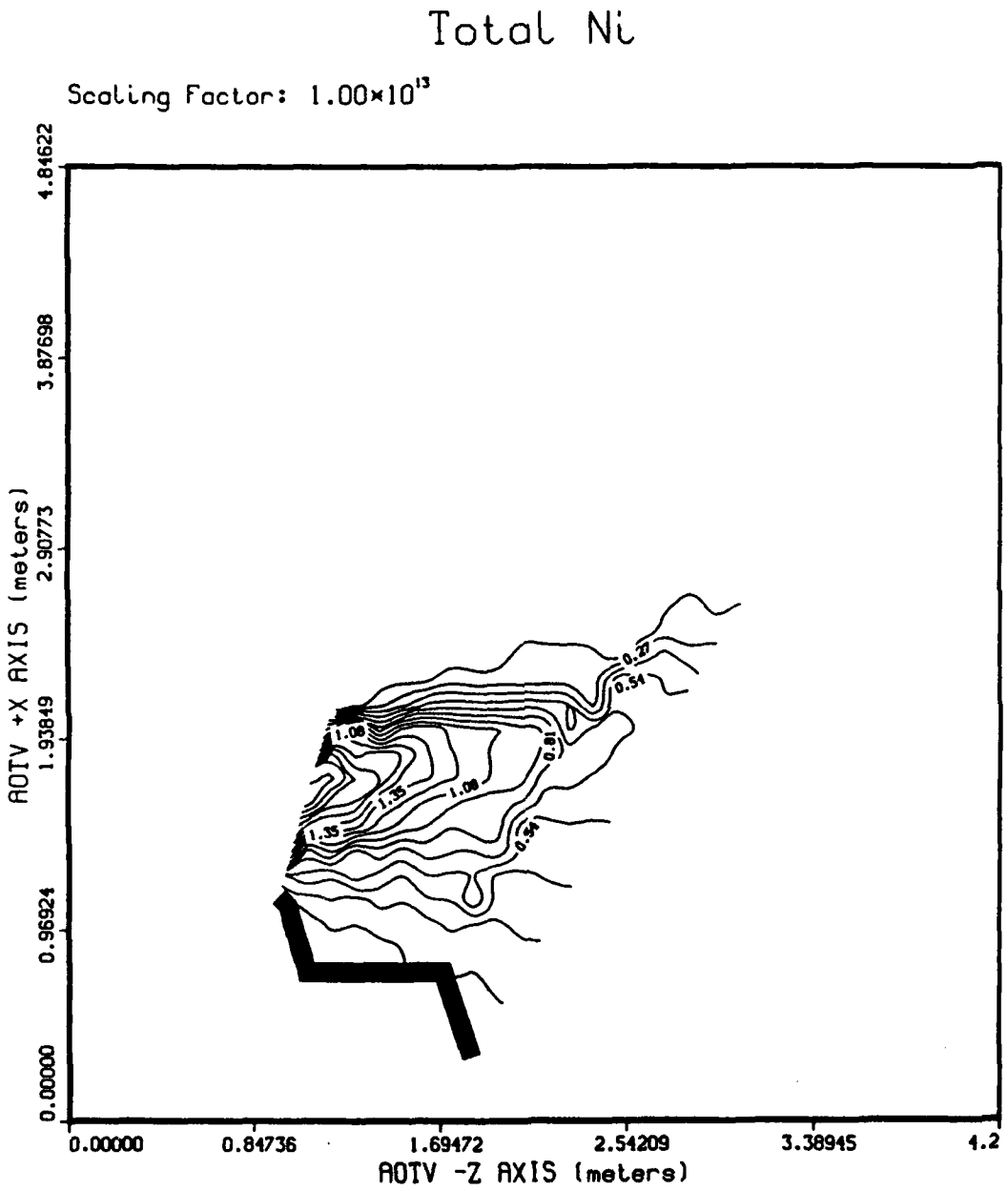

Fig. 36c. Results obtained by Gnoffo

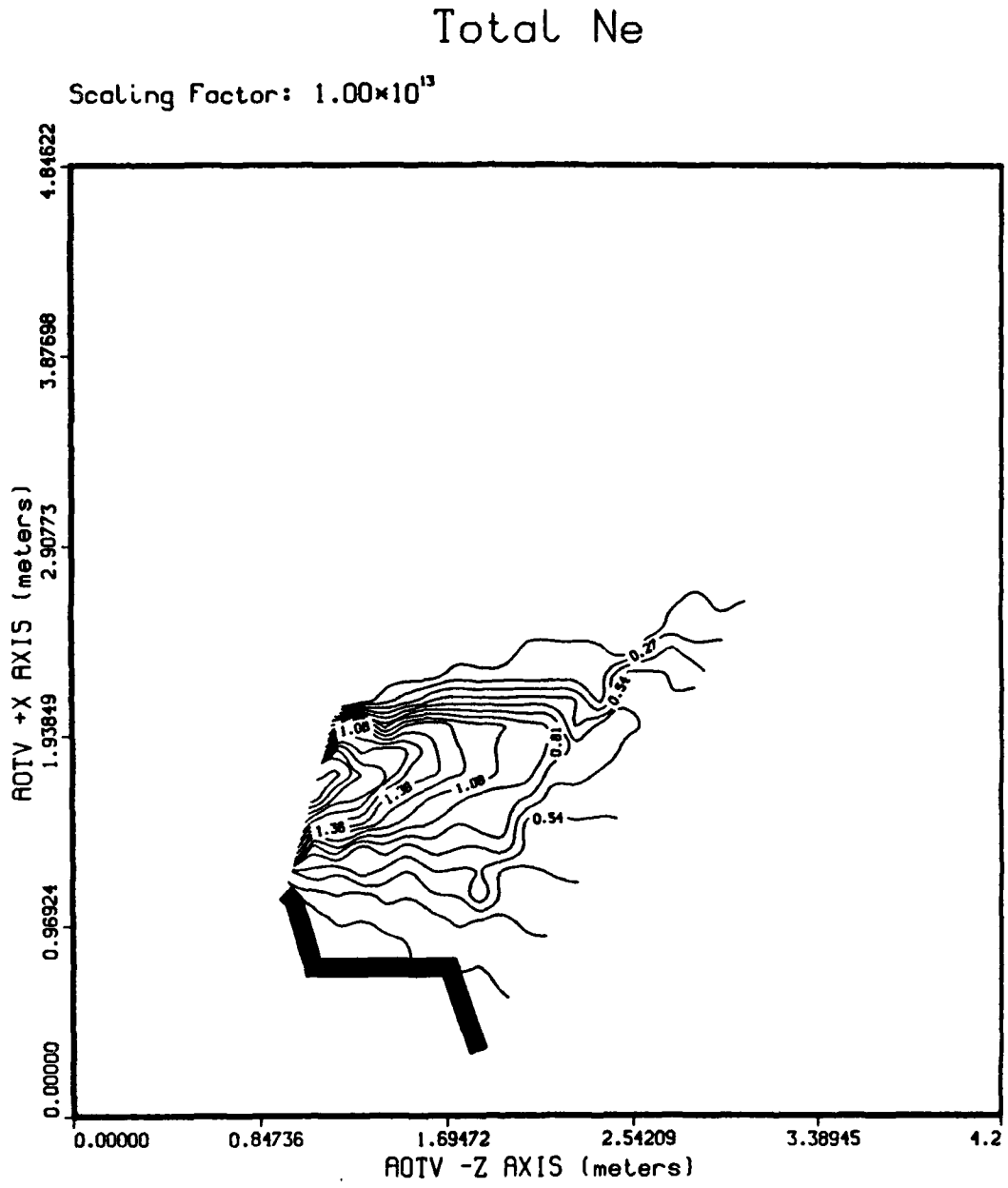

Fig. 36d. Results obtained by Gnoffo

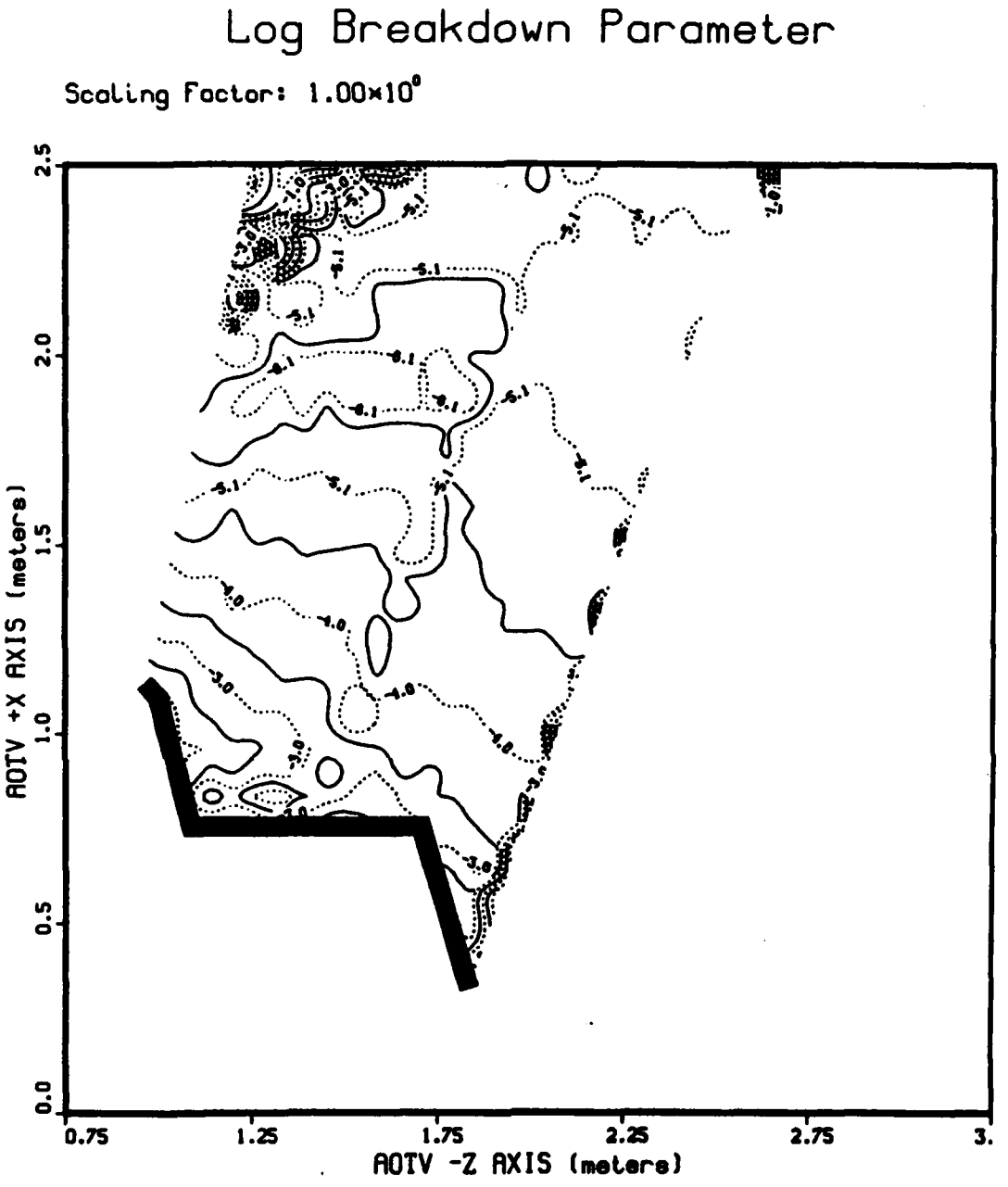

Fig. 36e. Results obtained by Gnoffo

monitor molecule duplication and removal across region boundaries, etc.

- Bird's code was specially designed to run on scalar computers such as personal computers or minicomputers. On these machines, typical computer runs are very long, on the order of several days. To make the code more like an engineering tool, supercomputers should be used and attempts should therefore be made to vectorize the source code.
- Do a more extensive literature search on wake flow in hypersonic and rarefied gas conditions. An initial computer search done with NASA RECON revealed no relevant material, but further work in this area is warranted.

8. Conclusions

Characterizing the expansion of SF_6 gases into the wake of the Aerobraking Orbital Transfer Vehicle is a very complex problem. This expansion depends strongly upon the flow characteristics of the ambient air, which has previously been subjected to a very intense shock wave and to momentum and thermal exchange with the body surface. Our approach to this problem has therefore been a step by step approach.

The first task consisted of simulating the expansion of the ambient air into the wake of the AOTV. Since the gas in the wake of an AOTV remains in rarefied conditions throughout the passage of the vehicle through the atmosphere, we tried using Bird's DSMC code, which has been widely accepted in the rarefied gas flow community, to perform this first task. Results shown in this report indicate that this code can satisfactorily represent the flow field in the wake of the AOTV. Many of the features here are similar to those observed in continuum wake flows. We are not able to attribute the absence of a corresponding feature or a difference in the intensity to the simulation numerics (physics simulation in the code and code implementation) or the actual physics (less transport of vorticity in transition than in continuum). Further work in this area is warranted, such as determining the effect of the computational grid structure on the results.

The second task examined the flow of the SF_6 gas into the air flow field background. Would the SF_6 be confined to the vortex region and "leak" through the neck at the foot of the wake flow, or would the SF_6 gas flow "overpower" the air flow and destroy the recirculation vortices? We performed a numerical experiment of this, adding a SF_6 source into the DSMC simulation of the air flow. Results shown in this report indicate that, for a SF_6 injection flux sufficient to ensure a 1% SF_6/air mole fraction over a fairly large volume, the SF_6 is the dominant species controlling the flow near the vehicle, is well mixed with the ambient gas, and is largely confined to the wake.

These two tasks were preliminary steps which allowed us to develop and test our simulation tools, and to explore the fundamental physics involved in hypersonic rarefied wake flows. In view of the present results, the following two tasks should now be performed to obtain a good first order estimate of the potential of injecting SF_6 to alleviate blackout:

- Perform simulations in 3-D (assuming axisymmetric geometry).
- Anchor these simulations to the results obtained by NASA-Langley for the ram flow field.

Further improvements in these simulations could be made at a later stage in two areas:

- Include chemistry between elections and SF_6. These chemical kinetics can be entered readily into the DSMC simulation code.
- Introduce electric and magnetic fields in the simulation. The present DSMC code does not allow this. However, SAIC is in the process of merging the DMSC code with proprietary particle-in-a-cell (PIC) codes for simulating problems involving electromagnetic fields and ionized plasmas.

References

1. Szuszczewicz, E. and D. Rault, "Feasibility of Radio Blackout Mitigation in the Braking Phase of AOTV Operations," Year End Contract Report, TRN 03005 (30 September 1987).
2. Berger, S. A., Laminar Wakes, American Elsvier Publishing Company, New York (1971).
3. Berman, H. A., J. D. Anderson, and J. P. Drummond, "Supersonic Flow Over a Rearward Facing Step with Transverse Nonreacting Hydrogen Injection," AIAA Journal 21, 12 (1983).
4. Eidelman, S., P. Collela, and R. P. Shreeve, "Applications of the Godunov Method and Its Second Order Extension to Cascade Flow Modelling," AIAA Journal 22, 10 (1984).
5. Eidelman, S., "The Problem of Gradual Opening in Wave Rotor Passage," J. Propulsion and Power 1, 3 (January 1985).
6. Eidelman, S., and R. P. Shreeve, "Numerical Modelling of the Nonsteady Thrust Produced by Intermittent Pressure Rise in a Diverging Channel," ASMA Winter Annual Meeting, New Orleans (1984).
7. Schlickting, S., Boundary Layer Theory, McGraw-Hill, New York (1968).
8. Bird, G., "General Programs for Numerical Simulation of Rarfied Gas Flows," (January 5, 1988).
9. Bird, G., Molecular Gas Dynamics, Clarendon Press, Oxford (1976).
10. Moss, J. and J. N. Price, "Direct Simulation of Radiative and Convective Heating for an Aeroassist Flight Experiment Vehicle," Sixteenth International Symposium on Rarefied Gas Dynamics, Pasadena, California (July 1988).
11. Celenligil, J., M. Moss, and G. Bird, "Direct Simulation of Three-Dimensional Flow About an Aeroassist Flight Experiment Vehicle," Sixteenth International Symposium on Rarefied Gas Dynamics, Pasadena, California (July 1988).
12. Gnoffo, P., private communication.
13. Bird, G., "Direct Simulation of Gas Flows at the Molecular Level," First World Congress on Computational Mechanics, University of Texas, Austin (September 1986).
14. Borganakke, C., and P. S. Larsen, "Statistical Collision Model for Monte Carlo Simulation of a Polyatonic Gas Mixture," J. Comp. Phys. 18, 405-420 (1979).

BLANK

Appendix A
Direct Simulation Monte Carlo (DSMC) Model

Direct Simulation Monte Carlo (DSMC) Model

A Monte Carlo method is a generic method based on random numbers. The Direct Simulation Monte Carlo method (DSMC) method tracks the gas molecules and treats the collisions between molecules and betweem molecules and the walls in a probabilistic manner (as opposed to deterministic), with random numbers used to evaluate the probability of a given event.

In this appendix, the DSMC method is first described for the simplest gas, i.e., a monatomic gas, with no internal degrees of freedom. In the second part, we describe the extension of the method to gases with internal energy, nonequilibrium, chemical reactions, ionization and radiation transport.

1. Monatomic Gas Simulation

The DSMC model is a particle simulation in which a very small sample of the gas molecules is selected and tracked as they collide with themselves and the wall boundaries in a simulated physical space in which all the other molecules have been removed. The gas is therefore assumed to be composed of N "simulated molecules," with N being such that the density of simulated molecules is on the order of 10-100 per cubic mean free path. (At 1 mTorr, the gas density is 10^{14} per cubic mean free path in a real gas). The value of N is a compromise between high values, which are computer time and storage intensive, and low values, which lead to exceedingly high fluctuations for the macroscopic thermodynamic and flow quantities.

1.1 Computational Grid Definition and Time Step

Just like for a continuum hydrocode, the flowfield around the body is broken down into a grid-like arrangement of cells, the size of which is typically 1/3 to 1/2 the local mean free path. The simulation is performed using a time step, Δt, which is typically on the order of 1/3 to 1/2 of the mean collision time given by $1/\sigma N V_r$, where σ is the molecular kinetic cross section and V_r is the relative velocity between the two molecules.

1.2 Molecular Motion

To help in tracking the simulated molecules, the physical motion of the molecules and the collision events are treated as independent events. The flow is "frozen" while the collisions are treated as described below. At the end of the time step, the molecules are moved according to the actual velocities they have after the collisions, namely,

$$\Delta x_i^j = V_i^j \Delta t$$

where V_i^j is the velocity component in the coordinate i for the simulated molecule j, and, Δx_i^j is the increment in the coordinate i for the molecule j. The computed coordinates are checked to identify collisions of molecules with the wall, and wall reflection is treated as described below.

1.3 Intermolecular collision modelling

Collisions are considered only between a given simulated molecule and its nearest neighbors, namely molecules belonging to the same cell. Since each simulated molecule in fact represents a large number of actual molecules, the simulated molecules should be viewed as a class of molecules within the cell, characterized by a certain range of velocity vectors. Hence, when dealing with collisions, the computed location of the molecules within the cell is ignored. For a given molecule, collision partners are selected with a probability proportional to the relative velocity between the collision partners. The collision mechanics are computed exactly, assuming hard sphere collisions that conserve momentum. The collision angles are selected at random between 0 and 2π. This Variable Hard Sphere (VHS) model has been adopted for DMSC because it has been shown that, for engineering problems, the angular scattering characteristics have little input on the flowfield solution.

1.4 Wall reflection

The physics of molecule-wall interaction is very complex and poorly known. Two simple models are used in DSMC, namely diffuse and specular reflections. In a specular reflection, the gas molecules do not transfer energy or parallel momentum to the wall, only normal momentum. In a diffuse reflection, the molecules lose all "memory" of their pre-collision velocity and are reflected back with an isotropic angular pattern and a Maxwellian velocity magnitude distribution at a temperature T_w. If full thermal accommodation is assured, T_w is the wall temperature. There is experimental evidence, however, that these two asymptotic models are inadequate in many instances, and that the flowfield is very sensitive to the gas- wall interaction model used.

1.5 Startup and Termination of the Simulation

The DSMC is always a nonsteady simulation which evolves from a well defined state to a steady state. The initial state, for example, could be a uniform flow velocity throughout, or a vacuum and uniform velocity combination. The characteristics of the simulated molecules in the initial state are selected at random, velocity components are selected from a drifted Maxwellian distribution and the molecular positions within the cell are chosen with equiprobability in each dimension.

The simulation is terminated when steady state is reached, i.e., when some macro-

scopic properties, such as heat transfer to the body walls, have reached asymptotic values.

1.6 Computer Time and Storage Requirements

For a typical problem, the DSMC model involves the simultaneous computation of the trajectories of thousands of simulated molecules, for which velocity components, position coordinates, and possibly internal energy status, species composition, etc., must be stored.

Use can be made of the flowfield symmetry and dimensionality (1-D, 2-D, 3-D) to decrease the storage requirements. The collisions, however, are always treated as 3-D phenomena, and the three velocity components of each molecules must be stored. Typically, machine storage limitation (for micro and minicomputers) restrict the number of cells to a few thousand so that a compromise must be made between the available machine storage and the desired flowfield resolution.

For a given body geometry, computation requirements increase significantly with increasing freestream density since both the time step and the cell size must be reduced, while the number of simulated molecules must remain constant.

1.7 Recent Development of the Method

When high density gases expand into a space vacuum, the gas density may vary by several orders of magnitude within the flowfield of interest. To solve such problems with the DSMC method, Bird (Ref. 9) proposes a computational scheme whereby low density regions are associated with longer time steps and a lower ratio of real to simulated molecules, so that, on the average, the flux across cell boundaries is conserved.

2. Complex Simulation

The rotational excitation and relaxation model implemented in the DSMC code is based on the scheme proposed by Borgnakke and Larsen (Ref. 14). This model, which satisfies the principle of detailed balancing, regards a fraction of the collisions as inelastic, with the new rotational energies of the collision partners sampled from the equilibrium rotational energy distribution of the gas (Local Thermodynamic Equilibrium). The relative translational energy of the collision partners sets the temperature of the rotational energy distribution. The fraction of inelastic collision is chosen to match the real gas rotational relaxation rate. Bird admits that this phenomenological model is not physically realistic, but it is simple and gives "satisfactory results in all applications."

The vibrational and electronic excitation and relaxation mechanisms can also be implemented with Borgnakke and Larsen's scheme. Alternatively, the molecules in

different energy states can be treated as different species.

2.1 Chemical Reactions

The particle nature of the DSMC model makes it particularly well suited to treatment of chemical reactions with a chemical physics approach. Chemical reactions occur if the relative energy of the collision partners is larger than some activation energy, with a probability proportional to the ratio of chemical to kinetic cross sections. This ratio, which is itself a function of the relative energy of the collision, can be determined from chemical rate data, when available.

2.2 Charged Particles and Ionization

Ionization can be treated as a chemical reaction. Electrons, however, are very mobile due to their low mass, so special procedures are needed to track them. In regions of the flowfield where the Debye length is much smaller than the local mean free path, each electron can be assumed to be "glued" to a given ion. In regions characterized by large gradients (gradient scale smaller than the Debye length), ambipolar diffusion must be allowed to occur. The ambipolar electric field E can be computed from the electron density distributions, n_e, using

$$E = \frac{kT_e}{e} \Delta n_e / n_e.$$

In these regions of large gradients, electrons and ions are therefore subjected not only to collisions, but also to a "restoring" electric field.

BLANK

Appendix B
Diagnostics Developed for DMSC Code

Diagnostics Developed for DMSC Code

The DSMC code developed by Bird is not easily mastered. The physics are undoubtedly well represented in the code, as witnessed by the coherent results obtained by the many users in the engineering community. Any user would like to monitor the time evaluation of the code and ensure a proper initial setup so that the code can be made to run in the most optimal conditions with regards to computer time and required memory.

Graphics produced by the SAIC-developed diagnostic routines allows us to quickly verify the input data file, and therefore, easily spot any serious input data error. They also allow us to check the gas velocity, density, and temperature at all inlets, all surface characteristics (accommodation coefficients, temperature, outgasing, absorption), etc. (See Figs. 11 and 16 in this report).

The time evaluation of the code during a run can be monitored with Figs. B1 through B6. Figure B1 shows the number of simulated molecules in each cell at a given time. These numbers are color coded from red (for too low a number) to black (for too high a number). The number of simulated molecule in a cell should be about 10. Higher numbers unduly penalize computer time and memory, whereas lower numbers impair the statistics for both collisions and macroscopic property evaluation. (Note that numbers are limited at 99 on the graph.) Fig. B2 is similar to Fig. B1, but represents the number of simulated molecules averaged over the time interval from the initial time to the present. The same remarks apply as to the optimal number of simulated molecules per cell.

Figs. B3 and B4 give the ratio of the local mean free path to the cell size in both the horizontal and vertical directions. Proper operation of the code requires that this number to be about 3. Lower values tend to smear gradients while higher values unduly penalize computer time and memory. In a high vorticity region, howerver, higher values are desirable. These numbers can be adjusted in each region by varying the local value of the ratio of the number of real molecules to simulated molecules.

Figs. B5 and B6 represent the ratio of the cell size in both horizontal and vertical directions to the distance transversed by a molecule during a time step. To ensure proper collision dynamics, this number should be about 3. These numbers can be adjusted in each region by varying the local clock time increment.

These diagnostic tools allowed us to tune the code to run under optimal conditions, and, if necessary, place emphasis on specific regions within the computational domain.

PR= 31 NPRNT= 12 (IFX= 0 IOS= 0 INS= 0 RWF= 0.00 NIS= 10 NSP= 10 NPS= 11)

FNUM()= 15.3/ 15.3/ 13.3/ 15.8/ 14.8/ 14.7/ 15.0/ 13.3/ 13.7/
DTM()= -5.0/-5.3/-4.2/-4.7/-4.0/-4.7/-4.7/-3.9/-3.9/
TIME()= -1.4/-1.7/-0.6/-1.1/-0.4/-1.1/-1.1/-0.3/-0.3/
DUPLIC(W.R.T. REG. 2)= 0.3/ 0.0/ 3.0/ 0.1/ 1.8/ 1.2/ 0.9/ 3.4/ 3.0/

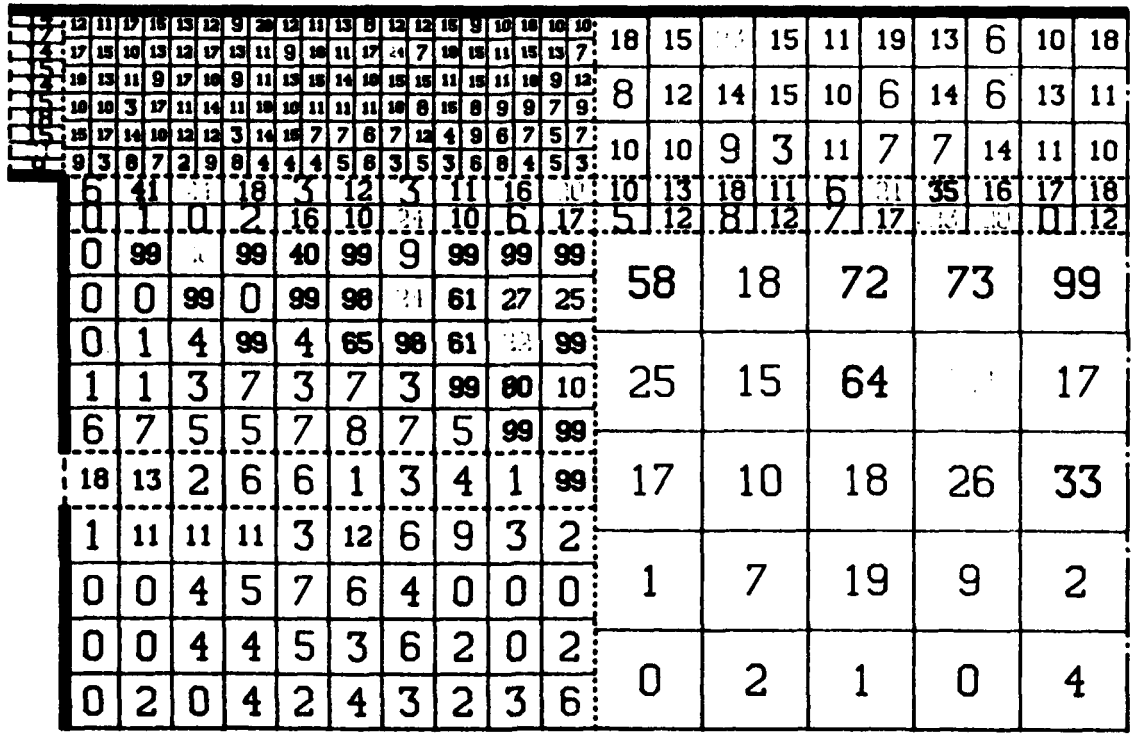

PRESENT SIMULATED MOLECULE TABLE DATE=22-Sep-88

SPECIES * MEAN TIME= 09:59:14 RUN * PROF7

Fig. B1 Diagnostics/Number of simulated molecules (present).

PR= 31 NPRNT= 12 (IFX= 0 IOS= 0 INS= 0 RWF= 0.00 NIS= 10 NSP= 10 NPS= 11)

FNUM()= 15.3/ 15.3/ 13.3/ 15.8/ 14.8/ 14.7/ 15.0/ 13.3/ 13.7/
DIM()= -5.0/-5.3/-4.2/-4.7/-4.0/-4.7/-4.7/-3.9/-3.9/
TIME()= -1.4/-1.7/-0.6/-1.1/-0.4/-1.1/-1.1/-0.3/-0.3/
DUPLIC(W.R.T. REG. 2)= 0.3/ 0.0/ 3.0/ 0.1/ 1.8/ 1.2/ 0.9/ 3.4/ 3.0/

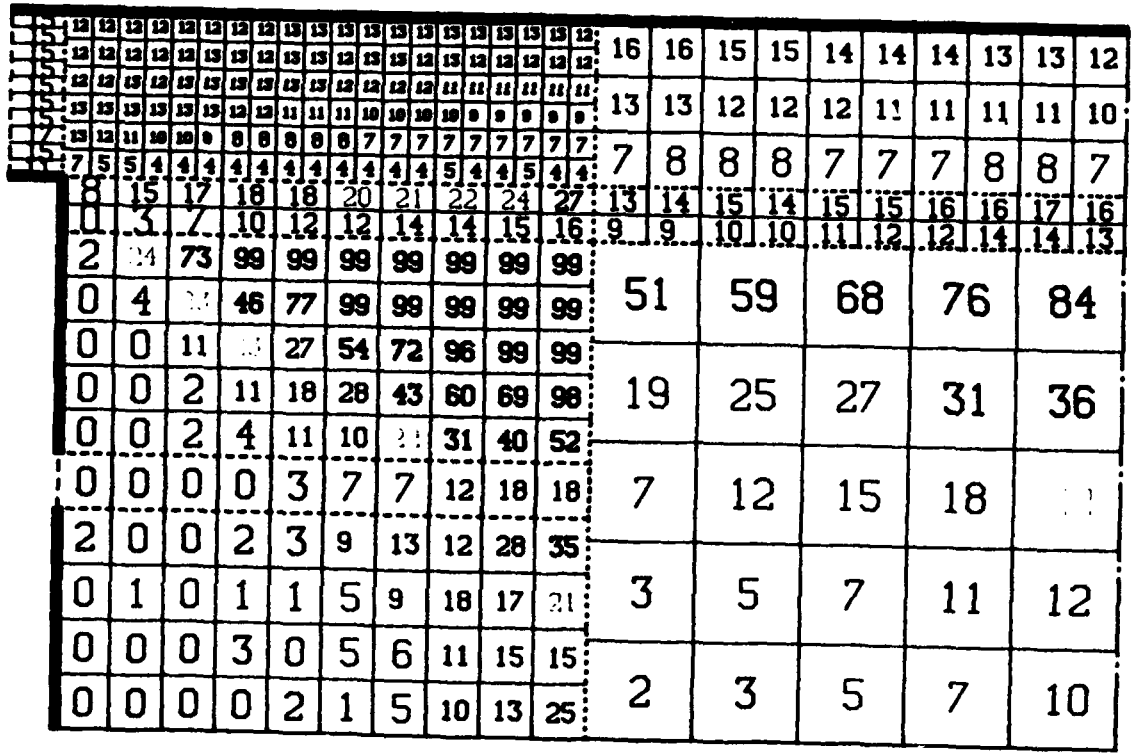

TIME AVERAGE SIMULATED MOLECULE TABLE DATE-22-Sep-88

SPECIES # 1 TIME- 09:59:14 RUN # PROF7

Fig. B2 Diagnostics/Number of simulated molecules (time mean).

PR= 31 NPRNT= 12 (IFX= 0 IOS= 0 INS= 0 RWF= 0.00 NIS= 10 NSP= 10 NPS= 11)

FNUM()= 15.3/ 15.3/ 13.3/ 15.8/ 14.8/ 14.7/ 15.0/ 13.3/ 13.7/
DTM()= -5.0/-5.3/-4.2/-4.7/-4.0/-4.7/-4.7/-3.9/-3.9/
TIME()= -1.4/-1.7/-0.6/-1.1/-0.4/-1.1/-1.1/-0.3/-0.3/
DUPLIC(W.R.T. REG. 2)= 0.3/ 0.0/ 0.0/ 3.0/ 0.1/ 1.8/ 1.2/ 0.9/ 3.4/ 3.0/

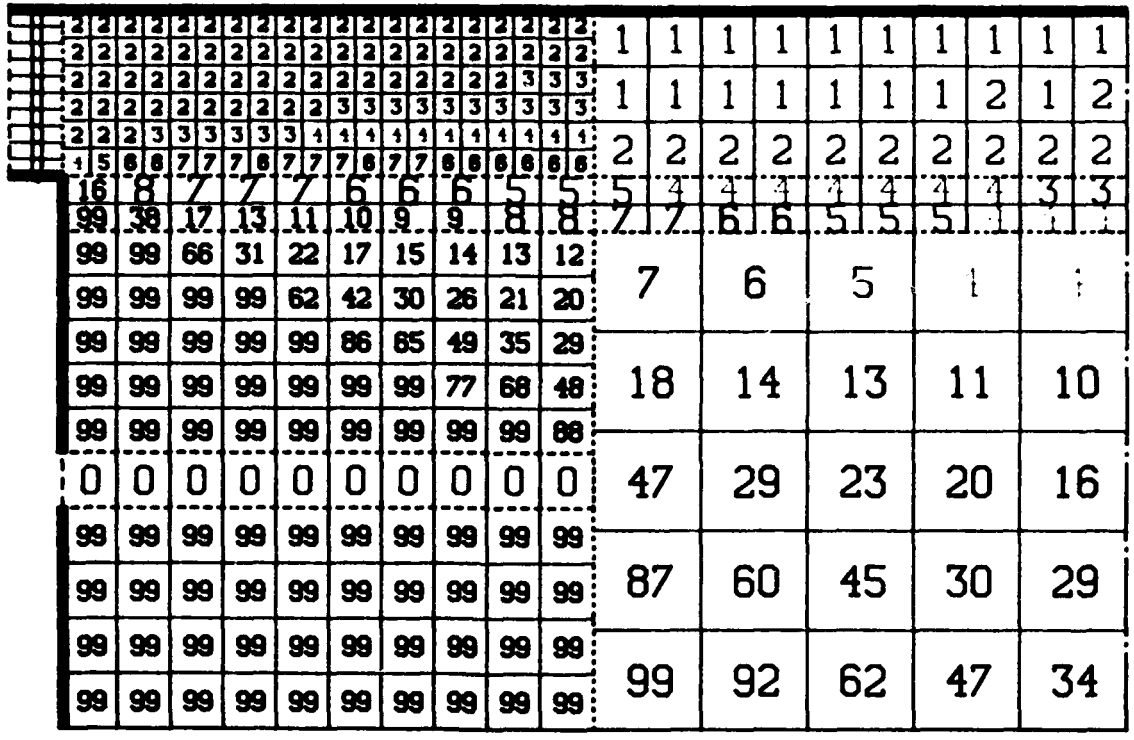

Fig. B3 Diagnostics/Comparison of cell size to mean free path (horizontal).

PR= 31 NPRNT= 12 (IFX= 0 IOS= 0 INS= 0 RWF= 0.00 NIS= 10 NSP= 10 NPS= 11)

FNUM()= 15.3/ 15.3/ 13.3/ 15.8/ 14.8/ 14.7/ 15.0/ 13.3/ 13.7/
DTM()= -5.0/-5.3/-4.2/-4.7/-4.0/-4.7/-4.7/-3.9/-3.9/
TIME()= -1.4/-1.7/-0.6/-1.1/-0.4/-1.1/-1.1/-0.3/-0.3/
DUPLIC(W.R.T. REG. 2)= 0.3/ 0.0/ 3.0/ 0.1/ 1.8/ 1.2/ 0.9/ 3.4/ 3.0/

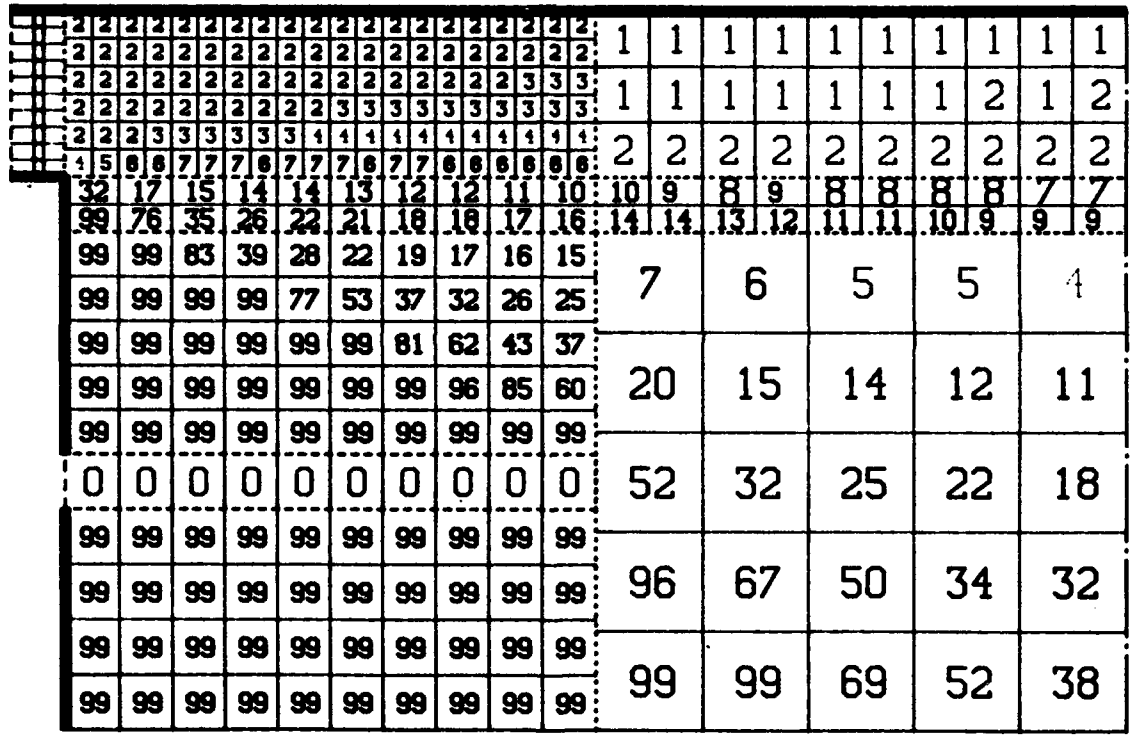

Fig. B4 Diagnostics/Comparison of cell size to mean free path (vertical).

PR= 31 NPRNT= 12 (IFX= 0 IOS= 0 INS= 0 RWF= 0.00 NIS= 10 NSP= 10 NPS= 11)

FNUM()= 15.3/ 15.3/ 13.3/ 15.8/ 14.8/ 14.7/ 15.0/ 13.3/ 13.7/
DTM()= -5.0/-5.3/-4.2/-4.7/-4.0/-4.7/-4.7/-3.9/-3.9/
TIME()= -1.4/-1.7/-0.6/-1.1/-0.4/-1.1/-1.1/-0.3/-0.3/
DUPLIC(W.R.T. REG. 2)= 0.3/ 0.0/ 3.0/ 0.1/ 1.8/ 1.2/ 0.9/ 3.4/ 3.0/

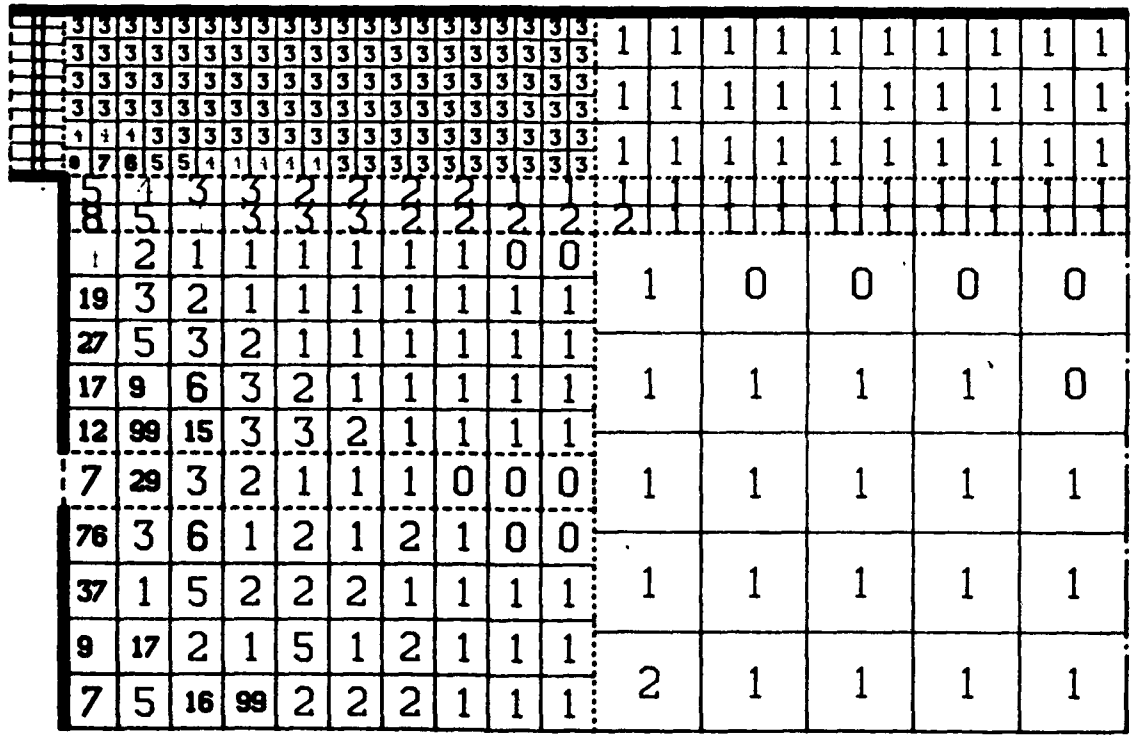

Fig. B5 Diagnostics/Comparison of cell size to horizontal distance.

PR= 31 NPRNT= 12 (IFX= 0 IOS= 0 INS= 0 RWF= 0.00 NIS= 10 NSP= 10 NPS= 11)

FNUM()= 15.3/ 15.3/ 13.3/ 15.8/ 14.8/ 14.7/ 15.0/ 13.3/ 13.7/
DTM()= -5.0/-5.3/-4.2/-4.7/-4.0/-4.7/-4.7/-3.9/-3.9/
TIME()= -1.4/-1.7/-0.6/-1.1/-0.4/-1.1/-1.1/-0.3/-0.3/
DUPLIC(W.R.T. REG. 2)= 0.3/ 0.0/ 3.0/ 0.1/ 1.8/ 1.2/ 0.9/ 3.4/ 3.0/

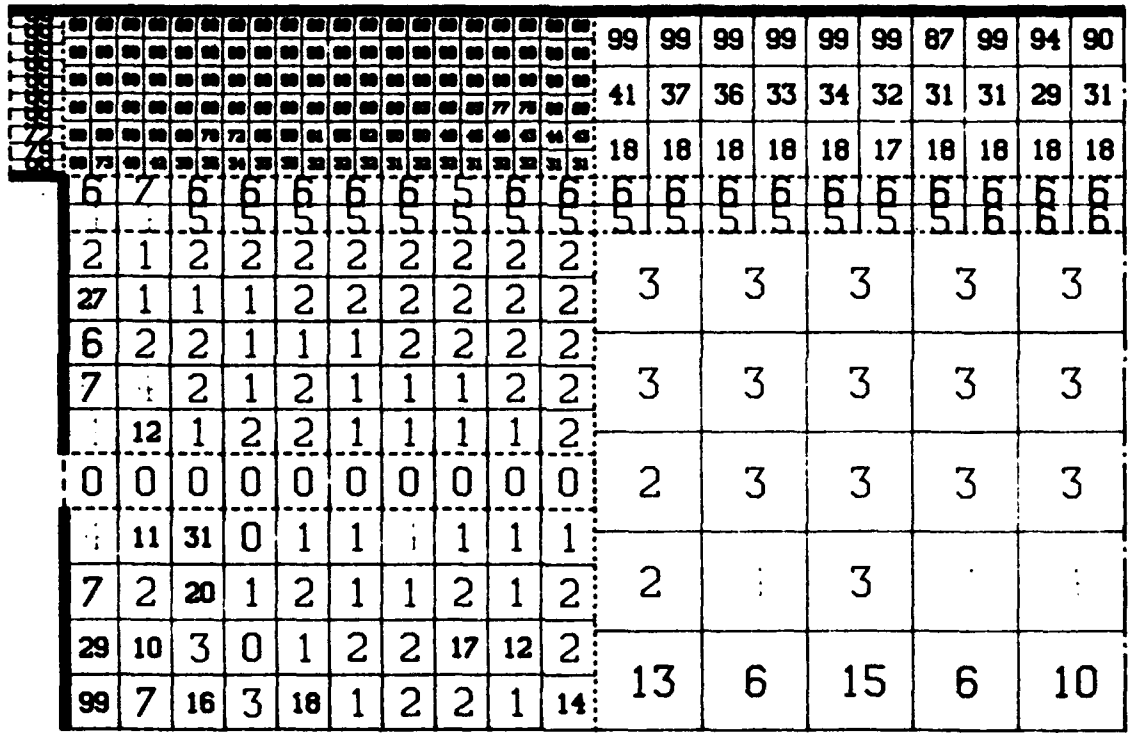

RATIO OF CELL SIZE Y / MEAN VEL. *DTM DATE-22-Sep-88

SPECIES * 1 TIME- 11:31:58 RUN * PROF7

Fig. B6 Diagnostics/Comparison of cell size to vertical distance.

Appendix C
Input Data Files

Data Deck for Computational Case #1

```
 &GENERAL
  IFX=0
  IQS=0
  MAXM=10000
  INS=0
  NIS=10
  NSP=10
  NPS=10
  NPT=10000
 &END
 &INIT
  ISQ=1
  VFX=1300.,VFY=0.,FND=1.E+19,FTMP=300.,FRACT(1)=1.
 &END
 &GAS
  NSS=1
  NSSR=1
 &END
 &GRID
  NREG=4
 &END
 &REGIONS
  FNUM(1)=1.E+16,DTM(1)=0.0001
    NC13(1)=1,NSC13(1)=1,NC24(1)=3,NSC24(1)=1
    NTS1(1)=2,XP1(1,1)=-0.1,YP1(1,1)=0.0,XP1(2,1)=0.0,YP1(2,1)=0.0,
      SZ1(1)=1.,NPR1(1)=1,NPS1(1)=1
    NTS3(1)=2,XP3(1,1)=-0.1,YP3(1,1)=0.3,XP3(2,1)=0.0,YP3(2,1)=0.3,
      SZ3(1)=1.,NPR3(1)=1,NPS3(1)=1
    NTS2(1)=1,
    NTS4(1)=1
    WT42(1)=1
  FNUM(2)=.2E+16,DTM(2)=0.00005
    NC13(2)=20,NSC13(2)=2,NC24(2)=6,NSC24(2)=2
    NTS1(2)=2,XP1(1,2)=0.0,YP1(1,2)=0.0,XP1(2,2)=1.0,YP1(2,2)=0.0,
      SZ1(2)=1.,NPR1(2)=1,NPS1(2)=1
    NTS3(2)=2,XP3(1,2)=0.0,YP3(1,2)=0.3,XP3(2,2)=1.0,YP3(2,2)=0.3,
      SZ3(2)=1.,NPR3(2)=1,NPS3(2)=1
    NTS2(2)=1,
    NTS4(2)=1
    WT42(2)=1
  FNUM(3)=2.E+15,DTM(3)=0.0001
    NC13(3)=20,NSC13(3)=4,NC24(3)=10,NSC24(3)=4
    NTS1(3)=2,XP1(1,3)=0.0,YP1(1,3)=-1.0,XP1(2,3)=2.0,YP1(2,3)=-1.0,
      SZ1(3)=1.,NPR1(3)=1,NPS1(3)=1
    NTS3(3)=2,XP3(1,3)=0.0,YP3(1,3)=0.0,XP3(2,3)=2.0,YP3(2,3)=0.0,
      SZ3(3)=1.,NPR3(3)=1,NPS3(3)=1
    NTS2(3)=1,
    NTS4(3)=1
    WT42(3)=1
  FNUM(4)=.2E+16,DTM(4)=0.0001
    NC13(4)=10,NSC13(4)=1,NC24(4)=3,NSC24(4)=1
    NTS1(4)=2,XP1(1,4)=1.0,YP1(1,4)=0.0,XP1(2,4)=2.0,YP1(2,4)=0.0,
      SZ1(4)=1.,NPR1(4)=1,NPS1(4)=1
    NTS3(4)=2,XP3(1,4)=1.0,YP3(1,4)=0.3,XP3(2,4)=2.0,YP3(2,4)=0.3,
      SZ3(4)=1.,NPR3(4)=1,NPS3(4)=1
    NTS2(4)=1,
    NTS4(4)=1
    WT42(4)=1
 &END
 &BOUNDARY
  MK(1,1)=5,MK(2,1)=3,MK(3,1)=5,MK(4,1)=7
    XGASVEL(1,2,1)=500.
    YGASVEL(1,2,1)=0.
```

```
   TEMPGAS(1,2,1)=300.
   DENSGAS(1,2,1)=1.E+19
   FRACTS(1,1,2,1)=1.
   MZ(1,1)=0.,MZ(3,1)=0.
   SURFTEMP(1,1,1)=300.,SURFTEMP(1,3,1)=300.
   SPECDIF(1,1,1)=.5, SPECDIF(1,3,1)=.5
   ABSORBD(1,1,1,1)=0.,ABSORBD(1,1,3,1)=0.
   KSIDE(4,1)=1,JSIDE(1,4,1)=2,IREGION(1,4,1)=2
 MK(1,2)=7,MK(2,2)=7,MK(3,2)=5,MK(4,2)=7
   MZ(3,2)=0.
   SURFTEMP(1,3,2)=300.
   SPECDIF(1,3,2)=.5
   ABSORBD(1,1,3,2)=0.
   KSIDE(1,2)=1,JSIDE(1,1,2)=3,IREGION(1,1,2)=3
   KSIDE(2,2)=1,JSIDE(1,2,2)=4,IREGION(1,2,2)=1
   KSIDE(4,2)=1,JSIDE(1,4,2)=2,IREGION(1,4,2)=4
 MK(1,3)=2,MK(2,3)=5,MK(3,3)=7,MK(4,3)=8
   MZ(1,3)=0., MZ(2,3)=0.
   SURFTEMP(1,1,3)=300.,SURFTEMP(1,2,3)=300.
   SPECDIF(1,1,3)=.5,SPECDIF(1,2,3)=.5
   ABSORBD(1,1,1,3)=0.,ABSORBD(1,1,2,3)=0.
   KSIDE(3,3)=2,JSIDE(1,3,3)=1,IREGION(1,3,3)=2,
                JSIDE(2,3,3)=1,IREGION(2,3,3)=4
 MK(1,4)=7,MK(2,4)=7,MK(3,4)=5,MK(4,4)=8
   MZ(3,4)=0.
   SURFTEMP(1,3,4)=300.
   SPECDIF(1,3,4)=.5
   ABSORBD(1,1,3,4)=0.
   KSIDE(1,4)=1,JSIDE(1,1,4)=3,IREGION(1,1,4)=3
   KSIDE(2,4)=1,JSIDE(1,2,4)=4,IREGION(1,2,4)=2
&END
```

Data Deck for Computational Case #2

```
$GENERAL
        IFX=0
        IQS=0
         MAXM=60000
         INS=0
         NIS=10
         NSP=10
         NPS=10
         NPT=30
$END
$INIT
        ISQ=1
        VFX=8000.,VFY=0.,FND=1.E+19,FTMP=300.,FRACT(1)=1.
$END
$GAS
        NSS=2
        NSSR=6
$END
$GRID
        NREG=9
$END
$REGIONS
        FNUM(1)=.2E+16,DTM(1)=0.00001
          NC13(1)=1,NSC13(1)=1,NC24(1)=10,NSC24(1)=1
          NTS1(1)=2,XP1(1,1)=-0.1,YP1(1,1)=0.0,XP1(2,1)=0.0,YP1(2,1)=0.0,
            SZ1(1)=1.,NPR1(1)=1,NPS1(1)=1
          NTS3(1)=2,XP3(1,1)=-0.1,YP3(1,1)=0.3,XP3(2,1)=0.0,YP3(2,1)=0.3,
            SZ3(1)=1.,NPR3(1)=1,NPS3(1)=1
          NTS2(1)=1,
          NTS4(1)=1
          WT42(1)=1
        FNUM(2)=.2E+16,DTM(2)=0.000005
          NC13(2)=20,NSC13(2)=2,NC24(2)=6,NSC24(2)=2
          NTS1(2)=2,XP1(1,2)=0.0,YP1(1,2)=0.0,XP1(2,2)=1.0,YP1(2,2)=0.0,
            SZ1(2)=1.,NPR1(2)=1,NPS1(2)=1
          NTS3(2)=2,XP3(1,2)=0.0,YP3(1,2)=0.3,XP3(2,2)=1.0,YP3(2,2)=0.3,
            SZ3(2)=1.,NPR3(2)=1,NPS3(2)=1
          NTS2(2)=1,
          NTS4(2)=1
          WT42(2)=1
        FNUM(3)=.022E+15,DTM(3)=0.00006
          NC13(3)=10,NSC13(3)=4,NC24(3)=5,NSC24(3)=4
          NTS1(3)=2,XP1(1,3)=0.0,YP1(1,3)=-.5,XP1(2,3)=1.0,YP1(2,3)=-.5,
            SZ1(3)=1.,NPR1(3)=1,NPS1(3)=1
          NTS3(3)=2,XP3(1,3)=0.0,YP3(1,3)=-.1,XP3(2,3)=1.0,YP3(2,3)=-.1,
            SZ3(3)=1.,NPR3(3)=1,NPS3(3)=1
          NTS2(3)=1,
          NTS4(3)=1
          WT42(3)=1
        FNUM(4)=.6E+16,DTM(4)=0.00002
          NC13(4)=10,NSC13(4)=1,NC24(4)=3,NSC24(4)=1
          NTS1(4)=2,XP1(1,4)=1.0,YP1(1,4)=0.0,XP1(2,4)=2.0,YP1(2,4)=0.0,
            SZ1(4)=1.,NPR1(4)=1,NPS1(4)=1
          NTS3(4)=2,XP3(1,4)=1.0,YP3(1,4)=0.3,XP3(2,4)=2.0,YP3(2,4)=0.3,
            SZ3(4)=1.,NPR3(4)=1,NPS3(4)=1
          NTS2(4)=1,
          NTS4(4)=1
          WT42(4)=1
        FNUM(5)=.066E+16,DTM(5)=0.0001
          NC13(5)=5,NSC13(5)=2,NC24(5)=5,NSC24(5)=2
          NTS1(5)=2,XP1(1,5)=1.0,YP1(1,5)=-1.0,XP1(2,5)=2.0,YP1(2,5)=-1.0,
            SZ1(5)=1.,NPR1(5)=1,NPS1(5)=1
          NTS3(5)=2,XP3(1,5)=1.0,YP3(1,5)=-.1,XP3(2,5)=2.0,YP3(2,5)=-.1,
```

```
      SZ3(5)=1.,NPR3(5)=1,NPS3(5)=1
    NTS2(5)=1,
    NTS4(5)=1
    WT42(5)=1
  FNUM(6)=.05E+16,DTM(6)=0.00002
    NC13(6)=10,NSC13(6)=4,NC24(6)=2,NSC24(6)=2
    NTS1(6)=2,XP1(1,6)=0.0,YP1(1,6)=-.1,XP1(2,6)=1.0,YP1(2,6)=-.1,
      SZ1(6)=1.,NPR1(6)=1,NPS1(6)=1
    NTS3(6)=2,XP3(1,6)=0.0,YP3(1,6)=0.0,XP3(2,6)=1.0,YP3(2,6)=0.0,
      SZ3(6)=1.,NPR3(6)=1,NPS3(6)=1
    NTS2(6)=1,
    NTS4(6)=1
    WT42(6)=1
  FNUM(7)=.1E+16,DTM(7)=0.00002
    NC13(7)=10,NSC13(7)=2,NC24(7)=2,NSC24(7)=2
    NTS1(7)=2,XP1(1,7)=1.0,YP1(1,7)=-.1,XP1(2,7)=2.0,YP1(2,7)=-.1,
      SZ1(7)=1.,NPR1(7)=1,NPS1(7)=1
    NTS3(7)=2,XP3(1,7)=1.0,YP3(1,7)=0.0,XP3(2,7)=2.0,YP3(2,7)=0.0,
      SZ3(7)=1.,NPR3(7)=1,NPS3(7)=1
    NTS2(7)=1,
    NTS4(7)=1
    WT42(7)=1
  FNUM(8)=.02E+15,DTM(8)=0.00012
    NC13(8)=10,NSC13(8)=4,NC24(8)=4,NSC24(8)=4
    NTS1(8)=2,XP1(1,8)=0.0,YP1(1,8)=-1.,XP1(2,8)=1.0,YP1(2,8)=-1.,
      SZ1(8)=1.,NPR1(8)=1,NPS1(8)=1
    NTS3(8)=2,XP3(1,8)=0.0,YP3(1,8)=-.6,XP3(2,8)=1.0,YP3(2,8)=-.6,
      SZ3(8)=1.,NPR3(8)=1,NPS3(8)=1
    NTS2(8)=1,
    NTS4(8)=1
    WT42(8)=1
  FNUM(9)=.05E+15,DTM(9)=0.00012
    NC13(9)=10,NSC13(9)=4,NC24(9)=1,NSC24(9)=4
    NTS1(9)=2,XP1(1,9)=0.,YP1(1,9)=-.6,XP1(2,9)=1.0,YP1(2,9)=-.6,
      SZ1(9)=1.,NPR1(9)=1,NPS1(9)=1
    NTS3(9)=2,XP3(1,9)=0.,YP3(1,9)=-.5,XP3(2,9)=1.0,YP3(2,9)=-.5,
      SZ3(9)=1.,NPR3(9)=1,NPS3(9)=1
    NTS2(9)=1,
    NTS4(9)=1
    WT42(9)=1
$END
$BOUNDARY
    MK(1,1)=5,MK(2,1)=4,MK(3,1)=5,MK(4,1)=7
      MU(2,1)=1
      XGASVEL(1,2,1)=500.
      YGASVEL(1,2,1)=0.
      TEMPGAS(1,2,1)=300.
      DENSGAS(1,2,1)=1.E+19
      FRACTS(1,1,2,1)=1.
      FRACTS(2,1,2,1)=0.
      XGASVEL(2,2,1)=1200.
      YGASVEL(2,2,1)=0.
      TEMPGAS(2,2,1)=300.
      DENSGAS(2,2,1)=1.E+19
      FRACTS(1,2,2,1)=1.
      FRACTS(2,2,2,1)=0.
      XGASVEL(3,2,1)=3000.
      YGASVEL(3,2,1)=0.
      TEMPGAS(3,2,1)=300.
      DENSGAS(3,2,1)=1.E+19
      FRACTS(1,3,2,1)=1.
      FRACTS(2,3,2,1)=0.
      XGASVEL(4,2,1)=3000.
```

```
      YGASVEL(4,2,1)=0.
      TEMPGAS(4,2,1)=300.
      DENSGAS(4,2,1)=1.E+19
      FRACTS(1,4,2,1)=1.
      FRACTS(2,4,2,1)=0.
      XGASVEL(5,2,1)=3000.
      YGASVEL(5,2,1)=0.
      TEMPGAS(5,2,1)=300.
      DENSGAS(5,2,1)=1.E+19
      FRACTS(1,5,2,1)=1.
      FRACTS(2,5,2,1)=0.
      XGASVEL(6,2,1)=3000.
      YGASVEL(6,2,1)=0.
      TEMPGAS(6,2,1)=300.
      DENSGAS(6,2,1)=1.E+19
      FRACTS(1,6,2,1)=1.
      FRACTS(2,6,2,1)=0.
      XGASVEL(7,2,1)=3000.
      YGASVEL(7,2,1)=0.
      TEMPGAS(7,2,1)=300.
      DENSGAS(7,2,1)=1.E+19
      FRACTS(1,7,2,1)=1.
      FRACTS(2,7,2,1)=0.
      XGASVEL(8,2,1)=3000.
      YGASVEL(8,2,1)=0.
      TEMPGAS(8,2,1)=300.
      DENSGAS(8,2,1)=1.E+19
      FRACTS(1,8,2,1)=1.
      FRACTS(2,8,2,1)=0.
      XGASVEL(9,2,1)=3000.
      YGASVEL(9,2,1)=0.
      TEMPGAS(9,2,1)=300.
      DENSGAS(9,2,1)=1.E+19
      FRACTS(1,9,2,1)=1.
      FRACTS(2,9,2,1)=0.
      XGASVEL(10,2,1)=3000.
      YGASVEL(10,2,1)=0.
      TEMPGAS(10,2,1)=300.
      DENSGAS(10,2,1)=1.E+19
      FRACTS(1,10,2,1)=1.
      FRACTS(2,10,2,1)=0.
      MZ(1,1)=0.,MZ(3,1)=0.
      SURFTEMP(1,1,1)=300.,SURFTEMP(1,3,1)=300.
      SPECDIF(1,1,1)=.5, SPECDIF(1,3,1)=1.
      ABSORBD(1,1,1,1)=0.,ABSORBD(1,1,3,1)=0.
      KSIDE(4,1)=1,JSIDE(1,4,1)=2,IREGION(1,4,1)=2
MK(1,2)=7,MK(2,2)=7,MK(3,2)=5,MK(4,2)=7
      MZ(3,2)=0.
      SURFTEMP(1,3,2)=300.
      SPECDIF(1,3,2)=1.
      ABSORBD(1,1,3,2)=0.
      KSIDE(1,2)=1,JSIDE(1,1,2)=3,IREGION(1,1,2)=6
      KSIDE(2,2)=1,JSIDE(1,2,2)=4,IREGION(1,2,2)=1
      KSIDE(4,2)=1,JSIDE(1,4,2)=2,IREGION(1,4,2)=4
MK(1,3)=7,MK(2,3)=5,MK(3,3)=7,MK(4,3)=7
      MZ(1,3)=0., MZ(2,3)=0.
      SURFTEMP(1,1,3)=300.,SURFTEMP(1,2,3)=300.
      SPECDIF(1,1,3)=.5,SPECDIF(1,2,3)=.5
      ABSORBD(1,1,1,3)=0.,ABSORBD(1,1,2,3)=0.
      KSIDE(1,3)=1,JSIDE(1,1,3)=3,IREGION(1,1,3)=9
      KSIDE(3,3)=1,JSIDE(1,3,3)=1,IREGION(1,3,3)=6
      KSIDE(4,3)=1,JSIDE(1,4,3)=2,IREGION(1,4,3)=5
MK(1,4)=7,MK(2,4)=7,MK(3,4)=5,MK(4,4)=8
```

```
      MZ(3,4)=0.
      SURFTEMP(1,3,4)=300.
      SPECDIF(1,3,4)=1.
      ABSORBD(1,1,3,4)=0.
      KSIDE(1,4)=1,JSIDE(1,1,4)=3,IREGION(1,1,4)=7
      KSIDE(2,4)=1,JSIDE(1,2,4)=4,IREGION(1,2,4)=2
    MK(1,5)=2,MK(2,5)=7,MK(3,5)=7,MK(4,5)=8
      KSIDE(2,5)=3,JSIDE(1,2,5)=4,IREGION(1,2,5)=8
                  ,JSIDE(2,2,5)=4,IREGION(2,2,5)=9
                  ,JSIDE(3,2,5)=4,IREGION(3,2,5)=3
      KSIDE(3,5)=1,JSIDE(1,3,5)=1,IREGION(1,3,5)=7
    MK(1,6)=7,MK(2,6)=5,MK(3,6)=7,MK(4,6)=7
      MZ(1,6)=0., MZ(2,6)=0.
      SURFTEMP(1,1,6)=300.,SURFTEMP(1,2,6)=300.
      SPECDIF(1,1,6)=.5,SPECDIF(1,2,6)=.5
      ABSORBD(1,1,1,6)=0.,ABSORBD(1,1,2,6)=0.
      KSIDE(1,6)=1,JSIDE(1,1,6)=3,IREGION(1,1,6)=3
      KSIDE(3,6)=1,JSIDE(1,3,6)=1,IREGION(1,3,6)=2
      KSIDE(4,6)=1,JSIDE(1,4,6)=2,IREGION(1,4,6)=7
    MK(1,7)=7,MK(2,7)=7,MK(3,7)=7,MK(4,7)=8
      KSIDE(1,7)=1,JSIDE(1,1,7)=3,IREGION(1,1,7)=5
      KSIDE(2,7)=1,JSIDE(1,2,7)=4,IREGION(1,2,7)=6
      KSIDE(3,7)=1,JSIDE(1,3,7)=1,IREGION(1,3,7)=4
    MK(1,8)=2,MK(2,8)=5,MK(3,8)=7,MK(4,8)=7
      MZ(1,8)=0., MZ(2,8)=0.
      SURFTEMP(1,1,8)=300.,SURFTEMP(1,2,8)=300.
      SPECDIF(1,1,8)=.5,SPECDIF(1,2,8)=.5
      ABSORBD(1,1,1,8)=0.,ABSORBD(1,1,2,8)=0.
      KSIDE(3,8)=1,JSIDE(1,3,8)=1,IREGION(1,3,8)=9
      KSIDE(4,8)=1,JSIDE(1,4,8)=2,IREGION(1,4,8)=5
    MK(1,9)=7,MK(2,9)=4,MK(3,9)=7,MK(4,9)=7
      MU(2,9)=0
      XGASVEL(1,2,9)=300.
      YGASVEL(1,2,9)=0.
      TEMPGAS(1,2,9)=300.
      DENSGAS(1,2,9)=1.E+17
      FRACTS(1,1,2,9)=0.
      FRACTS(2,1,2,9)=1.
      KSIDE(1,9)=1,JSIDE(1,1,9)=3,IREGION(1,1,9)=8
      KSIDE(3,9)=1,JSIDE(1,3,9)=1,IREGION(1,3,9)=3
      KSIDE(4,9)=1,JSIDE(1,4,9)=2,IREGION(1,4,9)=5
$END
```

Data Deck for Computational Case #3

```
$GENERAL
        IFX=0
        IQS=0
         MAXM=60000
         INS=0
         NIS=10
         NSP=10
         NPS=10
         NPT=30
$END
$INIT
         ISQ=1
         VFX=8000 ,VFY=0.,FND=1.E+19,FTMP=300.,FRACT(1)=1.
$END
$GAS
         NSS=2
         NSSR=6
$END
$GRID
         NREG=9
$END
$REGIONS
          FNUM(1)=.2E+16,DTM(1)=0.00001
            NC13(1)=1,NSC13(1)=1,NC24(1)=10,NSC24(1)=1
            NTS1(1)=2,XP1(1,1)=-0.1,YP1(1,1)=0.0,XP1(2,1)=0.0,YP1(2,1)=0.0,
               SZ1(1)=1.,NPR1(1)=1,NPS1(1)=1
            NTS3(1)=2,XP3(1,1)=-0.1,YP3(1,1)=0.3,XP3(2,1)=0.0,YP3(2,1)=0.3,
               SZ3(1)=1.,NPR3(1)=1,NPS3(1)=1
            NTS2(1)=1,
            NTS4(1)=1
            WT42(1)=1
          FNUM(2)=.2E+16,DTM(2)=0.000005
            NC13(2)=20,NSC13(2)=2,NC24(2)=6,NSC24(2)=2
            NTS1(2)=2,XP1(1,2)=0.0,YP1(1,2)=0.0,XP1(2,2)=1.0,YP1(2,2)=0.0,
               SZ1(2)=1.,NPR1(2)=1,NPS1(2)=1
            NTS3(2)=2,XP3(1,2)=0.0,YP3(1,2)=0.3,XP3(2,2)=1.0,YP3(2,2)=0.3,
               SZ3(2)=1.,NPR3(2)=1,NPS3(2)=1
            NTS2(2)=1,
            NTS4(2)=1
            WT42(2)=1
          FNUM(3)=.022E+15,DTM(3)=0.00006
            NC13(3)=10,NSC13(3)=4,NC24(3)=5,NSC24(3)=4
            NTS1(3)=2,XP1(1,3)=0.0,YP1(1,3)=-.5,XP1(2,3)=1.0,YP1(2,3)=-.5,
               SZ1(3)=1.,NPR1(3)=1,NPS1(3)=1
            NTS3(3)=2,XP3(1,3)=0.0,YP3(1,3)=-.1,XP3(2,3)=1.0,YP3(2,3)=-.1,
               SZ3(3)=1.,NPR3(3)=1,NPS3(3)=1
            NTS2(3)=1,
            NTS4(3)=1
            WT42(3)=1
          FNUM(4)=.6E+16,DTM(4)=0.00002
            NC13(4)=10,NSC13(4)=1,NC24(4)=3,NSC24(4)=1
            NTS1(4)=2,XP1(1,4)=1.0,YP1(1,4)=0.0,XP1(2,4)=2.0,YP1(2,4)=0.0,
               SZ1(4)=1.,NPR1(4)=1,NPS1(4)=1
            NTS3(4)=2,XP3(1,4)=1.0,YP3(1,4)=0.3,XP3(2,4)=2.0,YP3(2,4)=0.3,
               SZ3(4)=1.,NPR3(4)=1,NPS3(4)=1
            NTS2(4)=1,
            NTS4(4)=1
            WT42(4)=1
          FNUM(5)=.066E+16,DTM(5)=0.0001
            NC13(5)=5,NSC13(5)=2,NC24(5)=5,NSC24(5)=2
            NTS1(5)=2,XP1(1,5)=1.0,YP1(1,5)=-1.0,XP1(2,5)=2.0,YP1(2,5)=-1.0,
               SZ1(5)=1.,NPR1(5)=1,NPS1(5)=1
            NTS3(5)=2,XP3(1,5)=1.0,YP3(1,5)=-.1,XP3(2,5)=2.0,YP3(2,5)=-.1,
```

```
      SZ3(5)=1.,NPR3(5)=1,NPS3(5)=1
    NTS2(5)=1,
    NTS4(5)=1
    WT42(5)=1
  FNUM(6)=.05E+16,DTM(6)=0.00002
    NC13(6)=10,NSC13(6)=4,NC24(6)=2,NSC24(6)=2
    NTS1(6)=2,XP1(1,6)=0.0,YP1(1,6)=-.1,XP1(2,6)=1.0,YP1(2,6)=-.1,
      SZ1(6)=1.,NPR1(6)=1,NPS1(6)=1
    NTS3(6)=2,XP3(1,6)=0.0,YP3(1,6)=0.0,XP3(2,6)=1.0,YP3(2,6)=0.0,
      SZ3(6)=1.,NPR3(6)=1,NPS3(6)=1
    NTS2(6)=1,
    NTS4(6)=1
    WT42(6)=1
  FNUM(7)=.1E+16,DTM(7)=0.00002
    NC13(7)=10,NSC13(7)=2,NC24(7)=2,NSC24(7)=2
    NTS1(7)=2,XP1(1,7)=1.0,YP1(1,7)=-.1,XP1(2,7)=2.0,YP1(2,7)=-.1,
      SZ1(7)=1.,NPR1(7)=1,NPS1(7)=1
    NTS3(7)=2,XP3(1,7)=1.0,YP3(1,7)=0.0,XP3(2,7)=2.0,YP3(2,7)=0.0,
      SZ3(7)=1.,NPR3(7)=1,NPS3(7)=1
    NTS2(7)=1,
    NTS4(7)=1
    WT42(7)=1
  FNUM(8)=.02E+15,DTM(8)=0.00012
    NC13(8)=10,NSC13(8)=4,NC24(8)=4,NSC24(8)=4
    NTS1(8)=2,XP1(1,8)=0.0,YP1(1,8)=-1.,XP1(2,8)=1.0,YP1(2,8)=-1.,
      SZ1(8)=1.,NPR1(8)=1,NPS1(8)=1
    NTS3(8)=2,XP3(1,8)=0.0,YP3(1,8)=-.6,XP3(2,8)=1.0,YP3(2,8)=-.6,
      SZ3(8)=1.,NPR3(8)=1,NPS3(8)=1
    NTS2(8)=1,
    NTS4(8)=1
    WT42(8)=1
  FNUM(9)=.05E+15,DTM(9)=0.00012
    NC13(9)=10,NSC13(9)=4,NC24(9)=1,NSC24(9)=4
    NTS1(9)=2,XP1(1,9)=0.,YP1(1,9)=-.6,XP1(2,9)=1.0,YP1(2,9)=-.6,
      SZ1(9)=1.,NPR1(9)=1,NPS1(9)=1
    NTS3(9)=2,XP3(1,9)=0.,YP3(1,9)=-.5,XP3(2,9)=1.0,YP3(2,9)=-.5,
      SZ3(9)=1.,NPR3(9)=1,NPS3(9)=1
    NTS2(9)=1,
    NTS4(9)=1
    WT42(9)=1
$END
$BOUNDARY
  MK(1,1)=5,MK(2,1)=4,MK(3,1)=5,MK(4,1)=7
    MU(2,1)=1
    XGASVEL(1,2,1)=500.
    YGASVEL(1,2,1)=0.
    TEMPGAS(1,2,1)=300.
    DENSGAS(1,2,1)=1.E+19
    FRACTS(1,1,2,1)=1.
    FRACTS(2,1,2,1)=0.
    XGASVEL(2,2,1)=1200.
    YGASVEL(2,2,1)=0.
    TEMPGAS(2,2,1)=300.
    DENSGAS(2,2,1)=1.E+19
    FRACTS(1,2,2,1)=1.
    FRACTS(2,2,2,1)=0.
    XGASVEL(3,2,1)=3000.
    YGASVEL(3,2,1)=0.
    TEMPGAS(3,2,1)=300.
    DENSGAS(3,2,1)=1.E+19
    FRACTS(1,3,2,1)=1.
    FRACTS(2,3,2,1)=0.
    XGASVEL(4,2,1)=3000.
```

```
      YGASVEL(4,2,1)=0.
      TEMPGAS(4,2,1)=300.
      DENSGAS(4,2,1)=1.E+19
      FRACTS(1,4,2,1)=1.
      FRACTS(2,4,2,1)=0.
      XGASVEL(5,2,1)=3000.
      YGASVEL(5,2,1)=0.
      TEMPGAS(5,2,1)=300.
      DENSGAS(5,2,1)=1.E+19
      FRACTS(1,5,2,1)=1.
      FRACTS(2,5,2,1)=0.
      XGASVEL(6,2,1)=3000.
      YGASVEL(6,2,1)=0.
      TEMPGAS(6,2,1)=300.
      DENSGAS(6,2,1)=1.E+19
      FRACTS(1,6,2,1)=1.
      FRACTS(2,6,2,1)=0.
      XGASVEL(7,2,1)=3000.
      YGASVEL(7,2,1)=0.
      TEMPGAS(7,2,1)=300.
      DENSGAS(7,2,1)=1.E+19
      FRACTS(1,7,2,1)=1.
      FRACTS(2,7,2,1)=0.
      XGASVEL(8,2,1)=3000.
      YGASVEL(8,2,1)=0.
      TEMPGAS(8,2,1)=300.
      DENSGAS(8,2,1)=1.E+19
      FRACTS(1,8,2,1)=1.
      FRACTS(2,8,2,1)=0.
      XGASVEL(9,2,1)=3000.
      YGASVEL(9,2,1)=0.
      TEMPGAS(9,2,1)=300.
      DENSGAS(9,2,1)=1.E+19
      FRACTS(1,9,2,1)=1.
      FRACTS(2,9,2,1)=0.
      XGASVEL(10,2,1)=3000.
      YGASVEL(10,2,1)=0.
      TEMPGAS(10,2,1)=300.
      DENSGAS(10,2,1)=1.E+19
      FRACTS(1,10,2,1)=1.
      FRACTS(2,10,2,1)=0.
      MZ(1,1)=0.,MZ(3,1)=0.
      SURFTEMP(1,1,1)=300.,SURFTEMP(1,3,1)=300.
      SPECDIF(1,1,1)=.5, SPECDIF(1,3,1)=1.
      ABSORBD(1,1,1,1)=0.,ABSORBD(1,1,3,1)=0.
      KSIDE(4,1)=1,JSIDE(1,4,1)=2,IREGION(1,4,1)=2
MK(1,2)=7,MK(2,2)=7,MK(3,2)=5,MK(4,2)=7
      MZ(3,2)=0.
      SURFTEMP(1,3,2)=300.
      SPECDIF(1,3,2)=1.
      ABSORBD(1,1,3,2)=0.
      KSIDE(1,2)=1,JSIDE(1,1,2)=3,IREGION(1,1,2)=6
      KSIDE(2,2)=1,JSIDE(1,2,2)=4,IREGION(1,2,2)=1
      KSIDE(4,2)=1,JSIDE(1,4,2)=2,IREGION(1,4,2)=4
MK(1,3)=7,MK(2,3)=5,MK(3,3)=7,MK(4,3)=7
      MZ(1,3)=0., MZ(2,3)=0.
      SURFTEMP(1,1,3)=300.,SURFTEMP(1,2,3)=300.
      SPECDIF(1,1,3)=.5,SPECDIF(1,2,3)=.5
      ABSORBD(1,1,1,3)=0.,ABSORBD(1,1,2,3)=0.
      KSIDE(1,3)=1,JSIDE(1,1,3)=3,IREGION(1,1,3)=9
      KSIDE(3,3)=1,JSIDE(1,3,3)=1,IREGION(1,3,3)=8
      KSIDE(4,3)=1,JSIDE(1,4,3)=2,IREGION(1,4,3)=5
MK(1,4)=7,MK(2,4)=7,MK(3,4)=5,MK(4,4)=8
```

```
   MZ(3,4)=0.
   SURFTEMP(1,3,4)=300.
   SPECDIF(1,3,4)=1.
   ABSORBD(1,1,3,4)=0.
   KSIDE(1,4)=1,JSIDE(1,1,4)=3,IREGION(1,1,4)=7
   KSIDE(2,4)=1,JSIDE(1,2,4)=4,IREGION(1,2,4)=2
MK(1,5)=2,MK(2,5)=7,MK(3,5)=7,MK(4,5)=8
   KSIDE(2,5)=3,JSIDE(1,2,5)=4,IREGION(1,2,5)=8
                ,JSIDE(2,2,5)=4,IREGION(2,2,5)=9
                ,JSIDE(3,2,5)=4,IREGION(3,2,5)=3
   KSIDE(3,5)=1,JSIDE(1,3,5)=1,IREGION(1,3,5)=7
MK(1,6)=7,MK(2,6)=5,MK(3,6)=7,MK(4,6)=7
   MZ(1,6)=0., MZ(2,6)=0.
   SURFTEMP(1,1,6)=300.,SURFTEMP(1,2,6)=300.
   SPECDIF(1,1,6)=.5,SPECDIF(1,2,6)=.5
   ABSORBD(1,1,1,6)=0.,ABSORBD(1,1,2,6)=0.
   KSIDE(1,6)=1,JSIDE(1,1,6)=3,IREGION(1,1,6)=3
   KSIDE(3,6)=1,JSIDE(1,3,6)=1,IREGION(1,3,6)=2
   KSIDE(4,6)=1,JSIDE(1,4,6)=2,IREGION(1,4,6)=7
MK(1,7)=7,MK(2,7)=7,MK(3,7)=7,MK(4,7)=8
   KSIDE(1,7)=1,JSIDE(1,1,7)=3,IREGION(1,1,7)=5
   KSIDE(2,7)=1,JSIDE(1,2,7)=4,IREGION(1,2,7)=6
   KSIDE(3,7)=1,JSIDE(1,3,7)=1,IREGION(1,3,7)=4
MK(1,8)=2,MK(2,8)=5,MK(3,8)=7,MK(4,8)=7
   MZ(1,8)=0., MZ(2,8)=0.
   SURFTEMP(1,1,8)=300.,SURFTEMP(1,2,8)=300.
   SPECDIF(1,1,8)=.5,SPECDIF(1,2,8)=.5
   ABSORBD(1,1,1,8)=0.,ABSORBD(1,1,2,8)=0.
   KSIDE(3,8)=1,JSIDE(1,3,8)=1,IREGION(1,3,8)=9
   KSIDE(4,8)=1,JSIDE(1,4,8)=2,IREGION(1,4,8)=5
MK(1,9)=7,MK(2,9)=4,MK(3,9)=7,MK(4,9)=7
   MU(2,9)=0
   XGASVEL(1,2,9)=300.
   YGASVEL(1,2,9)=0.
   TEMPGAS(1,2,9)=300.
   DENSGAS(1,2,9)=1.E+18
   FRACTS(1,1,2,9)=0.
   FRACTS(2,1,2,9)=1.
   KSIDE(1,9)=1,JSIDE(1,1,9)=3,IREGION(1,1,9)=8
   KSIDE(3,9)=1,JSIDE(1,3,9)=1,IREGION(1,3,9)=3
   KSIDE(4,9)=1,JSIDE(1,4,9)=2,IREGION(1,4,9)=5
$END
```